Volume 19, Number 4, 2019 ISSN 1562-8353

NONLINEAR DYNAMICS AND SYSTEMS THEORY

An International Journal of Research and Surveys

Volume 19 Number 4 2019

CONTENTS

 ISSN 1562-8353 Printed in Ukraine
To receive contents and abstracts by e-mail, visit our Website at: **http://www.e-ndst.kiev.ua**

NONLINEAR DYNAMICS & SYSTEMS THEORY

Volume 19, No. 4, 2019

Nonlinear Dynamics and Systems Theory

An International Journal of Research and Surveys

InforMath Publishing Group
http://www.e-ndst.kiev.ua

Nonlinear Dynamics and Systems Theory

An International Journal of Research and Surveys

INSTRUCTIONS FOR CONTRIBUTORS

(1) General. Nonlinear Dynamics and Systems Theory (ND&ST) is an international journal devoted to publishing peer-refereed, high quality, original papers, brief notes and review articles focusing on nonlinear dynamics and systems theory and their practical applications in engineering, physical and life sciences. Submission of a manuscript is a representation that the submission has been approved by all of the authors and by the institution where the work was carried out. It also represents that the manuscript has not been previously published, has not been copyrighted, is not being submitted for publication elsewhere, and that the authors have agreed that the copyright in the article shall be assigned exclusively to InforMath Publishing Group by signing a transfer of copyright form. Before submission, the authors should visit the website:

http://www.e-ndst.kiev.ua

for information on the preparation of accepted manuscripts. Please download the archive Sample_NDST.zip containing example of article file (you can edit only the file Samplefilename.tex).

(2) Manuscript and Correspondence. Manuscripts should be in English and must meet common standards of usage and grammar. To submit a paper, send by e-mail a file in PDF format directly to

Professor A.A. Martynyuk, Institute of Mechanics,
Nesterov str.3, 03057, MSP 680, Kiev-57, Ukraine
e-mail: journalndst@gmail.com

or to one of the Regional Editors or to a member of the Editorial Board. Final version of the manuscript must typeset using LaTex program which is prepared in accordance with the style file of the Journal. Manuscript texts should contain the title of the article, name(s) of the author(s) and complete affiliations. Each article requires an abstract not exceeding 150 words. Formulas and citations should not be included in the abstract. AMS subject classifications and key words must be included in all accepted papers. Each article requires a running head (abbreviated form of the title) of no more than 30 characters. The sizes for regular papers, survey articles, brief notes, letters to editors and book reviews are: (i) 10-14 pages for regular papers, (ii) up to 24 pages for survey articles, and (iii) 2-3 pages for brief notes, letters to the editor and book reviews.

(3) Tables, Graphs and Illustrations. Each figure must be of a quality suitable for direct reproduction and must include a caption. Drawings should include all relevant details and should be drawn professionally in black ink on plain white drawing paper. In addition to a hard copy of the artwork, it is necessary to attach the electronic file of the artwork (preferably in PCX format).

(4) References. Each entry must be cited in the text by author(s) and number or by number alone. All references should be listed in their alphabetic order. Use please the following style:

Journal: [1] H. Poincare, Title of the article. *Title of the Journal* **volume** (issue) (year) pages. [Language]

Book: [2] A.M. Lyapunov, *Title of the Book.* Name of the Publishers, Town, year.

Proceeding: [3] R. Bellman, Title of the article. In: *Title of the Book.* (Eds.). Name of the Publishers, Town, year, pages. [Language]

(5) Proofs and Sample Copy. Proofs sent to authors should be returned to the Editorial Office with corrections within three days after receipt. The corresponding author will receive a sample copy of the issue of the Journal for which his/her paper is published.

(6) Editorial Policy. Every submission will undergo a stringent peer review process. An editor will be assigned to handle the review process of the paper. He/she will secure at least two reviewers' reports. The decision on acceptance, rejection or acceptance subject to revision will be made based on these reviewers' reports and the editor's own reading of the paper.

NONLINEAR DYNAMICS AND SYSTEMS THEORY
An International Journal of Research and Surveys
Published by InforMath Publishing Group since 2001

Volume 19 Number 4 2019

CONTENTS

Founded by A.A. Martynyuk in 2001.

Registered in Ukraine Number: KB 5267 / 04.07.2001.

NONLINEAR DYNAMICS AND SYSTEMS THEORY

An International Journal of Research and Surveys

Impact Factor from SCOPUS for 2017: SNIP – 0.707, SJR – 0.316

Nonlinear Dynamics and Systems Theory (ISSN 1562–8353 (Print), ISSN 1813–7385 (Online)) is an international journal published under the auspices of the S.P. Timoshenko Institute of Mechanics of National Academy of Sciences of Ukraine and Curtin University of Technology (Perth, Australia). It aims to publish high quality original scientific papers and surveys in areas of nonlinear dynamics and systems theory and their real world applications.

AIMS AND SCOPE

Nonlinear Dynamics and Systems Theory is a multidisciplinary journal. It publishes papers focusing on proofs of important theorems as well as papers presenting new ideas and new theory, conjectures, numerical algorithms and physical experiments in areas related to nonlinear dynamics and systems theory. Papers that deal with theoretical aspects of nonlinear dynamics and/or systems theory should contain significant mathematical results with an indication of their possible applications. Papers that emphasize applications should contain new mathematical models of real world phenomena and/or description of engineering problems. They should include rigorous analysis of data used and results obtained. Papers that integrate and interrelate ideas and methods of nonlinear dynamics and systems theory will be particularly welcomed. This journal and the individual contributions published therein are protected under the copyright by International InforMath Publishing Group.

PUBLICATION AND SUBSCRIPTION INFORMATION

Nonlinear Dynamics and Systems Theory will have 4 issues in 2020, printed in hard copy (ISSN 1562–8353) and available online (ISSN 1813–7385), by InforMath Publishing Group, Nesterov str., 3, Institute of Mechanics, Kiev, MSP 680, Ukraine, 03057. Subscription prices are available upon request from the Publisher, EBSCO Information Services (`mailto:journals@ebsco.com`), or website of the Journal: `http://e-ndst.kiev.ua`. Subscriptions are accepted on a calendar year basis. Issues are sent by airmail to all countries of the world. Claims for missing issues should be made within six months of the date of dispatch.

ABSTRACTING AND INDEXING SERVICES

Papers published in this journal are indexed or abstracted in: Mathematical Reviews / MathSciNet, Zentralblatt MATH / Mathematics Abstracts, PASCAL database (INIST–CNRS) and SCOPUS.

Nonlinear Dynamics and Systems Theory, **19** (4) (2019) 445–454

Diagonal Riccati Stability of a Class of Matrices and Applications

A. Yu. Aleksandrov * and N. O. Kovaleva

Saint Petersburg State University, 7–9 Universitetskaya Nab., St. Petersburg, 199034, Russia

Received: April 14, 2019; Revised: September 9, 2019

Abstract: Necessary and sufficient conditions of the diagonal Riccati stability are derived for a class of pairs of matrices with special structures. The obtained conditions are used in the problems of analysis and synthesis of some types of time-delay systems. Results of numerical simulation are presented to illustrate the effectiveness of the proposed approaches.

Keywords: *diagonal stability; delay; Lyapunov–Krasovskii functional; complex system; asymptotic stability; consensus.*

Mathematics Subject Classification (2010): 34D20, 34K20.

1 Introduction

The problem of diagonal Riccati stability was introduced in [15] and is motivated by the construction of the diagonal Lyapunov–Krasovskii functionals for linear time-delay systems.

In [4], a criterion for a given pair of matrices to be diagonally Riccati stable has been derived. This result extended the well known condition of Barker, Berman and Plemmons for the diagonal Lyapunov stability [7]. With the aid of this criterion, necessary and sufficient conditions of the existence of diagonal Lyapunov–Krasovskii functionals were found for linear positive differential and difference systems with delay [3, 4].

However, it should be noted that the conditions of the above criterion are not constructive enough. Therefore, an actual problem is to determine the classes of matrices for which simple and constructively verified necessary and sufficient conditions of the diagonal Riccati stability can be obtained. Some of such classes were found in [2, 5].

In the present paper, a class of pairs of matrices is studied. These matrices can be used for the modeling of complex systems composed of second order subsystems with a special structure of connections between the subsystems and with a delay in the feedback law. A criterion of the diagonal Riccati stability is derived for the matrices under consideration. Moreover, it is shown that the obtained result can be applied to the problems of analysis and synthesis of some types of time-delay systems.

* Corresponding author: mailto:a.u.aleksandrov@spbu.ru

2 Statement of the Problem

Let $\mathbb{R}$ be the field of real numbers, $\mathbb{R}^n$ and $\mathbb{R}^{n\times n}$ denote the vector spaces of n-tuples of real numbers and $n \times n$ matrices, respectively, $\|\cdot\|$ be the Euclidean norm of a vector.

For a matrix $C \in \mathbb{R}^{n\times n}$, we use the notation $C^\top$ for the transpose of C. The matrix C is Hurwitz if all of its eigenvalues have negative real parts, C is Metzler if its off-diagonal entries are all nonnegative, C is nonnegative if all of its entries are nonnegative. Let $\mathrm{diag}\{\lambda_1, \dots, \lambda_n\}$ be the diagonal matrix with the elements $\lambda_1, \dots, \lambda_n$ along the main diagonal.

Let matrices $A, B \in \mathbb{R}^{n\times n}$ be given.

Definition 2.1 (see [15]) The pair of matrices (A, B) is diagonally Riccati stable if there exist diagonal positive definite matrices $P = \mathrm{diag}\{p_1, \dots, p_n\}$ and $Q = \mathrm{diag}\{q_1, \dots, q_n\}$ such that the matrix

$$R = A^\top P + PA + Q + PBQ^{-1}B^\top P \tag{1}$$

is negative definite.

In [4, 5] the following results were obtained.

Proposition 2.1 *Let the matrix $A \in \mathbb{R}^{n\times n}$ be Metzler and the matrix $B \in \mathbb{R}^{n\times n}$ be nonnegative. Then the pair (A, B) is diagonally Riccati stable if and only if the matrix $A + B$ is Hurwitz.*

Proposition 2.2 *Let $A \in \mathbb{R}^{n\times n}$, $B \in \mathbb{R}^{n\times n}$ be given and let $D = \mathrm{diag}\{d_1, \dots, d_n\}$, $E = \mathrm{diag}\{e_1, \dots, e_n\}$ with $d_i \in \{-1; +1\}$, $e_i \in \{-1; +1\}$ for $i = 1, \dots, n$. The pair (A, B) is diagonally Riccati stable if and only if (DAD, DBE) is diagonally Riccati stable.*

In this contribution, we will look for the conditions of the diagonal Riccati stability for a special class of pairs of matrices. Assume that n is an even number ($n = 2k$, k is a positive integer), and the matrices A and B have the following forms:

$$A = \begin{pmatrix} a_{11} & a_{12} & 0 & 0 & 0 & 0 & \cdots & 0 & 0 & 0 \\ a_{21} & a_{22} & 0 & 0 & 0 & 0 & \cdots & 0 & 0 & 0 \\ 0 & 0 & a_{33} & a_{34} & 0 & 0 & \cdots & 0 & 0 & 0 \\ 0 & c_1 & a_{43} & a_{44} & 0 & 0 & \cdots & 0 & 0 & 0 \\ 0 & 0 & 0 & 0 & a_{55} & a_{56} & \cdots & 0 & 0 & 0 \\ 0 & 0 & 0 & c_2 & a_{65} & a_{66} & \cdots & 0 & 0 & 0 \\ \vdots & \vdots & \vdots & \vdots & \vdots & \vdots & \ddots & \vdots & \vdots & \vdots \\ 0 & 0 & 0 & 0 & 0 & 0 & \cdots & 0 & a_{n-1\,n-1} & a_{n-1\,n} \\ 0 & 0 & 0 & 0 & 0 & 0 & \cdots & c_{k-1} & a_{n\,n-1} & a_{n\,n} \end{pmatrix}, \tag{2}$$

$$B = \begin{pmatrix} 0 & 0 & 0 & \cdots & 0 & 0 \\ 0 & 0 & 0 & \cdots & 0 & b \\ 0 & 0 & 0 & \cdots & 0 & 0 \\ \vdots & \vdots & \vdots & \ddots & \vdots & \vdots \\ 0 & 0 & 0 & \cdots & 0 & 0 \\ 0 & 0 & 0 & \cdots & 0 & 0 \end{pmatrix}. \tag{3}$$

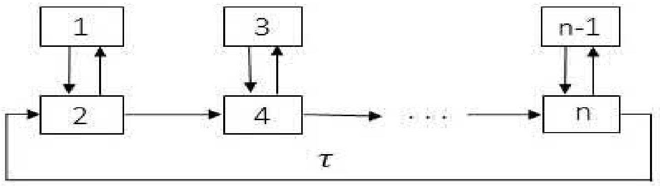

Figure 1: Structure of connections in a complex system.

Such matrices can be used for the modeling of complex systems composed of second order subsystems with a special structure of connections between the subsystems and with a delay in the feedback law (see Fig. 1).

Furthermore, we will apply the obtained conditions of the diagonal Riccati stability to the problems of analysis and synthesis for some classes of linear and nonlinear difference-differential systems.

3 A Criterion of the Diagonal Riccati Stability

Construct the auxiliary matrices

$$\widetilde{A} = \begin{pmatrix} a_{11} & \tilde{a}_{12} & 0 & 0 & 0 & 0 & \cdots & 0 & 0 & 0 \\ \tilde{a}_{21} & a_{22} & 0 & 0 & 0 & 0 & \cdots & 0 & 0 & 0 \\ 0 & 0 & a_{33} & \tilde{a}_{34} & 0 & 0 & \cdots & 0 & 0 & 0 \\ 0 & |c_1| & \tilde{a}_{43} & a_{44} & 0 & 0 & \cdots & 0 & 0 & 0 \\ 0 & 0 & 0 & 0 & a_{55} & \tilde{a}_{56} & \cdots & 0 & 0 & 0 \\ 0 & 0 & 0 & |c_2| & \tilde{a}_{65} & a_{66} & \cdots & 0 & 0 & 0 \\ \vdots & \vdots & \vdots & \vdots & \vdots & \vdots & \ddots & \vdots & \vdots & \vdots \\ 0 & 0 & 0 & 0 & 0 & 0 & \cdots & 0 & a_{n-1\,n-1} & \tilde{a}_{n-1\,n} \\ 0 & 0 & 0 & 0 & 0 & 0 & \cdots & |c_{k-1}| & \tilde{a}_{n\,n-1} & a_{n\,n} \end{pmatrix},$$

$$\widetilde{B} = \begin{pmatrix} 0 & 0 & 0 & \cdots & 0 & 0 \\ 0 & 0 & 0 & \cdots & 0 & |b| \\ 0 & 0 & 0 & \cdots & 0 & 0 \\ \vdots & \vdots & \vdots & \ddots & \vdots & \vdots \\ 0 & 0 & 0 & \cdots & 0 & 0 \\ 0 & 0 & 0 & \cdots & 0 & 0 \end{pmatrix}.$$

Here $\tilde{a}_{2j-1\,2j} = \tilde{a}_{2j\,2j-1} = 0$ for $a_{2j-1\,2j}a_{2j\,2j-1} < 0$, and $\tilde{a}_{2j-1\,2j} = |a_{2j-1\,2j}|$, $\tilde{a}_{2j\,2j-1} = |a_{2j\,2j-1}|$ for $a_{2j-1\,2j}a_{2j\,2j-1} \geq 0$, $j = 1, \ldots, k$.

Denote $\widetilde{\Delta}_{2j-1\,2j} = a_{2j-1\,2j-1}a_{2j\,2j} - \tilde{a}_{2j-1\,2j}\tilde{a}_{2j\,2j-1}$, $j = 1, \ldots, k$.

Theorem 3.1 *Let the matrices A and B be of the form (2) and (3), respectively. Then the pair (A, B) is diagonally Riccati stable if and only if the inequalities*

$$a_{ii} < 0, \quad i = 1, \ldots, n, \qquad \widetilde{\Delta}_{2j-1\,2j} > 0, \quad j = 1, \ldots, k, \tag{4}$$

$$\widetilde{\Delta}_{12}\widetilde{\Delta}_{34} \ldots \widetilde{\Delta}_{n-1\,n} > |a_{11}a_{33} \ldots a_{n-1\,n-1}c_1c_2 \ldots c_{k-1}b| \tag{5}$$

hold.

Proof. Let $P = \operatorname{diag}\{p_1, \dots, p_n\}$ and $Q = \operatorname{diag}\{q_1, \dots, q_n\}$ be positive definite diagonal matrices. Without loss of generality, assume that $q_n = 1$.

If the matrices A and B are defined by the formulae (2) and (3), then the matrix (1) can be represented in the form $R = \widetilde{R} + \operatorname{diag}\{q_1, q_2, \dots, q_{n-1}, 0\}$, where

$$\widetilde{R} = \begin{pmatrix} R_{12} & L_1 & 0 & 0 & 0 & \cdots & 0 & 0 \\ L_1 & R_{34} & L_2 & 0 & 0 & \cdots & 0 & 0 \\ 0 & L_2 & R_{56} & L_3 & 0 & \cdots & 0 & 0 \\ \vdots & \vdots & \vdots & \vdots & \vdots & \ddots & \vdots & \vdots \\ 0 & 0 & 0 & 0 & 0 & \cdots & R_{n-3\,n-2} & L_{k-1} \\ 0 & 0 & 0 & 0 & 0 & \cdots & L_{k-1} & R_{n-1\,n} \end{pmatrix},$$

$$R_{12} = \begin{pmatrix} 2p_1a_{11} & p_1a_{12} + p_2a_{21} \\ p_1a_{12} + p_2a_{21} & 2p_2a_{22} + p_2^2b^2 \end{pmatrix},$$

$$R_{2j-1\,2j} = \begin{pmatrix} 2p_{2j-1}a_{2j-1\,2j-1} & p_{2j-1}a_{2j-1\,2j} + p_{2j}a_{2j\,2j-1} \\ p_{2j-1}a_{2j-1\,2j} + p_{2j}a_{2j\,2j-1} & 2p_{2j}a_{2j\,2j} \end{pmatrix}, \quad j = 2, \dots, k-1,$$

$$R_{n-1\,n} = \begin{pmatrix} 2p_{n-1}a_{n-1\,n-1} & p_{n-1}a_{n-1\,n} + p_na_{n\,n-1} \\ p_{n-1}a_{n-1\,n} + p_na_{n\,n-1} & 2p_na_{nn} + 1 \end{pmatrix},$$

$$L_j = \begin{pmatrix} 0 & 0 \\ 0 & c_jp_{2j+2} \end{pmatrix}, \quad j = 1, \dots, k-1.$$

Thus, the pair (A, B) is diagonally Riccati stable if and only if there exist positive numbers $p_1, \dots, p_n$ for which the matrix $\widetilde{R}$ is negative definite.

Let Δ_i be the leading principal minor of the i-th order of the matrix $\widetilde{R}$, $i = 1, \dots, n$. Necessary and sufficient conditions of the negative definiteness of $\widetilde{R}$ can be formulated as follows: $a_{ii} < 0$, $i = 1, \dots, n$,

$$\det R_{2j-1\,2j} > 0, \quad \Delta_{2j} > 0, \quad j = 1, \dots, k. \tag{6}$$

Choose a number $l \in \{1, \dots, k\}$. Consider the inequalities from (6) depending on the corresponding parameter p_{2l-1}. We obtain $\det R_{2l-1\,2l} > 0$,

$$\Delta_{2j} > 0, \quad j = l, \dots, k. \tag{7}$$

Developing Δ_{2j} by the $(2l-1)$-th and $2l$-th columns, rewrite (7) in the form

$$\alpha_{lj} \frac{\det R_{2l-1\,2l}}{p_{2l-1}} > \beta_{lj}, \quad j = l, \dots, k,$$

where α_{lj} and β_{lj} are independent of p_{2l-1}, and $\alpha_{lj} > 0$.

Thus, to derive less conservative restrictions on the entries of the matrices A and B, one should take a value of p_{2l-1} for which $\det R_{2l-1\,2l}/p_{2l-1}$ is minimal. Hence,

$$p_{2l-1} = \begin{cases} p_{2l}a_{2l\,2l-1}/a_{2l-1\,2l} & \text{for} \ \ a_{2l-1\,2l}a_{2l\,2l-1} > 0, \\ -p_{2l}a_{2l\,2l-1}/a_{2l-1\,2l} & \text{for} \ \ a_{2l-1\,2l}a_{2l\,2l-1} < 0. \end{cases}$$

Moreover, taking into account Proposition 2.2, we can assume that $b \ge 0$, $c_s \ge 0$, $s = 1, \dots, k-1$, and $a_{2j-1\,2j} \ge 0$, $a_{2j\,2j-1} \ge 0$ for $a_{2j-1\,2j}a_{2j\,2j-1} \ge 0$.

As a result, we obtain that conditions of the diagonal Riccati stability for the pair (A, B) coincide with those for the pair $(\widetilde{A}, \widetilde{B})$.

The matrix $\widetilde{A}$ is Metzler and the matrix $\widetilde{B}$ is nonnegative. Hence (see Proposition 2.1), $(\widetilde{A}, \widetilde{B})$ is diagonally Riccati stable if and only if the matrix $\widetilde{A} + \widetilde{B}$ is Hurwitz. Verifying the Sevastyanov–Kotelyanskii conditions [10] for the matrix $\widetilde{A} + \widetilde{B}$, we arrive at the inequalities (4), (5). □

4 Applications

In this section, we will show how the result described above can be applied to some problems of analysis and synthesis of time-delay systems.

4.1 Absolute stability of the Persidskii-type systems

Let the nonlinear time-delay system

$$\dot{x}(t) = Af(x(t)) + Bf(x(t-\tau)) \tag{8}$$

be given. Here $x(t) = (x_1(t), \ldots, x_n(t))^\top$ is the state vector; $A \in \mathbb{R}^n$ and $B \in \mathbb{R}^n$ are constant matrices; τ is a constant nonnegative delay. The nonlinearity $f : \mathbb{R}^n \to \mathbb{R}^n$ is continuous, diagonal $f(x) = (f_1(x_1), \ldots, f_n(x_n))^\top$ and satisfies the sector-like conditions $x_i f_i(x_i) > 0$ for $x_i \neq 0$, $i = 1, \ldots, n$. Such a nonlinearity is said to be admissible.

The system (8) is a well-known Persidskii-type system [12, 14]. Such systems are widely used for the modeling of automatic control systems and neural networks.

From the properties of functions $f_1(x_1), \ldots, f_n(x_n)$ it follows that the system (8) possesses the zero solution.

We assume that the initial functions for (8) belong to the space $C([-\tau, 0], \mathbb{R}^n)$ of continuous functions $\varphi(\theta) : [-\tau, 0] \to \mathbb{R}^n$ with the uniform norm $\|\varphi\|_\tau = \sup_{\theta \in [-\tau, 0]} \|\varphi(\theta)\|$. In addition, let x_t stand for the restriction of a solution $x(t)$ of (8) to the segment $[t-\tau, t]$, i.e., $x_t : \theta \to x(t+\theta),\ \theta \in [-\tau, 0]$.

Definition 4.1 The system (8) is absolutely stable if its zero solution is asymptotically stable for any admissible nonlinearity and any constant nonnegative delay τ.

Theorem 4.1 *Let $n = 2k$, k be a positive integer, and the matrices A and B in* (8) *be of the form* (2) *and* (3)*, respectively. If the inequalities* (4) *and* (5) *are fulfilled, then the system* (8) *is absolutely stable.*

Proof. Under conditions (4) and (5), the pair (A, B) is diagonally Riccati stable. Choose positive definite diagonal matrices $P = \operatorname{diag}\{p_1, \ldots, p_n\}$ and $Q = \operatorname{diag}\{q_1, \ldots, q_n\}$ for which the matrix (1) is negative definite.

Using diagonal elements of P and Q, construct a Lyapunov–Krasovskii functional for (8) in the form

$$V(x_t) = \sum_{i=1}^{n} \left(2p_i \int_0^{x_i(t)} f_i(u)du + q_i \int_{t-\tau}^{t} f_i^2(x_i(\theta))d\theta \right).$$

It is easy to verify that there exists a number $\gamma > 0$ such that

$$\dot{V}\big|_{(8)} \leq -\gamma \left(\|f(x(t))\| + \|f(x(t-\tau))\| \right).$$

Hence (see [11]), the system (8) is absolutely stable. □

4.2 Stability analysis of a mechanical system

Consider a complex system describing the interaction of k mechanical systems with two degrees of freedom. Let equations of motion be of the form

$$\begin{aligned}
&\ddot{x}_1(t) + h\alpha_1\dot{x}_1(t) + \beta_{11}x_1(t) + \beta_{12}x_2(t) = 0,\\
&\ddot{x}_2(t) + h\alpha_2\dot{x}_2(t) + \beta_{21}x_1(t) + \beta_{22}x_2(t) = \omega_1 x_{2k}(t-\tau),\\
&\ddot{x}_{2j-1}(t) + h\alpha_{2j-1}\dot{x}_{2j-1}(t) + \beta_{2j-1\,2j-1}x_{2j-1}(t) + \beta_{2j-1\,2j}x_{2j}(t) = 0,\\
&\ddot{x}_{2j}(t) + h\alpha_{2j}\dot{x}_{2j}(t) + \beta_{2j\,2j-1}x_{2j-1}(t) + \beta_{2j\,2j}x_{2j}(t) = \omega_j x_{2j-2}(t), \;\; j = 2,\dots,k.
\end{aligned} \tag{9}$$

Here $x_i(t) \in \mathbb{R}$, $\alpha_i, \beta_i, \omega_j$ are constant coefficients, $i = 1,\dots,2k$, $j = 1,\dots,k$, h is a positive parameter, τ is a constant nonnegative delay.

Denote $n = 2k$, $x(t) = (x_1(t),\dots,x_n(t))^\top$. Then the equations (9) can be rewritten as follows:

$$\ddot{x}(t) + hD\dot{x}(t) + C_1x(t) + C_2x(t-\tau) = 0. \tag{10}$$

Here $D = \operatorname{diag}\{\alpha_1,\dots,\alpha_n\}$, and C_1, C_2 are constant matrices with the structures similar to those of (2) and (3), respectively.

We assume that the initial functions for (10) belong to the space $C^1([-\tau,0],\mathbb{R}^n)$ of continuously differentiable functions $\varphi(\theta) : [-\tau,0] \to \mathbb{R}^n$ with the uniform norm

$$\|\varphi\|_\tau = \sup_{\theta\in[-\tau,0]} \|\varphi(\theta)\| + \sup_{\theta\in[-\tau,0]} \|\dot{\varphi}(\theta)\|.$$

To derive delay-independent stability conditions for (10), we will use the decomposition method [13, 19, 20] and the approach proposed in [1, 6].

Consider the auxiliary isolated subsystems

$$\dot{y}(t) = Ay(t) + By(t-\tau), \tag{11}$$

$$\dot{z}(t) = -Dz(t), \tag{12}$$

where $y(t), z(t) \in \mathbb{R}^n$, $A = -D^{-1}C_1$, $B = -D^{-1}C_2$.

Assumption 4.1 Let $\alpha_i > 0$, $i = 1,\dots,n$.

Remark 4.1 Under Assumption 4.1, the system (12) is asymptotically stable.

Assumption 4.2 The inequalities (4) and (5) are valid for the entries of the matrices A and B.

Remark 4.2 Under Assumption 4.1, the subsystem (11) possesses a diagonal Lyapunov–Krasovskii functional of the form

$$V(y_t) = y^\top(t)Py(t) + \int_{t-\tau}^{t} y^\top(\theta)Qy(\theta)d\theta,$$

where P and Q are constant positive definite diagonal matrices.

Applying Theorem 1 from [6], we arrive at the following result.

Theorem 4.2 *Let Assumptions 4.1 and 4.2 be fulfilled. Then there exists a number $h_0 > 0$ such that if $h \geq h_0$, then the system* (10) *is asymptotically stable for any nonnegative delay.*

4.3 Synthesis of the decentralized control for a multiagent system

The problems of cooperative control of multiagent systems have attracted considerable attention in the last decade due to their wide applicability [8, 9, 17, 18]. The key goal of cooperative control is to reach a desired global group behavior by using global/local information shared among neighboring agents in a distributed fashion. One of the important cooperative control problems is that of consensus [8, 16].

In the present subsection, we are going to design a decentralized control ensuring consensus for a group of n mobile agents on a line with a special structure of communication topology.

Let $x_i(t) \in \mathbb{R}$ be the position of the i-th agent at time $t \geq 0$, $i = 1, \ldots, n$. We will assume that the following conditions are fulfilled:

(i) $n = 2k$, where k is a positive integer;

(ii) the $(2j-1)$-th agent is a satellite of the $2j$-th agent, and it receives information about the distance $x_{2j-1}(t) - x_{2j}(t)$, $j = 1, \ldots, k$;

(iii) the $2j$-th agent receives information about the distances $x_{2j}(t) - x_{2j-1}(t)$ and $x_{2j}(t) - x_{2j-2}(t)$, $j = 2, \ldots, k$;

(iv) the 2-th agent receives information about the distances $x_2(t) - x_1(t)$ and $x_2(t) - x_n(t-\tau)$, where τ is a constant nonnegative delay;

(iv) the 2-th agent is a leader: it knows the distance between itself and a desired position ξ.

Thus, the communication topology of the system has the structure depicted in Fig. 1.

First, consider the case where the dynamics of agents are described by the first order integrators

$$\dot{x}_i(t) = u_i, \quad i = 1, \ldots, n. \tag{13}$$

Here $u_i \in \mathbb{R}$ denotes the control input (or protocol) of agent i. We will say that the multiagent system achieves a consensus if $x_i(t) \to \xi$ as $t \to +\infty$, $i = 1, \ldots, n$.

Under conditions (i)–(iv), the control law can be chosen as follows:

$$\begin{aligned} &u_{2j-1} = \alpha_{2j-1}(x_{2j} - x_{2j-1}), \quad j = 1, \ldots, k, \\ &u_{2s} = \alpha_{2s}(x_{2s-1}(t) - x_{2s}(t)) + \beta_s(x_{2s-2}(t) - x_{2s}(t)), \quad s = 2, \ldots, k, \\ &u_2 = \alpha_2(x_1(t) - x_2(t)) + \beta_1(x_n(t-\tau) - x_2(t)) + \gamma(\xi - x_2(t)), \end{aligned} \tag{14}$$

where α_i, β_j, γ are constant coefficients, $i = 1, \ldots, n$, $j = 1, \ldots, k$.

Let $x(t) = (x_1(t), \ldots, x_n(t))^\top$. Then the system (13) closed by the control (14) takes the form

$$\dot{x}(t) = Ax(t) + Bx(t-\tau). \tag{15}$$

Here A and B are constant matrices with the structures similar to those of (2) and (3), respectively. The system (15) admits the equilibrium position $x = \bar{x}$, where $\bar{x} = (\xi, \ldots, \xi)^\top$.

Applying Theorem 4.1, we arrive at the following result.

Theorem 4.3 *Let the inequalities*

$$\begin{aligned} &\gamma > 0, \quad \alpha_{2j-1} > 0, \quad j = 1, \ldots, k, \\ &\beta_1 + \gamma + \min\{\alpha_2; 0\} > 0, \quad \beta_j + \min\{\alpha_{2j}; 0\} > 0, \quad j = 2, \ldots, k, \\ &(\beta_1 + \gamma + \min\{\alpha_2; 0\}) \prod_{j=2}^{k} (\beta_j + \min\{\alpha_{2j}; 0\}) > |\beta_1| \beta_2 \ldots \beta_k \end{aligned} \tag{16}$$

be valid. Then the equilibrium position $x = \bar{x}$ *of* (15) *is asymptotically stable for any nonnegative delay* τ*.*

Next, assume that the dynamics of agents are described by the double integrators

$$\ddot{x}_i(t) + h\dot{x}_i(t) = u_i, \quad i = 1, \dots, n. \tag{17}$$

Here $u_i \in \mathbb{R}$ is the control input of agent i, and h is a constant positive damping coefficient. We will say that the multiagent system achieves a consensus if $x_i(t) \to \xi$, $\dot{x}_i(t) \to 0$ as $t \to +\infty$, $i = 1, \dots, n$.

Choose a control law for (17) in the form (14). Then the corresponding closed-loop system can be rewritten as follows:

$$\ddot{x}(t) + h\dot{x}(t) = Ax(t) + Bx(t - \tau), \tag{18}$$

where A and B are constant matrices with the structures similar to those of (2) and (3), respectively.

With the aid of Theorem 4.2, it can be shown that the following theorem is valid.

Theorem 4.4 *Let the inequalities* (16) *hold. Then there exists a number* $h_0 > 0$ *such that if* $h \geq h_0$*, then the equilibrium position* $x = \bar{x}$*,* $\dot{x} = 0$ *of* (18) *is asymptotically stable for any nonnegative delay* τ*.*

5 Results of Numerical Simulation

To illustrate the effectiveness of the proposed approaches, consider a group consisting of six agents. Let the control law be of the form (14).

For the simulation, we choose $\alpha_1 = 1$, $\alpha_2 = -0.25$, $\alpha_3 = 1$, $\alpha_4 = -0.25$, $\alpha_5 = 1$, $\alpha_6 = -0.1$, $\beta_1 = -0.5$, $\beta_2 = 0.5$; $\beta_3 = 1$, $\gamma = 2$, $\tau = 10$, $\xi = 0.5$. In addition, it is assumed that $x(t) \equiv (0.1, 0.4667, 0.7, 0.2, 0.5, 0.2)^\top$ for $t \in [-10, 0]$.

Figure 2 corresponds to the case where the agent dynamics are described by the first order integrators. We can see the convergence of agents to the desired equilibrium position.

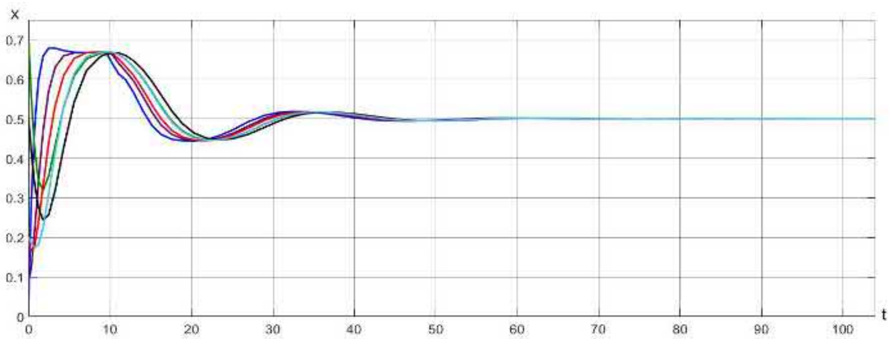

Figure 2: The agent time history (first order integrators).

Next, consider the double integrators (17). Figures 3 and 4 demonstrate that if $h = 0.2$, then the equilibrium position is unstable, whereas if $h = 2$, then the agents achieve the consensus.

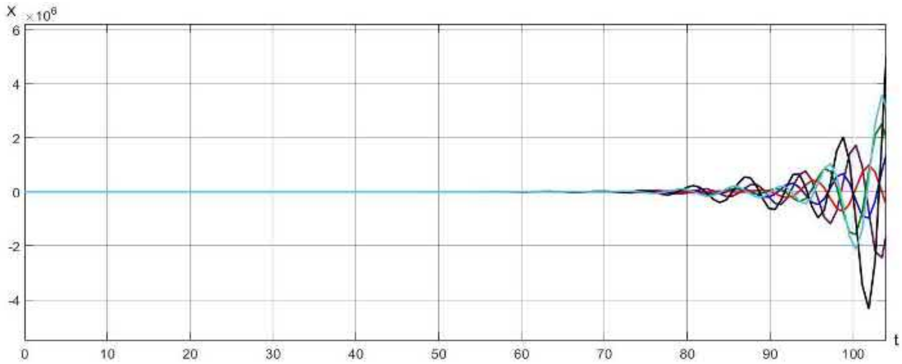

Figure 3: The agent time history (double integrators, $h = 0.2$).

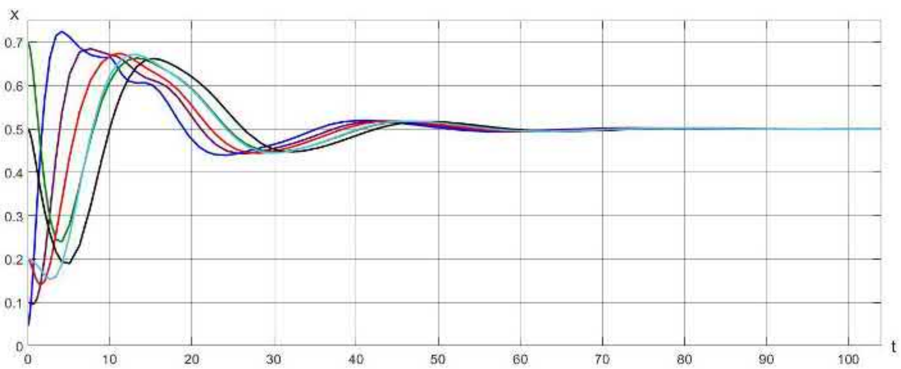

Figure 4: The agent time history (double integrators, $h = 2$).

6 Conclusion

In the present paper, simple necessary and sufficient conditions of the diagonal Riccati stability are derived for a class of pairs of matrices with special structures. These conditions are formulated in terms of algebraic inequalities for the entries of the matrices under consideration. We have shown that the obtained result can be used for the analysis of absolute stability of the Persidskii-type systems, the determination of delay-independent stability conditions for a mechanical system with a special structure of connections and the construction of decentralized controls providing the achievement of a consensus for some types of multiagent systems.

An application of the developed approaches to wider classes of matrices and time-delay systems is our future work.

Acknowledgment

The reported study was partially financially supported by the Russian Foundation for Basic Research (Grant Nos. 17-01-00672-a and 19-01-00146-a).

References

[1] A. Yu. Aleksandrov, E. B. Aleksandrova and A. P. Zhabko. Asymptotic stability conditions for certain classes of mechanical systems with time delay. *WSEAS Transactions on Systems and Control* **9** (2014) 388–397.

[2] A. Aleksandrov and N. Kovaleva. Diagonal Riccati stability of a class of time-delay systems. *Cybernetics and Physics* **7** (4) (2018) 167–173.

[3] A. Aleksandrov and O. Mason. Diagonal Lyapunov–Krasovskii functionals for discrete-time positive systems with delay. *Syst. Control Lett.* **63** (2014) 63–67.

[4] A. Aleksandrov and O. Mason. Diagonal Riccati stability and applications. *Linear Algebra & Appl.* **492** (2016) 38–51.

[5] A. Aleksandrov, O. Mason and A. Vorob'eva. Diagonal Riccati stability and the Hadamard product. *Linear Algebra & Appl.* **534** (2017) 158–173.

[6] A. Yu. Aleksandrov, A. P. Zhabko and Y. Chen. Stability analysis of gyroscopic systems with delay via decomposition. *AIP Conference Proceedings* **1959** (080002) (2018) 1–6.

[7] G. P. Barker, A. Berman, R. J. Plemmons. Positive diagonal solutions to the Lyapunov equations. *Linear Multilinear Algebra* **5** (4) (1978) 249–256.

[8] F. Bullo, J. Cortes and S. Martinez. *Distributed Control of Robotics Networks.* Princeton Univ. Press, Princeton, 2009.

[9] A. Feydi, S. Elloumi and N. Benhadj Braiek. Decentralized stabilization for a class of nonlinear interconnected systems using SDRE optimal control approach. *Nonlinear Dynamics and Systems Theory* **19** (1) (2019) 55–67.

[10] F. R. Gantmacher. *Matrix Theory.* Chelsea, New York, 1977.

[11] J. K. Hale and S. M. Verduyn Lunel, *Introduction to Functional Differential Equations.* Springer-Verlag, New York, 1993.

[12] E. Kazkurewicz and A. Bhaya. *Matrix Diagonal Stability in Systems and Computation.* Birkhauser, Boston, 1999.

[13] V. Lakshmikantham, S. Leela and A. A. Martynyuk. *Stability Analysis of Nonlinear Systems.* Marcel Dekker, New York, 1989.

[14] T. A. Lukyanova and A. A. Martynyuk. Stability analysis of impulsive Hopfield-type neuron system on time scale. *Nonlinear Dynamics and Systems Theory* **17** (3) (2017) 315–326.

[15] O. Mason. Diagonal Riccati stability and positive time-delay systems. *Syst. Control Lett.* **61** (2012) 6–10.

[16] R. Olfati-Saber and R. M. Murray. Consensus problems in networks of agents with switching topology and time delays. *IEEE Trans. Autom. Control* **49** (9) (2004) 1520–1533.

[17] W. Ren and W. Cao. *Distributed Coordination of Multi-Agent Networks.* Springer-Verlag, London, 2011.

[18] S. Rezzag. Boundedness results for a new hyperchaotic system and their application in chaos synchronization. *Nonlinear Dynamics and Systems Theory* **18** (4) (2018) 409–417.

[19] V. N. Tkhai and I. N. Barabanov. Extending the property of a system to admit a family of oscillations to coupled systems. *Nonlinear Dynamics and Systems Theory* **17** (1) (2017) 95–106.

[20] V. I. Zubov. *Analytical Dynamics of Gyroscopic Systems.* Sudostroenie, Leningrad, 1970. [Russian]

Nonlinear Dynamics and Systems Theory, **19** (4) (2019) 455–463

Kalman Filter Estimation of Identified Reduced Model Using Balanced Truncation: a Case Study of the Bengawan Solo River

D. K. Arif *, D. Adzkiya and H. N. Fadhilah

Department of Mathematics, Sepuluh Nopember Institute Of Technology, Sukolilo ITS Campus-Surabaya 60111, Indonesia

Received: May 16, 2019; Revised: September 23, 2019

Abstract: In this paper, we compare the estimation results for the reduced model and original model of water level in a river. First, we compute a reduced model from the original model using the balanced truncation method, then we estimate the reduced model using the Kalman filter. Since the orders of the state variables in the reduced model and original model are different, we cannot compare them directly. Therefore, we need an identification of the state variables in the reduced model such that we can determine the corresponding state variables in the original model or the real data. The selected river flow model is the Bengawan Solo river in Indonesia. The Bengawan Solo river is the longest river in Indonesia and often causes floods in the area around the river. With the river length of 548 km, it is difficult to obtain complete data at each point, and this will lead to a large order river flow model. Since the Bengawan Solo river flow model is a large order model, we need to reduce the model using the balanced truncation method. Next, to obtain data on the water levels at each unknown point, we estimate the reduced model using the Kalman filter method. Based on the simulation results, we see that if more points are removed, the error value is larger. However, if fewer points are known, the computational time is less.

Keywords: *estimation; Kalman filter; model reduction; balanced truncation; Bengawan Solo river.*

Mathematics Subject Classification (2010): 93E10.

* Corresponding author: mailto:didik@matematika.its.ac.id

1 Introduction

Indonesia is a maritime country with 2/3 of the area covered with water in the form of sea, lake, and river. River is one form of water that is useful for the life of Indonesian citizens. Furthermore, the river can also be disastrous if the volume of water in the river exceeds its capacity. Flood is a disaster in such event. One of the rivers in Indonesia that often causes floods is the Bengawan Solo river [1]. With the river length of 548 km, the Bengawan Solo river flows through 12 districts and is divided into 20 regions, i.e. upstream and downstream in Central Java and in East Java. The impact of flooding caused by the Bengawan Solo river is very large because it has a very long flow area. Therefore, the Bengawan Solo river water level is a system with a large order.

Thus, it is difficult to obtain complete data at each point. So, in anticipation of flooding due to the inability of the river to accommodate the increase in water volume, we estimate the river water level by taking into account the flow velocity using an estimator.

One of the well-known methods in estimation is the Kalman filter [2,3]. The Kalman filter was first introduced by Rudolph E. Kalman in 1960. There are some factors that cannot be modeled. Thus we added stochastic factors, such as the system noise and measurement noise. It follows that the system becomes a stochastic dynamical system. The Kalman filter consists of two processes: the time update and measurement update [4]. The time update is responsible for projecting forward in time the current state and error covariance estimates to obtain the a-priori estimates for the next time step. The measurement updates are responsible for the feedback for incorporating a new measurement into the a-priori estimate to obtain an improved a-posteriori estimate. After each time and measurement update, the process is repeated with the previous a-posteriori estimates used to project or predict the new a-priori estimates. This recursive nature is one of the very appealing features of the Kalman filter.

In the process of estimating the altitude of water level of the Bengawan Solo river, we use a shallow water equation, i.e. the Saint Venant equation. In this paper, the Saint Venant equation represents the original model which is widely used for the wave models in the atmosphere, rivers, lakes and oceans [5]. This equation is used to model the flow in open channels, such as the river flow. Since the Bengawan Solo river has many points of location denoted by states, the original model is a larger order model. Hence, in this paper, we also reduce the original model before we estimate the water level of the Bengawan Solo river using the Kalman filter.

Model reduction is used to simplify the size of realization in a model. This will reduce the computational time, and hopefully, the error is as small as possible [6]. Currently, there are many developed methods of model reduction such as the balanced truncation methods [7–9] and singular perturbation approximation [2, 10]. In [6], a Kalman filter algorithm has been developed in the reduced model and applied to the heat conduction distribution problem. The authors in [11] combine the Kalman filter estimation and model reduction without identification by using the balanced truncation method.

Since the orders of the state variables in the reduced and original models are different, we cannot compare them. Therefore, we need an identification of the state variables in the reduced model such that we can determine the corresponding state variables in the original model. In this paper, we want to determine a relationship between the state variables in the reduced and original model. We can compute the corresponding state variables in the original model using the reduced model [12]. The simulation results show that the Kalman filter estimation of the identified reduced model using balanced truncation can be carried out for several measurement points of the river water level.

2 The Bengawan Solo River

Bengawan Solo is the longest river on the island of Java, Indonesia. The river is around 548.53 km long and flows through two provinces, Central Java and East Java [1]. Data on the Bengawan Solo river can be seen in Figure 1 [1].

No	POS TMA	LEVEL SIAGA (TTG)			←	12 Aug 18					→
					WAKTU (WIB)						
					TELEMETRI				MANUAL		
Wilayah Hulu		SH	SK	SM	06.00	12.00	18.00	00.00	06.00	12.00	18.00
1	Ngadipiro (Kab. Wonogiri)	151.00	152.00	153.00					146.52	146.51	146.50
2	Ngrembang (Kab. Wonogiri)	147.00	148.00	149.00		139.42	139.42		142.80	142.80	142.80
3	Colo Weir (Kab. Sukoharjo)	108.60	109.00	109.40	107.21	107.21	107.21		107.20	107.20	107.20
4	Jarum (Kab. Klaten)	94.00	95.00	95.50	89.80	89.87	89.82		89.94	89.94	89.94
5	Serenan (Kab. Sukoharjo)	92.00	93.00	94.00					86.24	86.23	86.22
6	Peren (Kab. Sukoharjo)	89.41	90.41	91.41					87.37	87.36	87.36
7	Jurug (Kota Surakarta)	82.73	83.73	84.73							
8	Kedungupit (Kab. Sragen)	74.00	75.00	76.00	69.11	69.11	69.11		69.11	69.11	
9	Wonogiri Dam (Kab. Wonogiri)	135.30	136.00	137.20	131.71	131.71	131.71		131.73	131.72	131.70
Wilayah Madiun		SH	SK	SM	06.00	12.00	18.00	00.00	06.00	12.00	18.00
10	Sekayu (Kab. Ponorogo)	97.50	98.00	98.50					0.00	0.00	0.00
11	AhmadYani (Kab. Madiun)	67.16	67.91	68.66					63.08	63.08	63.08
12	Napel (Kb. Ngawi)	43.50	44.50	45.50	38.36	38.35	38.36		38.28	38.27	38.27
13	Ketonggo Bridge (Kab. Ngawi)	47.00	48.00	49.00	37.45	37.88	37.59				
14	Jati Weir (Kab. Magetan)	96.45	97.05	97.65					74.00		74.00
15	Arjowinangun - Pacitan (Kab. Pacitan)	20.19	20.69	21.19					10.25	10.30	10.20
Wilayah Hilir		SH	SK	SM	06.00	12.00	18.00	00.00	06.00	12.00	18.00
16	Cepu (Kab. Bojonegoro)	34.87	35.87	36.87					-3.63	28.05	28.04
17	Bengkelo_lor	20.73	21.48	22.23							
18	Bojonegoro - Kali Kethek (Kab. Bojonegoro)	20.04	21.04	22.04							
19	Boboh Kali Lamong (Kab. Gresik)	14.48	14.73	14.98							
20	Karanggeneng (Kab. Lamongan)	6.50	7.50	8.50							

Figure 1: Data on the water level of the Bengawan Solo river.

Because of the length of the river, the recording of the river water level data is not easy. The river water level data are often not recorded properly as in Figure 1. So, it is necessary to estimate the river water level in order to anticipate floods. Since the BBWS data are not available at all for the water level data in the Karanggeneng area, we will estimate the water level at 19 points or locations. In this paper, we use the data on water level of the Bengawan Solo river for the period of June, 2018 – August, 2018 [1].

3 Model Representation

We discuss the shallow water equation that describes the flow of water in rivers [13]:

$$
\begin{aligned}
\frac{\partial h}{\partial t} + D\frac{\partial v}{\partial x} &= 0, \\
\frac{\partial v}{\partial t} + g\frac{\partial h}{\partial x} + C_f u &= 0,
\end{aligned} \tag{1}
$$

where the initial conditions are taken from the measurement data of water level in the Bengawan Solo river at $t = 1$ [1] and the boundary conditions are [2]

$$h(0,t) = h(x-1,t), \qquad h(L,t) = h(2,t), \tag{2}$$

where $h(x,t)$ is the water level above the reference plane at the position (or city) x and time t, t is the time variable, x is the position (or city) along the river, D is the water depth, g is the gravitational acceleration and C_f is a friction constant.

4 Discretization

The shallow water equation in (1) will be discretized using the Lax-Wendroff scheme. We can obtain a discrete-time system that is suitable for the Kalman filter and model reduction. The result of discretization in (1) is as follows [2]:

$$\begin{aligned} h_i^{k+1} &= \frac{1}{2}(h_{i+1}^k + h_{i-1}^k) - \frac{D\Delta t}{2\Delta x}(u_{i+1}^k - u_{i-1}^k), \\ u_i^{k+1} &= \frac{(1 - C_f\Delta t)}{2}(u_{i+1}^k + u_{i-1}^k) - \frac{g\Delta t}{2\Delta x}(h_{i+1}^k - h_{i-1}^k), \end{aligned} \tag{3}$$

where h represents the water level and u represents the water velocity. The Lax-Wendroff scheme is a combination of the Lax-Friedrichs scheme and Leapfrog scheme [2]. The Leapfrog scheme works by replacing Δt with $2\Delta t$ such that $g\Delta t$ or $D\Delta t$ has smaller value than Δx in order to achieve the desired accuracy. The result of discretization of h_i^{k+1} and u_i^{k+1} is as follow:

$$\begin{aligned} h_i^{k+1} &= h_i^k - a(u_{i+1}^k - u_{i-1}^k) + c(h_{i+1}^k - 2h_i^k + h_{i-1}^k), \\ u_i^{k+1} &= du_i^k - b(h_{i+1}^k - h_{i-1}^k) + c(u_{i+1}^k - 2u_i^k + u_{i-1}^k), \end{aligned} \tag{4}$$

where

$$a = \frac{D\Delta t}{\Delta x}(1 - C_f\Delta t),\ b = \frac{g\Delta t}{\Delta x},\ c = \frac{Dg\Delta t^2}{2\Delta x^2},\ d = (1 - 2C_f\Delta t).$$

Thus, we can write (4) in matrix realization as follows:

$$\begin{cases} x_{k+1} &= Ax_k + Bu_k, \\ y_k &= Cx_k + Du_k, \end{cases} \tag{5}$$

where

$$x_{k+1} = \begin{bmatrix} h_1^{k+1} \\ u_1^{k+1} \\ h_2^{k+1} \\ u_2^{k+1} \\ h_3^{k+1} \\ u_3^{k+1} \\ h_4^{k+1} \\ u_4^{k+1} \\ \vdots \\ h_{N-1}^{k+1} \\ u_{N-1}^{k+1} \end{bmatrix}, \qquad x_k = \begin{bmatrix} h_1^k \\ u_1^k \\ h_2^k \\ u_2^k \\ h_3^k \\ u_3^k \\ h_4^k \\ u_4^k \\ \vdots \\ h_{N-1}^k \\ u_{N-1}^k \end{bmatrix}, \qquad u_k = \begin{bmatrix} h_0^k \\ u_0^k \\ h_N^k \\ u_N^k \end{bmatrix}.$$

For the measurement matrix C, we use the number of the Bengawan Solo river elevation points which do not have the real data, and for the matrix D, it is assumed that 0 is the adjusted size.

5 Estimation and Identification of Model Reduction

The Kalman filter is one of the data assimilation methods, i.e. estimation of state variables based on the noisy model and measurement systems [14]. The Kalman filter is divided into two processes: the time update and measurement update [4]. The time updates are responsible for projecting forward in time the current state and error covariance estimates to obtain the a-priori estimates for the next time step. The measurement updates are responsible for the feedback for incorporating a new measurement into the a-priori estimate to obtain an improved a-posteriori estimate. The estimation of large-order model needs a long computational time, so in this case we use the model reduction to simplify the model without any significant error.

Model reduction is used to simplify the large order system without any significant error. The behavior of the reduced system is almost the same as that of the original system [10]. There are many methods of model reduction and one of them is the balanced truncation method. Before we apply the balanced truncation method [7–9], the realization of the system has to be balanced, i.e. the controllability Gramian is the same as the observability Gramian [10]. In order to do so, we apply a transformation matrix T to the original system (A, B, C, D)

$$\tilde{A} = T^{-1}AT, \qquad \tilde{B} = T^{-1}B, \qquad \tilde{C} = CT, \qquad \tilde{D} = D.$$

The balanced system $(\tilde{A}, \tilde{B}, \tilde{C}, \tilde{D})$ can be written as

$$\begin{cases} \tilde{x}_{k+1} &= \tilde{A}\tilde{x}_k + \tilde{B}\tilde{u}_k, \\ \tilde{y}_k &= \tilde{C}\tilde{x}_k + \tilde{D}\tilde{u}_k. \end{cases} \tag{6}$$

After we obtain the balanced system in (6), we partition the Gramian Σ such that $\Sigma = diag(\Sigma_1, \Sigma_2)$, where $\Sigma_1 = diag(\sigma_1, \sigma_2, ..., \sigma_r)$ and $\Sigma_2 = diag(\sigma_{r+1}, \sigma_{r+2}, ..., \sigma_n)$. Then the balanced system is partitioned into

$$\begin{bmatrix} \tilde{x}_1(k+1) \\ \tilde{x}_2(k+1) \end{bmatrix} = \begin{bmatrix} \tilde{A}_{11} & \tilde{A}_{12} \\ \tilde{A}_{21} & \tilde{A}_{22} \end{bmatrix} \begin{bmatrix} \tilde{x}_1(k) \\ \tilde{x}_2(k) \end{bmatrix} + \begin{bmatrix} \tilde{B}_1 \\ \tilde{B}_2 \end{bmatrix} u(k), \tag{7}$$

$$\tilde{y}(k) = \begin{bmatrix} \tilde{C}_1 & \tilde{C}_2 \end{bmatrix} \begin{bmatrix} \tilde{x}_1(k) \\ \tilde{x}_2(k) \end{bmatrix} + \tilde{D}u(k), \tag{8}$$

where, $\tilde{x}_1(k) \in \mathbb{R}^r$ corresponds to Σ_1 and $\tilde{x}_2(k) \in \mathbb{R}^{n-r}$ corresponds to Σ_2.

Model reduction by using the balanced truncation method is done by assuming $\tilde{x}_2(k+1) = 0$. The reduced system can be written as [9]

$$\begin{cases} \tilde{x}_{rk+1} &= \tilde{A}_r\tilde{x}_{rk} + \tilde{B}_r\tilde{u}_k, \\ \tilde{y}_{rk} &= \tilde{C}_r\tilde{x}_{rk} + \tilde{D}_r\tilde{u}_k. \end{cases} \tag{9}$$

Because there are differences in the size of the original system matrix and the reduced system, the results cannot be compared directly. In order to produce a reduced system that corresponds to the original system, it is necessary to identify the relationship between the states of the two systems. The identification can be obtained from the transformation matrix T [12]

$$x_k = T\tilde{x}_k. \tag{10}$$

Equation (10) can be written as

$$x_{id} = T_r\tilde{x}_{rk}, \tag{11}$$

where x_{id} is the state of the identified reduced model with size $n \times 1$, T_r is obtained by reducing the first part of the inverse transformation matrix T of size $n \times r$, and x_{rk} is the reduced model of size $r \times 1$.

6 Simulation Results

The shallow water equation (1) describes the relationship between the water level h and water debit u. In this paper, we focus on the estimation of water level in the Bengawan Solo river. Due to the unavailability of water debit data, the initial value of u is defined as 0. We use the following values for the parameters in shallow water equations:

$$D = 150m, \quad C_f = 0.0002, \quad \Delta x = 548km, \quad \Delta t = 100, \quad g = 9.8m/s^2.$$

With the parameters above, we estimate the water level h using the Kalman filter by using the real data for the period of June, 2018 - August, 2018 [1]. First, we reduce the number of state variables in the model. Each state represents the water level point. Thus, we will reduce the number of the water level points. The original model has 19 states, it means that the number of the water level points is 19. In the second simulation, the states in the original model will be reduced to 4-18 states (or points). The simulation results of the Kalman filter estimation of the identified reduced model using balanced truncation for 10 and 15 water level points are shown in Figure 2-3.

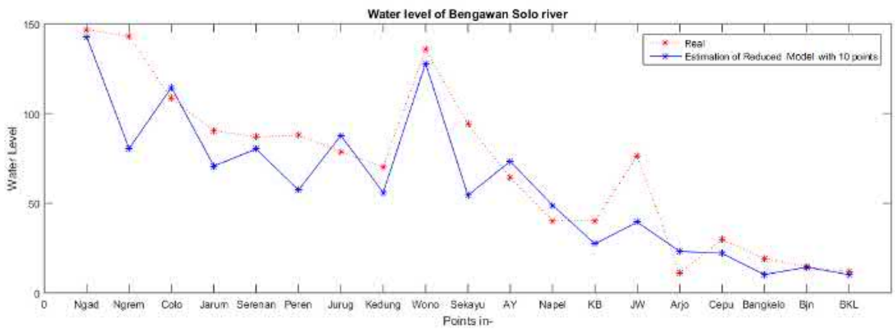

Figure 2: Estimation of the reduced system with 10 water level points.

From Figures 2-3, we can see that the simulation results of the Kalman filter estimation of the identified reduced model using balanced truncation are quite accurate or almost the same as those for the original model for several points. For more detailed values, we describe the relative error value and computational time for each known point in Table 1.

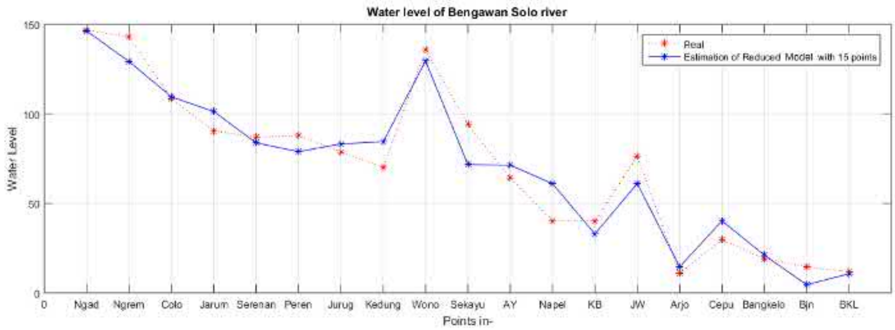

Figure 3: Estimation of the reduced system with 15 water level points.

Known points	Relative Error		Computational time	
	Original model	Reduced model	Original model	Reduced model
2	1.11E-04	1.1660	0.125465	0.024951
3	1.77E-04	1.1269	0.130171	0.025277
4	1.14E-04	1.0989	0.129215	0.032373
5	8.63E-05	1.0398	0.212791	0.032134
6	7.02E-05	1.0348	0.134526	0.032752
7	1.32E-04	1.0298	0.134507	0.035429
8	1.73E-04	0.6755	0.133507	0.025639
9	1.51E-04	0.4274	0.133474	0.047240
10	1.31E-04	0.4239	0.133721	0.029778
11	9.37E-05	0.4139	0.131884	0.033390
12	1.23E-04	0.3837	0.135993	0.031910
13	9.26E-05	0.3357	0.128158	0.035152
14	1.33E-04	0.3018	0.134753	0.035960
15	1.49E-04	0.2321	0.127770	0.042461
16	1.09E-04	0.1819	0.129831	0.041342
17	8.10E-05	0.1526	0.132840	0.048576
18	8.62E-05	0.0085	0.137477	0.059243

Table 1: Comparison between the error and computational time for estimation of the original and reduced models.

Based on Table 1, we conclude that the Kalman filter estimation of the original model is better than the Kalman filter estimation of the identified reduced model using balanced truncation. This result is reasonable, because the reduced model cannot achieve better performance than the best estimation of the original model. In terms of the computational time, the Kalman filter estimation of the identified reduced model using balanced truncation is faster than that of the original one. This result is also reasonable, because the order of the reduced model is smaller than that of the original model.

Based on Table 1, we can see that the error of 18 (from 19) water level points is 0.0085 and the computational time is 0.059243 seconds. On the other hand, the error of 2 (from 19) water level points is 1.1660 and the computational time is 0.024951 seconds. If the order of the reduced model is smaller, the error value is larger and inversely proportional to the computational time. We can see in Table 1 that the computational time for the Kalman filter estimation of the identified reduced model using balanced truncation is less than that for the Kalman filter estimation of the original model.

7 Conclusions

In this work, we estimate the water level in the reduced model using balanced truncation. Since the orders of the state variables in the reduced and original models are different, we cannot compare them directly. Therefore, we need an identification of the state variables in the reduced model such that we can determine the corresponding state variables in the original model. The simulation result shows that the Kalman filter estimation of the identified reduced model using balanced truncation has an error larger than that of the original model, but the average computational time to estimate the reduced system is 26% less compared to the estimation of the original model. Thus, for the model reduction, we can choose the number of water level points based on our needs.

References

[1] Situs Resmi BBWS Bengawan Solo. http://bbwsbengawansolo.net. Indonesia, 2018.

[2] V. Rachmawati, D. K. Arif and D. Adzkiya. Implementation of Kalman filter algorithm on models reduced using singular pertubation approximation method and its application to measurement of water level. *Journal of Physics: Conference Series* **974** (1) (2018) 012018.

[3] P. Aditya, E. Apriliani, D. K. Arif and K. Baihaqi. Estimation of Three-Dimensional Radar Tracking Using Modified Extended Kalman Filter. *Journal of Physics: Conference Series* **974** (1) (2018) 012018.

[4] G. Welch and G. Bishop. *An Introduction to the Kalman Filter*. University of North Carolina, Chapel Hill, 2001.

[5] M. Ersoy. *Shallow Water Equation: Modelling, Numerics and Applications*. University of Sussex, UK, 2013.

[6] D. K. Arif, Widodo, Salmah and E. Apriliani. Construction of the Kalman Filter Algorithm on the Model Reduction. *International Journal of Control and Automation* **7** (9) (2014) 257–270.

[7] Y. I. Sari, D. K. Arif, E. Apriliani and D. Adzkiya. A study on model order reduction of stable discrete-time linear-time-invariant systems using balanced truncation methods. *Journal of Physics: Conference Series* **1867** (1) (2017) 020049.

[8] D. A. Kartika, D. K. Arif, E. Apriliani and D. Adzkiya. A study on model order reduction of stable continuous-time linear-time-invariant systems using balanced truncation methods. *Journal of Physics: Conference Series* **1867** (1) (2017) 020050.

[9] D. K. Arif, D. Adzkiya, E. Apriliani and I. N. Khasanah. Model Reduction of Non-minimal Discrete-Time Linear-Time-Invariant Systems. *Malaysian Journal of Mathematical Science* **11** (3) (2017) 377–391.

[10] D. K. Arif, H. N. Fadhilah, D. Adzkiya, L. N. Rochmah, N. A. W. Yoga, H. Setiawan, R. Kamilah and R. R. N. Cahyani. Accelerating simulation time of unstable discrete-time systems using Singular Perturbation Approximation. In: *Proc. International Conf. on Instrumentation, Control, and Automation*. Yogyakarta, Indonesia, 2017, 7–12.

[11] K. Mustaqim, D. K. Arif, E. Apriliani and D. Adzkiya. Model reduction of unstable systems using balanced truncation method and its application to shallow water equations. *Journal of Physics: Conference Series* **855** (1) (2017) 012029.

[12] T. P. Lesnussa, D. K. Arif, D. Adzkiya and E. Apriliani. Identification and estimation of state variables on reduced model using balanced truncation method. *Journal of Physics: Conference Series* **855** (1) (2017) 012023.

[13] M. Verlaan. Efficient Kalman Filtering Algorithms for Hydrodynamic Models. PhD Thesis. Delft University of Technology, The Netherlands, 1998.

[14] J. Humpherys, P. Redd and J. West. A Fresh Look at the Kalman Filter. *SIAM Review* **54** (4) (2012) 801–823.

Nonlinear Dynamics and Systems Theory, **19** (4) (2019) 464–473

Uniform Asymptotic Stability in Probability of Nontrivial Solution of Nonlinear Stochastic Systems

A. Barbata [1*], M. Zasadzinski [2*], R. Chatbouri [3] and H. Souley Ali [2]

[1] *UR Analysis and Control of PDEs, University of Monastir, Tunisia;*
[2] *Research Center for Automatic Control (CRAN, UMR 7039, CNRS), University of Lorraine, 186 rue de Lorraine, 54400 Cosnes et Romain, France;*
[3] *Laboratory of Mathematics, Physics and Special Functions, University of Sousse, Tunisia*

Received: July 1, 2019; Revised: September 16, 2019

Abstract: The aim of this paper is to study the uniform asymptotic stability in probability when a nonlinear stochastic differential equation does not have a trivial solution. For nontrivial solutions of a nonlinear stochastic differential equation, the problem of uniform asymptotic stability in probability is reformulated for a ball of radius $R > 0$. Based on this new formulation, a theorem for the uniform asymptotic stability in probability for this ball is proposed by using a Lyapunov approach.

Keywords: *stochastic systems; Itô formula; Brownian motions; stability in probability; asymptotic stability in probability.*

Mathematics Subject Classification (2010): 93E03, 93E15.

1 Introduction

In this paper, we discuss a new concept of uniform asymptotic stability in probability for stochastic systems which are described by stochastic differential equations (SDEs) driven by multiplicative noises. These systems differ from ordinary differential equations (ODEs) modeling deterministic processes. Unlike an ODE, a SDE contains two terms: the drift for the evolution of time and the diffusion for the action of the Brownian motion. These systems correspond to Itô processes, and the noises that affect them are Brownian motions, also called the Wiener processes. This kind of equations is extensively studied in [8, 16, 17] and references therein.

Numerous phenomena are described by this class of models when a deterministic description is not satisfactory: in finance (financial mathematics and stock prices), biology

* Corresponding author: mailto:barbata_asma@yahoo.fr

(geographical and population evolution), geology (earthquakes), engineering (synthesis of control taking into account the failures that may appear randomly), computing (modeling networks), electricity (modeling of electrical circuits taking account of noise of electrical circuits), physical and mechanical processes (particle movements in a gas or ionized medium, quantum physics), etc.

The notion of stability of the solutions of SDE was introduced by Kats and Krasovskii [9]. Then, in the works of Kushner [11, 12], Has'minski [8], Kozin [10], Wonham [19], Zakai [22, 23], Gikhman and Skorokhod [5] and Friedman [4], several types of stability have been defined for the SDE and a Lyapunov-type approach to study these stabilities has been developed and elaborated.

In the literature, the asymptotic stability in probability has been extensively studied in many works. Without exhaustivity, we can cite the textbooks [8, 16], the survey papers [10, 13] and the papers [6, 7, 14, 18, 20, 21, 24], with references therein. It is the asymptotic stability in probability of the equilibrium point $x = 0$ which is treated in the works mentioned above and the case where the stochastic differential equation has a nontrivial solution $x \neq 0$ is not considered.

In [2], the authors consider that the equilibrium point of the stochastic differential equation is not the origin and that the differential stochastic equation is perturbed by an external disturbance. There is a study of the stability of nontrivial solution in [1, 3, 15].

To deal with the existence of nontrivial solutions $x \neq 0$ of a stochastic differential equation, we propose to study the uniform asymptotic stability in probability for a ball with a given radius $R > 0$ and the classical concepts of uniform stability in probability and uniform asymptotic stability in probability are reformulated for this ball. Sufficient conditions are derived by using a Lyapunov approach in order to guarantee that a solution initialized outside of the ball converges asymptotically in probability to the border of the ball.

The paper is organized as follows. The concepts of uniform stability in probability and uniform asymptotic stability in probability for a ball of radius $R > 0$ are given in Section 2. A new theorem guaranteeing the uniform asymptotic stability in probability for this ball is proposed in Section 3. This theorem is illustrated by an example in Section 4.

Notations. $\mathbb{R}^n$ denotes the n-dimensional Euclidean space.

$$\|A\| = \sqrt{\sum_{i,j} A_{i,j}^2} = \sqrt{\mathrm{tr}(A^T A)}$$

is the Euclidean norm of the matrix A, while $\|x\| = \sqrt{x^T x}$ is the Euclidean norm of the vector x. $a \vee b$ is the maximum of reals a and b. $a \wedge b$ is the minimum of reals a and b. The SDE means a stochastic differential equation. The probability measure associated with the random variable x is denoted $\mathbf{P}\{x\}$. $\mathbf{E}\{x\}$ stands for the mathematical expectation operator with respect to the given probability measure $\mathbf{P}\{x\}$. Let $\mathbf{K}$ denote the family of all continuous and nondecreasing functions $\mu : \mathbb{R}_+ \to \mathbb{R}_+$ such that $\mu(0) = 0$ and $\mu(r) > 0$ if $r > 0$.

2 Concepts of Stability in Probability

Consider the following nonlinear stochastic differential equation (SDE):

$$\mathrm{d}\, x = f(x)\, \mathrm{d}\, t + g(x)\, \mathrm{d}\, w, \tag{1}$$

where $x \in \mathbb{R}^n$ is the state vector, $w \in \mathbb{R}^d$ is a multi-dimensional independent Wiener processes (or Brownian motions). The initial condition is given by $x_0 = x(t_0)$. We assume that $f(0) \neq 0$ or $g(0) \neq 0$, i.e. the stochastic differential equation (1) does not have the trivial solution $x = 0$.

The functions $f(x)$ and $g(x)$ verify the following standard assumptions for Itô calculus [8, 16, 17] :

$$\int_0^T \|f(x(s))\| \,\mathrm{d}\, s < \infty \qquad \text{a.s.} \qquad \forall T > 0, \tag{2a}$$

$$\int_0^T \|g(x(s))\|^2 \,\mathrm{d}\, s < \infty \qquad \text{a.s.} \qquad \forall T > 0. \tag{2b}$$

To guarantee the existence and the uniqueness of the solution $x(t)$ of the SDE (1), the functions $f(x)$ and $g(x)$ satisfy the following relations $\forall x \in \mathbb{R}^n$ and $\forall \overline{x} \in \mathbb{R}^n$ ([8, 16, 17]):

$$\|f(x)\|^2 + \|g(x)\|^2 \leqslant k_1(1 + \|x\|^2), \tag{3a}$$

$$\|f(x) - f(\overline{x})\| \vee \|g(x) - g(\overline{x})\| \leqslant k_2 \|x - \overline{x}\|, \tag{3b}$$

where k_1 and k_2 are given strictly positive reals.

In this paper, we study the uniform stability in probability of the solution of a SDE when the origin is not an equilibrium point. The considered stability is characterized by the convergence of the solution in probability to a border of a ball B_R defined as follows.

Definition 2.1 Let $R > 0$ be a real. The ball B_R is defined by

$$B_R = \{x \in \mathbb{R}^n : \|x\| \leqslant R\}. \tag{4}$$

Definition 2.2 The ball B_R is said to be uniformly stable in probability for the SDE (1) if, for any $0 < \varepsilon < 1$ and for any $r > 0$, there exists $\delta(\varepsilon, r, t_0) > 0$ such that

$$\mathbf{P}\{x(t) \in \mathbb{R}^n : R < \|x(t)\| \leqslant R + r \text{ for all } t \geqslant t_0\} \geqslant 1 - \varepsilon, \\ \forall x_0 \in \mathbb{R}^n \text{ and } R < \|x_0\| \leqslant R + \delta(t_0, \varepsilon, r). \tag{5}$$

Definition 2.3 The ball B_R is uniformly asymptotically stable in probability for the SDE (1) if the ball is uniformy stable in probability and, for any $0 < \varepsilon < 1$, there exists $\delta(\varepsilon, t_0) > 0$ such that

$$\mathbf{P}\{x(t) \in \mathbb{R}^n : \limsup_{t \to +\infty} \|x(t)\| = R\} \geqslant 1 - \varepsilon, \quad \forall x_0 \in \mathbb{R}^n, \quad R < \|x_0\| \leqslant R + \delta(\varepsilon, t_0). \tag{6}$$

3 Uniform Asymptotic Stability in Probability of Nontrivial Solution of SDE

Let $V(x,t)$ be a function valued on $\mathbb{R}$ which is continuously twice differentiable in $x \in \mathbb{R}^n$ and once differentiable in $t \in \mathbb{R}_+$. Applying the Itô formula to $V(x,t)$ with SDE (1) yields [8, 16, 17]

$$\mathrm{d}\, V(x,t) = \mathfrak{L}V(x,t)\,\mathrm{d}\, t + \mathfrak{B}V(x,t)\,\mathrm{d}\, w \tag{7}$$

with

$$\mathfrak{L}V(x,t) = V_t(x,t) + V_x(x,t) f(x) + \frac{1}{2}\operatorname{tr}(g^T(x) V_{xx}(x,t) g(x)), \tag{8a}$$

$$\mathfrak{B}V(x,t) = V_x(x,t) g(x), \tag{8b}$$

where

$$V_t(x,t) = \frac{\partial V(x,t)}{\partial t},$$
$$V_x(x,t) = \begin{bmatrix} \frac{\partial V(x,t)}{\partial x_1} & \dots & \frac{\partial V(x,t)}{\partial x_n} \end{bmatrix},$$
$$V_{xx}(x,t) = \begin{bmatrix} \frac{\partial^2 V(x,t)}{\partial x_1 \partial x_1} & \dots & \frac{\partial^2 V(x,t)}{\partial x_1 \partial x_n} \\ \vdots & \ddots & \vdots \\ \frac{\partial^2 V(x,t)}{\partial x_n \partial x_1} & \dots & \frac{\partial^2 V(x,t)}{\partial x_n \partial x_n} \end{bmatrix}.$$

In the sequel, it is assumed that $V_t(x,t) = 0$, so $V(x,t)$ is replaced by $V(x)$.

The following theorem solves the problem of the uniform asymptotic stability in probability of SDE (1).

Theorem 3.1 *Let $V(x)$ be a positive definite Lyapunov function. If there exist three functions μ_1, μ_2 and μ_3 in $\mathbf{K}$ and a scalar $\gamma > 0$ and $R > 0$, such that*

$$\mu_1(\|x\|) \leqslant V(x) \leqslant \mu_2(\|x\|), \tag{9}$$
$$\mathfrak{L}V(x) \leqslant -\mu_3(\|x\|) + \gamma, \tag{10}$$
$$-\mu_3(\|x\|) + \gamma < 0, \quad \forall\ \|x\| > R, \tag{11}$$
$$\mu_1(R) = \mu_2(R), \tag{12}$$

then the ball B_R is uniformly asymptotically stable in probability for the SDE (1).

Proof. First step: The ball B_R is uniformly stable in probability.

Fix $t_0 \in \mathbb{R}^+$. Let $0 < \epsilon < 1$ and $r > 0$, we define $x(t)$ as the solution of the system (1), we suppose that $\forall t \geqslant t_0$, we have $\|x\| > R$.

The following stopping time

$$\tau_r = \inf\{t \geqslant t_0 \text{ such that } \|x(t)\| > R + r\} \tag{13}$$

is defined to eliminate all the solutions that go beyond $R + r$.

From (7), (8a), (10) and (11), we have

$$\mathrm{d}\, V(x) = \mathfrak{L}V(x)\,\mathrm{d}\, t + V_x g(x)\,\mathrm{d}\, w(t) \tag{14}$$

and

$$\mathfrak{L}V(x) \leqslant -\mu_3(\|x\|) + \gamma < 0, \quad \forall\ \|x\| > R. \tag{15}$$

Applying the expectation to the previous inequality leads to

$$\mathbf{E}\left\{\int_{t_0}^{t\wedge\tau_r} \mathrm{d}\, V(x(s))\right\} = \mathbf{E}\left\{\int_{t_0}^{t\wedge\tau_r} (\mathfrak{L}V(x(s)\,\mathrm{d}\, s + V_x g(x(s))\,\mathrm{d}\, w(s))\right\}. \tag{16}$$

In view of (15) and the following relation

$$\mathbf{E}\left\{\int_{t_0}^{t\wedge\tau_r} V_x g(x(s))\,\mathrm{d}\, w(s)\right\} = 0, \tag{17}$$

the equation (16) becomes

$$\mathbf{E}\left\{\int_{t_0}^{t\wedge\tau_r} \mathrm{d}\, V(x(s))\right\} = \mathbf{E}\left\{\int_{t_0}^{t\wedge\tau_r} \mathfrak{L}V(x(s))\,\mathrm{d}\, s\right\} \leqslant 0. \tag{18}$$

Integrating (18) gives

$$\mathbf{E}\{V(x(t\wedge\tau_r)) - V(x_0)\} \leqslant 0. \tag{19}$$

The previous inequality is equivalent to

$$\mathbf{E}\{V(x(t\wedge\tau_r)) - \mu_1(R)\} \leqslant \mathbf{E}\{V(x_0) - \mu_1(R)\}, \tag{20}$$

and, if $\tau_r \leqslant t$, we obtain

$$\mathbf{P}\{\tau_r \leqslant t\}\ \mathbf{E}\{V(x(\tau_r)) - \mu_1(R)\} \leqslant \mathbf{E}\{V(x_0) - \mu_1(R)\}. \tag{21}$$

Condition (9) yields $\mu_1(R+r) \leqslant V(x(\tau_r))$, then we have

$$\mathbf{P}\{\tau_r \leqslant t\}(\mu_1(R+r) - \mu_1(R)) \leqslant (V(x_0) - \mu_1(R)). \tag{22}$$

So, if $t \to +\infty$, the following inequality holds true:

$$\mathbf{P}\{\tau_r \leqslant +\infty\} \leqslant \frac{V(x_0) - \mu_1(R)}{\mu_1(R+r) - \mu_1(R)}. \tag{23}$$

Since we have $\mu_1(R) = \mu_2(R)$ (because of the continuity at the point R of μ_2), there exists $0 < \delta_0(t_0, \epsilon, r) < r$ such that $R < \|x_0\| < R + \delta_0(t_0, \epsilon, r)$, then we have

$$\mu_2(\|x_0\|) - \mu_2(R) \leqslant \epsilon(\mu_1(R+r) - \mu_1(R)). \tag{24}$$

Using the inequality above we have

$$V(x_0) - \mu_1(R) \leqslant \epsilon(\mu_2(\|x_0\|) - \mu_2(R)) \leqslant \epsilon(\mu_1(R+r) - \mu_1(R)).$$

From (**??**) we can deduce that

$$\frac{V(x_0) - \mu_1(R)}{\mu_1(R+r) - \mu_1(R)} \leqslant \epsilon. \tag{25}$$

Fix $x_0 \in \mathbb{R}^n$ such that $R < \|x_0\| < R + \delta_0(\varepsilon, r, t_0)$. From the existence and uniqueness of the solution x to the SDE (1) (see (2a) and (2b)), we assume that there exists $x(t)$ such that $\|x(t)\| > R$, $\forall t \geqslant t_0$.

Using x_0 chosen above and the inequality (25), we have

$$\mathbf{P}\{\tau_r \leqslant +\infty\} \leqslant \varepsilon. \tag{26}$$

Finally, we have $\forall R < \|x_0\| < (R + \delta_0(\epsilon, t_0, r)) \leqslant R + r$. Then, we obtain

$$\mathbf{P}\{x(t) \in \mathbb{R}^n : R < \|x(t)\| \leqslant R + r \text{ for all } t \geqslant t_0\} \geqslant 1 - \varepsilon \tag{27}$$

and the condition (5) in Definition 2.2 is proved.

Second step: The ball B_R is uniformly asymptotically stable in probability.

Since the ball B_R is uniformly stable in probability (see step 1), $\forall \varepsilon$ and r with $0 < \varepsilon < 1$ and $r > 0$, $\exists \, \delta_0(\varepsilon, r, t_0)$ such that $R < \|x_0\| < R + \delta_0(\varepsilon, r, t_0)$. From the existence and uniqueness of the solution x to the SDE (1) (see (2a) and (2b)), we assume that there exists $x(t)$ such that $\|x(t)\| > R$, $\forall t \geqslant t_0$. So, the following relation

$$\mathbf{P}\Big\{x(t) \in \mathbb{R}^n : R < \|x(t)\| \leqslant R + \frac{r}{2}, t \geqslant t_0\Big\} \geqslant 1 - \frac{\varepsilon}{4} \tag{28}$$

holds.

In view of the theorem of continuity on $\mu_2(R)$ and since $R < \|x_0\|$, for all β with $R < \beta < \|x_0\|$, there exists α such that $R < \alpha < \beta$ and

$$\frac{\mu_2(\alpha) - \mu_2(R)}{\mu_1(\beta) - \mu_1(R)} \leqslant \frac{\varepsilon}{4}. \tag{29}$$

We define the stopping times as follows:

$$\tau_\alpha = \inf\{t \geqslant t_0 \text{ such that } \|x(t)\| \leqslant \alpha\}, \tag{30}$$

$$\tau_r = \inf\Big\{t \geqslant t_0 \text{ such that } \|x(t)\| > R + \frac{r}{2}\Big\}. \tag{31}$$

Applying the Itô formula to $V(x)$, we have

$$\mathbf{E}\{V(x(\tau_\alpha \wedge \tau_r \wedge t))\} = \mathbf{E}\{V(x(t_0))\} + \mathbf{E}\Big\{\int_{t_0}^{\tau_\alpha \wedge \tau_r \wedge t} \mathfrak{L}V(x(s))\,\mathrm{d}\,s\Big\}. \tag{32}$$

If $t < \tau_\alpha \wedge \tau_r$, we have $\|x(t)\| > \alpha$ and, using (10), we obtain

$$\mathfrak{L}V(x(t)) \leqslant -\mu_3(\|x\|) + \gamma \leqslant -\mu_3(\alpha) + \gamma. \tag{33}$$

Integrating (32) and using (33) yield

$$\mathbf{E}\{V(x(\tau_\alpha \wedge \tau_r \wedge t))\} \leqslant \mathbf{E}\{V(x(t_0))\} + (\gamma - \mu_3(\alpha))(t - t_0)\mathbf{P}\{t < \tau_\alpha \wedge \tau_r\}. \tag{34}$$

Since the left term in inequality (34) is positive, we obtain

$$(t - t_0)(\mu_3(\alpha) - \gamma)\mathbf{P}\{t < \tau_\alpha \wedge \tau_r\} \leqslant \mathbf{E}\{V(x_0)\}. \tag{35}$$

Since the term $(t - t_0)(\mu_3(\alpha) - \gamma)\mathbf{P}\{t < \tau_\alpha \wedge \tau_r\}$ is bounded and using condition (11), we have

$$\mathbf{P}\{\tau_\alpha \wedge \tau_r = +\infty\} = 0 \tag{36}$$

when $t \to +\infty$. So we deduce

$$\mathbf{P}\{\tau_\alpha \wedge \tau_r < +\infty\} = 1. \tag{37}$$

Also, from the beginning of the second step of the proof, we get

$$\mathbf{P}\{\tau_r < +\infty\} \leqslant \frac{\varepsilon}{4}. \tag{38}$$

Then, using (37) and (38), the following relation

$$1 = \mathbf{P}\{\tau_\alpha \wedge \tau_r < +\infty\} \leqslant \mathbf{P}\{\tau_\alpha < +\infty\} + \mathbf{P}\{\tau_r < +\infty\} \leqslant \mathbf{P}\{\tau_\alpha < +\infty\} + \frac{\varepsilon}{4} \tag{39}$$

is obtained. Finally, we deduce

$$\mathbf{P}\{\tau_\alpha < +\infty\} \geqslant 1 - \frac{\varepsilon}{4}. \tag{40}$$

Now, we choose $\theta > 0$ sufficiently large such that

$$\mathbf{P}\{\tau_\alpha < \theta\} \geqslant 1 - \frac{\varepsilon}{2}, \tag{41}$$

and relations (38) and (41) lead to

$$\begin{aligned} \mathbf{P}\{\tau_\alpha < \tau_r \wedge \theta\} &\geqslant \mathbf{P}\{(\tau_\alpha < \theta) \cap (\tau_r = +\infty)\} \\ &\geqslant \mathbf{P}\{(\tau_\alpha < \theta)\}\mathbf{P}\{\tau_r = +\infty\} \\ &= \mathbf{P}\{(\tau_\alpha < \theta)\}(1 - \mathbf{P}\{\tau_r < +\infty\}) \\ &\geqslant \mathbf{P}(\tau_\alpha < \theta) - \mathbf{P}\{\tau_r < +\infty\} \\ &\geqslant 1 - \frac{3\varepsilon}{4}. \end{aligned} \tag{42}$$

We define the time σ and the stopping time τ_β as follows:

$$\sigma = \begin{cases} \tau_\alpha, & \text{if} \quad \tau_\alpha < \tau_r \wedge \theta, \\ +\infty, \end{cases} \tag{43}$$

$$\tau_\beta = \inf\{t > \sigma, \|x(t)\| > \beta\}. \tag{44}$$

Taking $t \geqslant \theta$, applying the Itô formula to the function $V(x)$ and using conditions (10) and (11), the following relation

$$\mathbf{E}\left\{\int_{\sigma\wedge t}^{\tau_\beta \wedge t} \mathrm{d}\, V(x(s))\right\} = \mathbf{E}\left\{\int_{\sigma\wedge t}^{\tau_\beta\wedge t} \mathfrak{L}V(x(s))\,\mathrm{d}\, s\right\} \leqslant 0 \tag{45}$$

is obtained.

Integrating (45) gives

$$\mathbf{E}\{V(x(\tau_\beta \wedge t))\} \leqslant \mathbf{E}\{V(x(\sigma \wedge t))\}. \tag{46}$$

The previous inequality is equivalent to

$$\mathbf{E}\{V(x(\tau_\beta \wedge t)) - \mu_2(R)\} \leqslant \mathbf{E}\{V(x(\sigma \wedge t)) - \mu_2(R)\}. \tag{47}$$

If $\tau_\alpha < \tau_r \wedge \theta$, in view of (43), the inequality (47) becomes

$$\mathbf{E}\{V(x(\tau_\beta \wedge t)) - \mu_2(R)\} \leqslant E\{V(x(\tau_\alpha \wedge t)) - \mu_2(R)\}. \tag{48}$$

If $\tau_\beta < t$, then $\tau_\alpha < t$, and the previous inequality becomes

$$\mathbf{P}\{\tau_\beta < t\}\mathbf{E}\{V(x(\tau_\beta)) - \mu_2(R)\} \leqslant \mathbf{E}\{V(x(\tau_\alpha)) - \mu_2(R)\}. \tag{49}$$

So, using condition (9), we obtain

$$\mathbf{P}\{\tau_\beta < t\}(\mu_1(\beta) - \mu_2(R)) \leqslant \mu_2(\alpha) - \mu_2(R). \tag{50}$$

Then, using (29), the following inequality

$$\mathbf{P}\{\tau_\beta < t\} \leqslant \frac{\mu_2(\alpha) - \mu_2(R)}{\mu_1(\beta) - \mu_2(R)} \leqslant \frac{\varepsilon}{4} \tag{51}$$

is satisfied and, if $t \to +\infty$, we have

$$\mathbf{P}\{\tau_\beta < +\infty\} \leqslant \frac{\varepsilon}{4}. \tag{52}$$

Then, relations (42) and (52) lead to

$$\begin{aligned} \mathbf{P}\{(\sigma < +\infty) \cap (\tau_\beta = +\infty)\} &\geqslant \mathbf{P}\{\sigma < +\infty\}\mathbf{P}\{\tau_\beta = +\infty\} \\ &= \mathbf{P}\{\sigma < +\infty\}(1 - \mathbf{P}\{\tau_\beta < +\infty\}) \\ &\geqslant \mathbf{P}\{\sigma < +\infty\} - \mathbf{P}\{\tau_\beta < +\infty\} \\ &\geqslant \mathbf{P}\{\tau_\alpha < \tau_r \wedge \theta\} - \mathbf{P}\{\tau_\beta < +\infty\} \\ &\geqslant 1 - \frac{3\varepsilon}{4} - \frac{\varepsilon}{4} = 1 - \varepsilon, \end{aligned} \tag{53}$$

and, with (43) and (44), we obtain

$$\mathbf{P}\{x(t) \in \mathbb{R}^n : R \leqslant \lim_{t\to+\infty} \sup \|x(t)\| \leqslant \beta\} \geqslant 1 - \varepsilon, \qquad \forall\, \beta > R. \tag{54}$$

Since β is arbitrary, if $\beta \to R$, we obtain

$$\mathbf{P}\{x(t) \in \mathbb{R}^n : \limsup_{t\to+\infty} \|x(t)\| = R\} \geqslant 1 - \varepsilon. \tag{55}$$

The proof is ended.

4 Example

To illustrate Theorem 3.1, we consider the SDE (1) given by

$$\mathrm{d}\, x = (-x + 1)\, \mathrm{d}\, t + \beta\, \mathrm{d}\, w. \tag{56}$$

This SDE does not have the trivial solution $x = 0$ since $f(0) = 1$.

Let $V(x)$ be the following Lyapunov function

$$V(x) = \frac{1}{2}x^2 \tag{57}$$

and the functions $\mu_1(x)$, $\mu_2(x)$ and $\mu_3(x)$ be given by

$$\mu_1(x) = \mu_2(x) = \mu_3(x) = \frac{1}{2}x^2. \tag{58}$$

Applying the Itô formula to $V(x)$ leads to

$$\mathfrak{L}V(x) = -x^2 + x + \frac{1}{2}\beta^2 \leqslant \frac{-1}{2}x^2 + \frac{1}{2}(1 + \beta^2).$$

Then we have

$$\mathfrak{L}V(x) < 0, \ \forall\ |x| > \sqrt{1 + \beta^2}. \tag{59}$$

The radius of the ball B_R is equal to $R = \sqrt{1 + \beta^2}$.

Finally, the ball $S_{\sqrt{1+\beta^2}} = \{x \in \mathbb{R}, |x| = \sqrt{1 + \beta^2}\}$ is uniformly asymptotically stable in probability as can be seen in Figure 1 with $\beta = 0.01$.

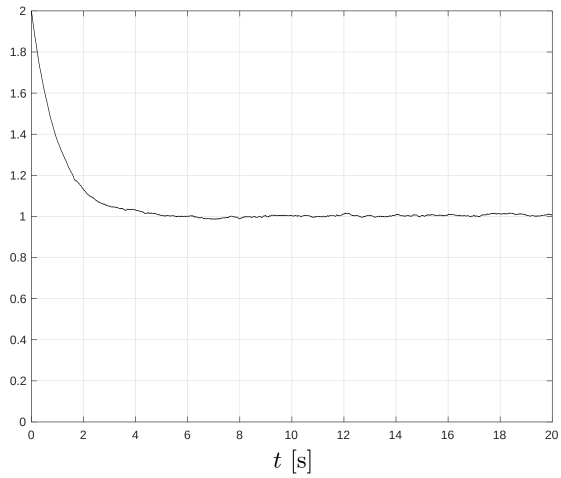

Figure 1: State x.

5 Conclusion

In this paper, the concept of uniform asymptotic stability in probability of nontrivial solutions of a SDE is studied. A new theorem is proposed to check this uniform asymptotic stability in probability. This theorem is based on sufficient conditions to be verified for a given Lyapunov function. An example is given to illustrate our approach.

References

[1] A. Barbata, M. Zasadzinski, H. Souley Ali and H. Messaoud. Exponential disturbance rejection with decay rate for stochastic systems. In: *Proc. IEEE American Control Conf.* Washington, USA, 2013, 5424-5428.

[2] A. Barbata, M. Zasadzinski, R. Chatbouri, H. Souley Ali and H. Messaoud. Almost sure practical exponential stability of nonlinear disturbed stochastic systems with guaranteed decay rate. *Asian Journal of Control* **1** (6) (2017) 1954–1965.

[3] T. Caraballo, M. A. Hammami and L. Mchiri. On the practical global uniform asymptotic stability of stochastic differential equations. *Stochastics: An International Journal of Probability and Stochastic Processes* **88** (1) (2016) 45–56.

[4] A. Friedman. *Stochastic Differential Equations and Applications.* Academic Press, New York, 1975.

[5] I. I. Gikhman, and A. V. Skorokhod. *Stochastic Differential Equations.* Springer Verlag, New York, 1972.

[6] H. Deng and M. Krstić. Stochastic nonlinear stabilization − I: A backstepping design. *Systems and Control Letters* **32** (3) (1997)143–150.

[7] H. Deng and M. Krstić. Output-feedback stochastic nonlinear stabilization. *IEEE Transactions on Automatic Control* **44** (2) (1999) 328–333.

[8] R. Z. Has'minskii. *Stochastic Stability of Differential Equations* (2nd ed.). Springer, Berlin, 2012.

[9] I. I. Kats and N. N. Krasovskii. On the stability of systems with random parameters. *Journal of Applied Mathematics and Mechanics* **24** (5) (1961) 1225–1246

[10] F. Kozin. A survey of stability of stochastic systems. *Automatica* **5** (1) (1969) 95–112.

[11] H. J. Kushner. On the construction of stochastic Liapunov functions. *IEEE Transactions on Automatic Control* **10** (4) (1965) 477–478.

[12] H. J. Kushner. *Stochastic Stability and Control*. Academic Press, New York, 1967.

[13] H. J. Kushner. A partial history of the early development of continuous-time nonlinear stochastic systems theory. *Automatica* **50** (2) (2014) 303–334.

[14] Y. G. Liu and J. F. Zhang. Reduced-order observer-based control design for nonlinear stochastic systems. *Systems and Control Letters* **52** (2) (2004) 123–135.

[15] T. T. T. Lan and N. H. Dang. Exponential stability of nontrivial solutions of stochastic differential equations. *Scientia, Series A: Mathematical Sciences* **29** (2011) 97–106.

[16] X. Mao. *Stochastic Differential Equations & Applications*. Horwood, London, 1997.

[17] B. Øksendal. *Stochastic Differential Equations: an Introduction with Applications* (6th ed.). Springer-Verlag, New York, 2003.

[18] A. S. Rufino Ferreira, M. Arcak and E. D. Sontag. Stability certification of large scale stochastic systems using dissipativity. *Automatica* **48** (11) (2012) 2956–2964.

[19] W. M. Wonham. Liapunov criteria for weak stochastic stability. *Journal of Differential Equations* **2** (2) (1966) 195–207.

[20] X. J. Xie and J. Tian. Adaptive state-feedback stabilization of high-order stochastic systems with nonlinear parameterization. *Automatica* **45** (1) (2009) 126–133.

[21] S. Xiong, Q. Zhu and F. Jiang. Globally asymptotic stabilization of stochastic nonlinear systems in strict-feedback form. *Journal of the Franklin Institute* **352** (11) (2015) 5106–5121.

[22] M. Zakai. On the ultimate boundedness of moments associated with solutions of stochastic differential equations. *SIAM Journal of Control and Optimization* **5** (4) (1967) 588–593.

[23] M. Zakai. A Lyapunov criterion for the existence of stationary probability distributions for systems perturbed by noise. *SIAM Journal of Control and Optimization* **7** (3) (1969) 390–397.

[24] Z. Y. Zhang and F. Kozin. On almost sure sample stability of nonlinear stochastic dynamic systems. *IEEE Transactions on Automatic Control* **39** (3) (1994) 560–565.

Nonlinear Dynamics and Systems Theory, **19** (4) (2019) 474–485

Oscillation and Nonoscillation for Caputo–Hadamard Impulsive Fractional Differential Equations

Mouffak Benchohra [1,2*], Samira Hamani [3], and Juan Nieto [4]

[1] *Laboratory of Mathematics, Djillali Liabes University of Sidi Bel-Abbès, P.O. Box 89, Sidi Bel-Abbès 22000, Algeria;*
[2] *Department of Mathematics, College of Science, King Saud University, P.O. Box 2455, Riyadh 11451, Saudi Arabia;*
[3] *Laboratory of Applied and Pure Mathematics, University of Mostaganem, B.P. 227, 27000, Mostaganem, Algérie;*
[4] *Department of Statistics, Mathematical Analysis and Optimization, Institute of Mathematics, University of Santiago de Compostela, Santiago de Compostela, Spain*

Received: September 16, 2018; Revised: September 10, 2019

Abstract: In this paper, the concept of the upper and lower solutions method combined with the fixed point theorem is used to investigate the existence of oscillatory and nonoscillatory solutions for a class of initial value problems for Caputo–Hadamard impulsive fractional differential equations.

Keywords: *impulsive fractional differential equations; Caputo–Hadamard fractional derivative; fixed point; upper solution; lower solution, oscillation, nonoscillation.*

Mathematics Subject Classification (2010): 26A33, 34A37, 34D10.

1 Introduction

Fractional differential equations and integrals are valuable tools in the modeling of many phenomena in various fields of science and engineering. Indeed, there are numerous applications in viscoelasticity, electrochemistry, control, porous media, electromagnetism, etc. In the monographs [1, 3, 4, 11, 12, 15], we can find the mathematical background and various applications of fractional calculus. Recently, many researchers studied different fractional problems involving the Riemaan-Liouville, Caputo and Hadamard derivatives; see, for example, the papers [2, 17]. Sufficient conditions for the oscillation of solutions of differential equations are given in [9, 14, 16].

* Corresponding author: mailto:benchohra@univ-sba.dz

The method of upper and lower solutions has been successfully applied to study the existence of solutions for ordinary and fractional differential equations and inclusions. See the monograph [13], and the papers [8, 18, 19], and the references therein.

This paper deals with the existence of oscillatory and nonoscillatory solutions for the following class of initial value problems for Caputo–Hadamard impulsive fractional differential equations:

$$^{Hc}D^{\alpha}_{t_k}y(t) = f(t, y(t)),\ t \in (t_k, t_{k+1}), \tag{1}$$

$$y(t_k^+) = I_k(y(t_k^-)), \quad k = 1, 2, \ldots, \tag{2}$$

$$y(1) = y_*, \tag{3}$$

where $^{Hc}D^{\alpha}_{t_k}$ is the Caputo–Hadamard fractional derivative of order $0 < \alpha \leq 1$, $f : J \times \mathbb{R} \to \mathbb{R}$ is a given function, $y_* \in \mathbb{R}$, $I_k \in C(\mathbb{R}, \mathbb{R})$, $1 = t_0 < t_1 < \ldots < t_m < t_{m+1} < \cdots < \infty$, $y(t_k^+) = \lim_{h\to 0^+} y(t_k + h)$ and $y(t_k^-) = \lim_{h\to 0^+} y(t_k - h)$ represent the right and left limits of $y(t)$ at $t = t_k,\ k = 1, 2, \ldots$

This paper initiates the study of oscillatory and nonoscillatory solutions for impulsive fractional differential equations involving the Caputo–Hadamard fractional derivative.

2 Preliminaries

In this section, we introduce notations, definitions, and preliminary facts that will be used in the remainder of this paper. Let $C(J, \mathbb{R})$ be the space of all continuous functions from J into $\mathbb{R}$.

$$\|y\|_\infty = \sup_{t\in J} |y(t)|.$$

Let $BC(J, \mathbb{R})$ be the Banach space of all continuous and bounded functions from J into $\mathbb{R}$ with the norm

$$\|y\|_\infty = \sup_{t\in J} |y(t)|,$$

and let $L^1(J, \mathbb{R})$ be the Banach space of Lebesgue integrable functions $y : J \longrightarrow \mathbb{R}$ with the norm

$$\|y\|_{L^1} = \int_1^T |y(t)|dt.$$

Denote by $AC(J, \mathbb{R})$ the space of absolutely continuous functions from J into $\mathbb{R}$.

Let us recall some definitions and properties of the Hadamard fractional integration and differentiation. Let $\delta = t\dfrac{d}{dt}$, and set

$$AC^n_\delta(J, \mathbb{R}) = \{y : J \longrightarrow \mathbb{R}, \delta^{n-1}y(t) \in AC(J, \mathbb{R})\}.$$

Definition 2.1 [12] The Hadamard fractional integral of order $r > 0$ for a function $h \in L^1([1, +\infty), \mathbb{R})$ is defined as

$$^{H}I^r h(t) = \frac{1}{\Gamma(r)} \int_1^t \left(\log \frac{t}{s}\right)^{r-1} \frac{h(s)}{s} ds,$$

provided the integral exists for a.e. $t > 1$.

Example 2.1 Let $q > 0$. Then

$$^{H}I_1^q \ln t = \frac{1}{\Gamma(2+q)}(\ln t)^{1+q}; \; for \; a.e. \; t \in [1, +\infty).$$

Definition 2.2 [12] The Hadamard fractional derivative of order $r > 0$ applied to the function $h \in AC_\delta^n([1, +\infty), \mathbb{R})$ is defined as

$$(^{H}D_1^q h)(t) = \delta^n(^{H}I_1^{n-r} h)(t),$$

where $n - 1 < r < n, \; n = [r] + 1$, and $[r]$ is the integer part of r.

Definition 2.3 [10] For a given function $h \in AC_\delta^n([a, b], \mathbb{R})$, such that $0 < a < b$, the Caputo–Hadamard fractional derivative of order $r > 0$ is defined as follows:

$$^{Hc}D^r y(t) = ^{H} D^r \left[y(s) - \sum_{k=0}^{n-1} \frac{\delta^k y(a)}{k!} \left(\log \frac{s}{a} \right)^k \right](t),$$

where $Re(\alpha) \geq 0$ and $n = [Re(\alpha)] + 1$.

Lemma 2.1 *[10] Let $y \in AC_\delta^n([a, b], \mathbb{R})$ or $C_\delta^n([a, b], \mathbb{R})$ and $\alpha \in \mathbb{C}$. Then*

$$^{H}I^r(^{Hc}D^r y)(t) = y(t) - \sum_{k=0}^{n-1} \frac{\delta^k y(a)}{k!} \left(\log \frac{t}{a} \right)^k.$$

3 Main Results

We consider the space

$$PC(J, \mathbb{R}) = \{ y : J \to \mathbb{R}, \, y \in C((t_k, t_{k+1}], \mathbb{R}), \, k = 0, 1, \ldots,$$

$$\text{and there exist}\, y(t_k^+) \; \text{and} \; y(t_k^-), \, k = 1, 2, \ldots, \; \text{with} \; y(t_k^-) = y(t_k) \}.$$

This set is a Banach space with the norm

$$\|y\|_{PC} = \sup_{t \in J} |y(t)|.$$

Let us start by defining what we mean by a solution of problem (1)–(3).

Definition 3.1 A function $y \in PC \cap C^1((t_k, t_{k+1}), \mathbb{R}), \; k = 0, 1, \ldots$, is said to be a solution of (1)–(3) if y satisfies the equation $^{Hc}D_{t_k}^\alpha y(t) = f(t, y(t))$ on (t_k, t_{k+1}) and conditions $y(t_k^+) = I_k(y(t_k^-))$, k=1,2,…, $y(1) = y_*$.

Definition 3.2 A function $u \in PC \cap C^1((t_k, t_{k+1}), \mathbb{R}), k = 0, 1, \ldots$, is said to be a lower solution of (1)–(3) if $^{Hc}D_{t_k}^\alpha u(t) \leq f(t, u(t))$ on (t_k, t_{k+1}) and $u(t_k^+) \leq I_k(u(t_k)), k = 1, \ldots$. Similarly, a function $v \in PC \cap C^1((t_k, t_{k+1}), \mathbb{R}), k = 0, \ldots$, is said to be an upper solution of (1)–(3) if $^{Hc}D_{t_k}^\alpha v(t) \geq f(t, v(t))$ on (t_k, t_{k+1}) and $v(t_k^+) \geq I_k(v(t_k)), k = 1, 2, \ldots$.

For the study of this problem we first list the following hypotheses:

(H1) The function $f : J \times \mathbb{R} \to \mathbb{R}$ is continuous;

(H2) For all $r > 0$ there exists a function $h_r \in C(J, \mathbb{R}^+)$ such that

$$|f(t,y)| \leq h_r(t) \text{ for all } \ t \in J \text{ and all } |y| \leq r;$$

(H3) There exist u and $v \in PC \cap C^1((t_k, t_{k+1}), \mathbb{R}),\ k = 0, \ldots,$ which are the lower and upper solutions for the problem (1)–(3) such that $u \leq v$;

(H4)

$$u(t_k^+) \leq \min_{y \in [u(t_k^-), v(t_k^-)]} I_k(y) \leq \max_{y \in [u(t_k^-), v(t_k^-)]} I_k(y) \leq v(t_k^+),\ k = 1, 2, \ldots .$$

Theorem 3.1 *Assume that hypotheses (H1)-(H4) hold. Then the problem (1)–(3) has at least one solution y such that*

$$u(t) \leq y(t) \leq v(t) \quad \textit{for all } t \in J.$$

Proof. The proof will be given in several steps.

Step 1: Consider the problem

$$^{Hc}D^{\alpha}_{t_0} y(t) = f(t, y(t)),\ t \in J_1 := [t_0, t_1], \tag{4}$$

$$y(1) = y_*. \tag{5}$$

Transform the problem (4)–(5) into a fixed point problem. Consider the following modified problem:

$$^{Hc}D^{\alpha}_{t_0} y(t) = f_1(t, y(t)),\ t \in J_1, \tag{6}$$

$$y(1) = y_*, \tag{7}$$

where

$$f_1(t,y) = f(t, \tau(t,y))$$

$$\tau(t,y) = \max\{u(t), \min(y, v(t))\}$$

and

$$\overline{y}(t) = \tau(t,y).$$

A solution to (6)–(7) is a fixed point of the operator $N : C([t_0,t_1], \mathbb{R}) \longrightarrow C([t_0,t_1], \mathbb{R})$ defined by

$$y(t) = y_* + \frac{1}{\Gamma(\alpha)} \int_{t_0}^{t} \left(\log \frac{t}{s}\right)^{\alpha - 1} f_1(s, y(s)) \frac{ds}{s}.$$

Remark 3.1 (i) Notice that f_1 is a continuous function, and from (H2) there exists $M^* > 0$ such that

$$|f_1(t,y)| \leq M^* \text{ for each } (t,y) \in J_1 \times \mathbb{R}.$$

(ii) By the definition of τ it is clear that

$$u(t_k^+) \leq I_k(\tau(t_k, y(t_k))) \leq v(t_k^+),\ k = 1, 2, \ldots .$$

In order to apply the nonlinear alternative of Leray–Schauder type, we first show that N is continuous and completely continuous.

Claim 1: *N is continuous.*

Let $\{y_n\}$ be a sequence such that $y_n \to y$ in $C([t_0,t_1],\mathbb{R})$. Then

$$|N(y_n)(t) - N(y)(t)| \leq \frac{1}{\Gamma(\alpha)} \int_{t_0}^{t} \left(\log \frac{t}{s}\right)^{\alpha-1} |f_1(s,\overline{y}_n(s)) - f_1(s,\overline{y}(s))| \frac{ds}{s}.$$

Since f_1 is a continuous function, we have

$$\|N(y_n) - N(y)\|_\infty \leq \frac{\left(\log \frac{t_1}{t_0}\right)^{\alpha}}{\Gamma(\alpha+1)} \|f_1(\cdot,\overline{y}_n(\cdot)) - f_1(\cdot,\overline{y}(\cdot))\|_\infty.$$

Thus

$$\|N(y_n) - N(y)\|_\infty \to 0 \quad as\ n \to \infty.$$

Claim 2: *N maps bounded sets into bounded sets in $C([t_0,t_1],\mathbb{R})$.*

Indeed, it is enough to show that there exists a positive constant ℓ such that for each $y \in B_q = \{y \in C([t_0,t_1],\mathbb{R}) : \|y\|_\infty \leq q\}$ one has $\|Ny\|_\infty \leq \ell$. Let $y \in B_q$. Then for each $t \in J_1$ we have

$$y(t) = y_* + \frac{1}{\Gamma(\alpha)} \int_{t_0}^{t} \left(\log \frac{t}{s}\right)^{\alpha-1} f_1(s,y(s)) \frac{ds}{s}.$$

By (H1) and Remark 3.1 we have for each $t \in J_1$

$$\begin{aligned} |Ny(t)| &\leq |y_*| + \frac{1}{\Gamma(\alpha)} \int_{t_0}^{t} \left(\log \frac{t}{s}\right)^{\alpha-1} |f_1(s,y(s))| \frac{ds}{s} \\ &\leq |y_*| + \frac{M\left(\log \frac{t_1}{t_0}\right)^{\alpha}}{\Gamma(\alpha+1)} := \ell. \end{aligned}$$

Thus $\|N(y)\|_\infty \leq \ell$.

Claim 3: *N maps bounded set into equicontinuous sets of PC.*

Let $\tau_1,\tau_2 \in J_1,\ \tau_1 < \tau_2$ and B_q be a bounded set of PC as in Claim 2. Let $y \in B_q$, then

$$|N(u_2) - N(u_1)| \leq \frac{M\left(\log \frac{\tau_2}{\tau_1}\right)^{\alpha}}{\Gamma(\alpha+1)}.$$

As $\tau_2 \longrightarrow \tau_1$ the right-hand side of the above inequality tends to zero.

As a consequence of Claims 1 to 3 together with the Arzela–Ascoli theorem we can conclude that $N : C([t_0,t_1],\mathbb{R}) \longrightarrow C([t_0,t_1],\mathbb{R})$ is continuous and completely continuous.

Claim 4: *A priori bounds on solutions.*

Let y be a possible solution of $y = \lambda N(y)$ with $\lambda \in [0,1]$. Then we have

$$y(t) = \lambda\left[|y_*| + \frac{1}{\Gamma(\alpha)}\int_{t_0}^{t}\left(\log\frac{t}{s}\right)^{\alpha-1}|f_1(s,y(s))|\frac{ds}{s}\right].$$

This implies by Remark 3.1 that for each $t \in J_1$ we have

$$\begin{aligned}|Ny(t)| &\leq |y_*| + \frac{1}{\Gamma(\alpha)}\int_{t_0}^{t}\left(\log\frac{t}{s}\right)^{\alpha-1}|f_1(s,y(s))|\frac{ds}{s}\\ &\leq |y_*| + \frac{M\left(\log\frac{t_1}{t_0}\right)^{\alpha}}{\Gamma(\alpha+1)} := M_1.\end{aligned}$$

Set

$$U = \{y \in C([t_0,t_1],\mathbb{R}) : \|y\|_\infty < M_1 + 1\}.$$

From the choice of U there is no $y \in \partial U$ such that $y = \lambda N(y)$ for some $\lambda \in (0,1)$. As a consequence of the nonlinear alternative of Leray–Schauder type, we deduce that N has a fixed point y in U which is a solution of the problem (6)–(7).

Claim 5: *Every solution y of $(6)-(7)$ satisfies*

$$u(t) \leq y(t) \leq v(t) \text{ for all } t \in J_1.$$

Let y be a solution of $(6)-(7)$. We prove that

$$u(t) \leq y(t) \text{ for all } t \in J_1.$$

Suppose not. Then there exist $\tau_1,\, \tau_2$ with $\tau_1 < \tau_2$ such that $u(\tau_1) = y(\tau_1)$ and

$$u(t) > y(t) \text{ for all } t \in (\tau_1,\, \tau_2).$$

In view of the definition of τ one has

$${}^{Hc}D^\alpha y(t) = f(t,u(t)) \text{ for all } t \in (\tau_1,\, \tau_2).$$

An integration on $(\tau_1,\, t]$ with $t \in (\tau_1,\, \tau_2)$ yields

$$y(t) - y(\tau_1) = \frac{1}{\Gamma(\alpha)}\int_{\tau_1}^{t}\left(\log\frac{t}{s}\right)^{\alpha-1}f(s,u(s))\frac{ds}{s}.$$

Since u is a lower solution to $(4)-(5)$, we have

$$u(t) - u(\tau_1) \leq \frac{1}{\Gamma(\alpha)}\int_{\tau_1}^{t}\left(\log\frac{t}{s}\right)^{\alpha-1}f(s,u(s))\frac{ds}{s};\ t \in (\tau_1,\, \tau_2).$$

It follows from $y(\tau_1) = u(\tau_1)$ that

$$u(t) \leq y(t);\ \text{for all } t \in (\tau_1,\, \tau_2),$$

which is a contradiction, since $u(t) > y(t)$ for all $t \in (\tau_1, \tau_2)$. Consequently,

$$u(t) \leq y(t) \text{ for all } t \in J_1.$$

Analogously, we can prove that

$$y(t) \leq v(t) \text{ for all } t \in J_1.$$

This shows that

$$u(t) \leq y(t) \leq v(t) \text{ for all } t \in J_1.$$

Consequently, the problem $(4) - (5)$ has a solution y satisfying $u \leq y \leq v$. Denote this solution by y_0.

Step 2: Consider the following problem:

$$^{Hc}D^{\alpha}_{t_1} y(t) = f(t, y(t)),\ t \in J_2 := [t_1, t_2], \tag{8}$$

$$y(t_1^+) = I_1(y_0(t_1^-)). \tag{9}$$

Consider the following modified problem:

$$^{Hc}D^{\alpha}_{t_1} y(t) = f_1(t, y(t)),\ t \in J_2, \tag{10}$$

$$y(t_1^+) = I_1(y_0(t_1^-)). \tag{11}$$

A solution to (10)–(11) is a fixed point of the operator $N_1 : C([t_1, t_2], \mathbb{R}) \longrightarrow C([t_1, t_2], \mathbb{R})$ defined by

$$N_1(y)(t) = \frac{1}{\Gamma(\alpha)} \int_{t_0}^{t} \left(\log \frac{t}{s}\right)^{\alpha-1} f_1(s, y(s)) \frac{ds}{s} + I_1(y_0(t_1^-)).$$

Since $y_0(t_1) \in [u(t_1^-), v(t_1^-)]$, (H4) implies that

$$u(t_1^+) \leq I_1(y_0(t_1^-)) \leq v(t_1^+),$$

that is

$$u(t_1^+) \leq y(t_1^+) \leq v(t_1^+).$$

Using the same reasoning as that used for problem (4)–(5), we can conclude the existence of at least one solution y to (10)–(11). We now show that this solution satisfies

$$u(t) \leq y(t) \leq v(t) \quad \text{for all} \quad t \in J_2.$$

Let y be the above solution to (10)–(11). We show that

$$u(t) \leq y(t) \quad \text{for all} \quad t \in J_2.$$

Let y be a solution of $(6) - (7)$. We prove that

$$u(t) \leq y(t) \text{ for all } t \in J_1.$$

Suppose not. Then there exist τ_3, τ_4 with $\tau_3 < \tau_4$ such that $u(\tau_3) = y(\tau_4)$ and

$$u(t) > y(t) \text{ for all } t \in (\tau_3, \tau_4).$$

In view of the definition of τ one has

$$^{Hc}D^{\alpha}y(t) = f(t, u(t)) \text{ for all } t \in (\tau_3,\, \tau_4).$$

An integration on $(\tau_3,\, t]$ with $t \in (\tau_3,\, \tau_4)$ yields

$$y(t) - y(\tau_3) = \frac{1}{\Gamma(\alpha)} \int_{\tau_3}^{t} \left(\log \frac{t}{s}\right)^{\alpha-1} f(s, u(s)) \frac{ds}{s}.$$

Since u is a lower solution to (4) $-$ (5), we have

$$u(t) - u(\tau_3) \leq \frac{1}{\Gamma(\alpha)} \int_{\tau_3}^{t} \left(\log \frac{t}{s}\right)^{\alpha-1} f(s, u(s)) \frac{ds}{s};\ t \in (\tau_3,\, \tau_4).$$

It follows from $y(\tau_3) = u(\tau_3)$ that

$$u(t) \leq y(t) \text{ for all } t \in (\tau_3,\, \tau_4),$$

which is a contradiction, since $u(t) > y(t)$ for all $t \in (\tau_3,\, \tau_4)$. Consequently,

$$u(t) \leq y(t) \text{ for all } t \in J_2.$$

Analogously, we can prove that

$$y(t) \leq v(t) \text{ for all } t \in J_2.$$

This shows that

$$u(t) \leq y(t) \leq v(t) \text{ for all } t \in J_2.$$

Denote this solution by y_1.

Step 3: We continue this process and take into account that $y_m := y|_{[t_{m-1}, t_m]}$ is a solution to the problem

$$^{Hc}D^{\alpha}_{t_{m-1}}y(t) = f(t, y(t)),\ t \in J_m := [t_{m-1}, t_m], \tag{12}$$

$$y(t_m^+) = I_m(y_{m-1}(t_{m-1}^-)). \tag{13}$$

Consider the following modified problem:

$$^{Hc}D^{r}_{t_{m-1}}y(t) = f_1(t, y(t)),\ t \in J_m, \tag{14}$$

$$y(t_m^+) = I_m(y_{m-1}(t_{m-1}^-)). \tag{15}$$

A solution to (14)–(15) is a fixed point of the operator $N_m : C([t_{m-1}, t_m], \mathbb{R}) \longrightarrow C([t_{m-1}, t_m], \mathbb{R})$ defined by

$$N_m(y)(t) = \frac{1}{\Gamma(\alpha)} \int_{t_m}^{t} \left(\log \frac{t}{s}\right)^{\alpha-1} f(s, y(s)) \frac{ds}{s} + I_m(y(t_{m-1}^-)).$$

Using the same reasoning as that used for problems (4)-(5) and (8)–(9) we can conclude the existence of at least one solution y to (12)–(13). Denote this solution by y_{m-1}.

The solution y of the problem (1)–(3) is then defined by

$$y(t) = \begin{cases} y_0(t), & t \in [t_0, t_1], \\ y_2(t), & t \in (t_1, t_2], \\ . \\ . \\ . \\ y_{m-1}(t), & t \in (t_{m-1}, t_m], \\ . \\ . \\ . \end{cases}$$

The proof is complete.

3.1 Nonoscillation and oscillation of solutions

The following theorem gives sufficient conditions to ensure the nonoscillation of solutions of problem (1)–(3).

Theorem 3.2 *Let u and v be lower and upper solutions, respectively, of (1)–(3) with $u \leq v$ and assume that*

(H5) u is eventually positive nondecreasing, or v is eventually negative nonincreasing.

Then every solution y of (1)–(3) such that $y \in [u, v]$ is nonoscillatory.

Proof. Assume that u is eventually positive. Thus there exists $T_u > t_0$ such that

$$u(t) > 0 \quad \text{for all} \quad t > T_u.$$

Hence $y(t) > 0$ for all $t > T_u$, and $t \neq t_k, k = 1, \ldots$ For some $k \in N$ and $t > t_u$, we have $y(t_k^+) = I_k(y(t_k))$. From (H4) we get $y(t_k^+) > u(t_k^+)$. Since for each $h > 0, u(t_k + h) \geq u(t_k) > 0$, one has $I_k(y(t_k)) > 0$ for all $t_k > T_u, k = 1, \ldots,$ which means that y is nonoscillatory. Analogously, if v is eventually negative, then there exists $T_v > t_0$ such that

$$y(t) < 0 \quad \text{for all} \quad t > T_v,$$

which means that y is nonoscillatory. This completes the proof.

The following theorem discusses the oscillation of solutions of problem (1)–(3).

Theorem 3.3 *Let u and v be lower and upper solutions, respectively, of (1)–(3), and assume that the sequences $u(t_k)$ and $v(t_k), k = 1, 2, \ldots,$ are oscillatory. Then every solution y of (1)–(3) such that $y \in [u, v]$ is oscillatory.*

Proof. Suppose on the contrary that y is a nonoscillatory solution of (1)–(3). Then there exists $T_y > 0$ such that $y(t) > 0$ for all $t > T_y$, or $y(t) < 0$ for all $t > T_y$. In the case when $y(t) > 0$ for all $t > T_y$ we have $v(t_k) > 0$ for all $t_k > T_y, k = 1, 2, \ldots,$ which is a contradiction since $v(t_k)$ is an oscillatory upper solution. Analogously, in the case $y(t) < 0$ for all $t > T_y$ we have $u(t_k) < 0$ for all $t_k > T_y, k = 1, 2, \ldots,$ which is also a contradiction, since $u(t_k)$ is an oscillatory lower solution.

3.2 An example

We consider the following impulsive fractional differential equation:

$$^{Hc}D^{\alpha}y(t) = f(t, y(t)), \quad \text{for each } t \in (t_k, t_{k+1}),\ 0 < \alpha < 1,\ \ k = 1, 2, \ldots, \tag{16}$$

$$y(t_k^+) = I_k(y(t_k^-)),\ k = 1, 2, \ldots, \tag{17}$$

$$y(1) = y_*, \tag{18}$$

where $f : J \times \mathbb{R} \to \mathbb{R}$. Assume that there exist $g_1(\cdot),\ g_2(\cdot) \in C(J, \mathbb{R})$ such that

$$g_1(t) \le f(t, y) \le g_2(t) \ \text{ for all } \ t \in J, \ \text{ and } \ y \in \mathbb{R},$$

and for each $t \in J$

$$\int_1^t g_1(s)\frac{ds}{s} \le I_k\left(\int_1^t g_1(s)\frac{ds}{s}\right),\ k \in \mathbb{N},$$

$$\int_1^t g_2(s)\frac{ds}{s} \ge I_k\left(\int_1^t g_2(s)\ \frac{ds}{s}\right),\ \ k \in \mathbb{N}.$$

Consider the functions $u(t) := \displaystyle\int_1^t g_1(s)\frac{ds}{s}$ and $v(t) := \displaystyle\int_1^t g_2(s)\frac{ds}{s}$. Clearly, u and v are lower and upper solutions of the problem (16)-(18), respectively; that is,

$$^{Hc}D^{\alpha}u(t) \le f(t, u(t)) \ \text{ for all } \ t \in J,$$

and

$$^{Hc}D^{\alpha}v(t) \ge f(t, v(t)) \ \text{ for all } \ t \in J.$$

Since all the conditions of Theorem 3.1 are satisfied, the problem (16)-(18) has at least one solution y on J with $u \le y \le v$. If $g_1(t) > 0$, then u is positive and nondecreasing, thus y is nonoscillatory. If $g_2(t) < 0$, then v is negative and nonincreasing, thus y is nonoscillatory. If the sequences $u(t_k)$ and $v(t_k)$ are both oscillatory, then y is oscillatory.

4 Conclusion

In this paper, we have provided some sufficient conditions guaranteeing the existence of the oscillatory and nonoscillatory solutions of a class of impulsive differential equations involving the Caputo–Hadamard fractional derivative. We use the concept of the upper and lower solutions method combined with the nonlinear alternative of Leray–Schauder type.

Acknowledgements

The research of J.J. Nieto has been partially supported by the Agencia Estatal de Investigación (AEI) of Spain under grant MTM2016-75140-P, co-financed by the European Community fund FEDER, and Xunta de Galicia, grants GRC 2015-004 and R 2016-022.

References

[1] S. Abbas, M. Benchohra, J.R. Graef and J. Henderson. *Implicit Fractional Differential and Integral Equations: Existence and Stability*. De Gruyter, Berlin, 2018.

[2] S. Abbas, M. Benchohra, J.E. Lazreg and Y. Zhou, A Survey on Hadamard and Hilfer fractional differential equations: Analysis and Stability. *Chaos, Solitons Fractals* **102** (2017) 47–71.

[3] S. Abbas, M. Benchohra and G.M. N'Guérékata. *Topics in Fractional Differential Equations*. Springer, New York, 2012.

[4] S. Abbas, M. Benchohra and G.M. N'Guérékata. *Advanced Fractional Differential and Integral Equations*. Nova Science Publishers, New York, 2015.

[5] M. Benchohra and S. Hamani, The method of upper and lower solution and impulsive fractional differential inclusions. *Nonlinear Anal.: Hybrid Syst.* **3** (2009) 433–440.

[6] M. Benchohra, S. Hamani and J. Henderson. Oscillation and nonoscillation for impulsive dynamic equations on certain time scales. *Adv. Difference Equ.* **2006** (2006), Art. 60860, 12 pages.

[7] M. Benchohra, J. Henderson and S. K. Ntouyas. *Impulsive Differential Equations and Inclusions*. Hindawi Publishing Corporation, Vol 2, New York, 2006.

[8] Z. Denton, P. W. Ng and A.S. Vatsala. Quasilinearization method via lower and upper solutions for Riemann-Liouville fractional differential equations. *Nonlinear Dyn. Syst. Theory* **11** (3) (2011) 239–251.

[9] J. Dzurina, E. Thandapani, B. Baculikova, C. Dharuman and N. Prabaharan. Oscillation of second order nonlinear differential equations with several sub-linear neutral terms. *Nonlinear Dyn. Syst. Theory* **19** (1) (2019) 124–132.

[10] F. Jarad, T. Abdeljawad, and D. Baleanu. Caputo-type modification of the Hadamard fractional derivatives. *Adv. Difference Equa.* 2012:142, 8 pages.

[11] R. Hilfer. *Applications of Fractional Calculus in Physics*. World Scientific, Singapore, 2000.

[12] A. A. Kilbas, Hari M. Srivastava, and Juan J. Trujillo. *Theory and Applications of Fractional Differential Equations*. North-Holland Mathematics Studies, 204. Elsevier Science B.V., Amsterdam, 2006.

[13] G. S. Ladde,V. Lakshmikanthan and A. S. Vatsala. *Monotone Iterative Technique for Nonlinear Differential Equations*. Pitman Advanced Publising Program, London, 1985.

[14] G. I. Melnikov, N. A. Dudarenko, K. S. Malykh, L. N. Ivanova and V. G. Melnikov. Mathematical models of nonlinear oscillations of mechanical systems with several degrees of freedom. *Nonlinear Dyn. Syst. Theory* **17** (4) (2017) 369–375.

[15] I. Podlubny. *Fractional Differential Equations*. Academic Press, San Diego, 1999.

[16] J. Singh, D. Kumar and J.J. Nieto. Analysis of an El Nino-Southern Oscillation model with a new fractional derivative. *Chaos, Solitons Fractals* **99** (2017) 109–115.

[17] V. Singh and D. N. Pandey. Mild solutions for multi-term time-fractional impulsive differential systems. *Nonlinear Dyn. Syst. Theory* **18** (2018) 307–318.

[18] M. Sowmya and A. S. Vatsala. Generalized iterative methods for Caputo fractional differential equations via coupled lower and upper solutions with superlinear convergence. *Nonlinear Dyn. Syst. Theory* **15** (2015) 198–208.

[19] D. Stutson and A. S. Vatsala. Generalized monotone method for Caputo fractional differential systems via coupled lower and upper solutions. *Dynam. Systems Appl.* **20** (2011) 495–503.

Nonlinear Dynamics and Systems Theory, **19** (4) (2019) 486–496

Higher-Order Sliding Mode Control of a Wind Energy Conversion System

S. Boulkhrachef[1], A. Moualdia[1*], DJ. Boudana[1] and P. Wira[2]

[1] *Laboratory of Electrical Engineering and Automatics (LREA), University of Medea, Algeria*
[2] *Laboratory of Modeling Intelligence Process Systems, University of Haute–Alsace (MIPS), Mulhouse, France*

Received: Jully 9, 2019;   Revised: September 30, 2019

Abstract: This work presents a control strategy employing the second-order sliding mode for a variable-speed wind energy system based on a double-fed asynchronous machine (DFIG). This technique finds its stronger justification in the problem of using a nonlinear control law robust to inaccuracies in the model. The objective is to apply this command to independently control the active and reactive power generated by the double-fed asynchronous machine decoupled from the flow direction. The use of this method provides very satisfactory performance for the DFIG control. The overall strategy has been validated on a 7.5 kW wind turbine driven by a DFIG using the Matlab/Simulink. The numerical simulation results show the growing importance of this control in the systems of wind energy conversion.

Keywords: *DFIG; PWM converters; MPPT, higher-order sliding mode controller; wind energy.*

Mathematics Subject Classification (2010): 03B52, 93C42, 94D05.

1 Introduction

The consumption of electricity has increased dramatically over the past decade because of the massive industrialization of some countries and the significant population increase. During the first half of the century, fossil fuels remain the main source of energy, which consequently causes environmental problems in terms of global warming and climate change. Nowadays, the renewable energy attracted the interest of several research teams. Thus, the development of wind turbines is a great investment in technological research.

* Corresponding author: mailto:amoualdia@gmail.com

Among these sources of renewable energy, wind energy has the greatest energy potential. With the power of wind turbines installed around the world increasing every year, wind systems can no longer act as active power generators in distribution or transmission networks, depending on the installed capacity. Indeed, they will certainly be led, in the short term, to provide system services (reactive power compensation, for example) such as conventional power plant generators and / or to participate in the improvement of the quality of electrical energy (filtering harmonic currents, in particular). Much of the wind turbines installed today are equipped with a double-fed induction machine (DFIG) [1, 2].

This generator allows power generation variable speed; this then allows better use of wind resources under different wind conditions. These turbines are also equipped with a propeller-pitch blade to accommodate variable wind conditions. The entire wind turbine is controlled to maximize the power produced continuously searching for the operating point at maximum power commonly called MPPT. However, this type of energy is an energy booster in relation to nuclear generation and remains largely predominant in many works presenting the DFIG with diverse control diagrams. These control diagrams are frequently based on the vector control notion with sliding mode controllers as proposed in [2, 3].

In the electromechanical conversion chain of a wind turbine system, three-phase static voltage converters are essential elements because they make it possible to control the active and reactive powers injected into the electrical network as a function of the wind speed applied to the wind turbine blades.

In recent years, the sliding mode control (SMC) methodology has been widely used for the control of nonlinear systems. It achieves a robust control by adding a discontinuous control signal across the sliding surface, satisfying the sliding condition. Nevertheless, this type of control has an essential disadvantage, which is the chattering phenomenon caused by the discontinuous control action. To treat these difficulties, several modifications to the original sliding mode control law have been proposed, the most common and recent strategy is using a second order sliding mode controller as in [1, 2].

The proposed control strategy is a second-order sliding mode for the DFIG control. This strategy possesses attractive features such as the chattering-free behavior and robustness. This work is organized as follows. In Section 2, we briefly review the modeling of the whole system under study. Section 3 provides the detail of the second-order sliding mode control technique and its application to the DFIG control.

The system under study is shown in Figure 1. This farm consists of three aerogenerators, where each one is connected to a variable-speed asynchronous generator. For operation at variable speed, three rectifiers are used to connect the generators to the DC bus. This bus is linked to the electrical network via a tow level inverter and an RL (resistance R and inductor L) filter. The subject of this paper consists in designing control strategies for a wind energy conversion system, connected to the network based on the rotor-powered dual-power asynchronous machine via two reversible PWM converters (one rotor side and the other network side) in back-to-back mode, realizing the electrical interface between the rotor of the machine and the network. The control of the latter consists in regulating the intermediate DC bus regardless of the power generated by the conversion system under variable frequency.

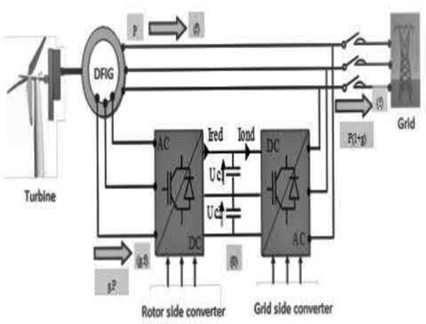

Figure 1: The overall pattern of a chain of wind energy conversion.

2 System Model

2.1 Wind turbine model

For a horizontal axis wind turbine, the mechanical power captured from the wind is given by [14]

$$P_t = \frac{1}{2} C_p(\lambda, \beta) R^2 \rho V^3, \tag{1}$$

where R is the radius of the turbine in (m), ρ is the air density (kg/m^3), V is the wind speed (meter/second), and (C_p) is the power coefficient which is a function of both the tip speed ratio λ and the blade pitch angle β (degre). In this work, the (C_p) equation is approximated using a non-linear function according to [15]

$$C_p = (0.5 - 0.167)(\beta - 2) \sin\left[\frac{\pi(\lambda + 0.1)}{18.5 - 0.3(\beta - 2)}\right] - 0.0018(\lambda - 3)(\beta - 2). \tag{2}$$

The tip speed ratio λ is given by

$$\lambda = \frac{R\Omega_t}{V}, \tag{3}$$

where Ω_t is the angular velocity of the wind turbine.

2.2 The DFIG model

The application of the Park transformation to the three-phase model of the DFIG permits to write the dynamic voltages and fluxes equations in an arbitrary dq reference frame:

$$\begin{cases} V_{sd} = R_s i_{sd} + \frac{d}{dt}\Phi_{sd} - \omega_s \Phi_{sq}, \\ V_{sq} = R_s i_{sq} + \frac{d}{dt}\Phi_{sq} + \omega_s \Phi_{sd}, \\ V_{rd} = R_r i_{rd} + \frac{d}{dt}\Phi_{rd} - \omega_r \Phi_{rq}, \\ V_{rq} = R_r i_{rq} + \frac{d}{dt}\Phi_{rq} + \omega_r \Phi_{rd}, \end{cases} \tag{4}$$

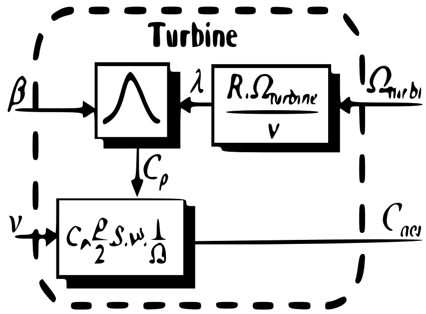

Figure 2: Turbine model.

$$\begin{cases} \Phi_{sd} = L_s i_{sd} + M i_{rd}, \\ \Phi_{sq} = L_s i_{sq} + M i_{rq}, \\ \Phi_{rd} = L_r i_{rd} + M i_{sd}, \\ \Phi_{rq} = L_r i_{rq} + M i_{sq}. \end{cases} \tag{5}$$

The stator and rotor angular velocities are linked by the following relation: $\omega_s = \omega + \omega_r$, where ω_s is the electrical pulsation of the stator and ω_r is the rotor one, ω is the mechanical pulsation of the DFIG. This electrical model is completed by the mechanical equation

$$C_{em} = C_r + J\frac{d\Omega}{dt} + f\Omega, \tag{6}$$

where C_r is the resisting torque, Ω is the mechanical speed of the DFIG, J is the inertia, f is the viscous friction and p is the number of the pairs of poles. In the two-phase reference, the stator active and reactive power of induction generator is written as

$$\begin{cases} P_s = V_{sd} i_{sd} + V_{sq} i_{sq}, \\ Q_s = V_{sq} i_{sd} - V_{sd} i_{sq}. \end{cases} \tag{7}$$

The wind farm is controlled to extract the maximum power available. According to the Betz theory, the power coefficients C_p do not exceed 0.593 [12,13], which corresponds to the Betz limit. Therefore, the power produced by a turbine is 59.3 % of the available power of wind. In this case, the variation of C_p as a function of λ for $\beta = 0$ is shown in Figure 4, then the maximum value of C_p ($C_{pmax} = 0.45$) corresponds to the optimal value of λ (λ_{opt} =8.1). The electromagnetic torque reference given by the MPPT strategy is defined by equation (7).

$$C_{em-Opt} = \frac{C_p \rho \pi R^5 \Omega_{mec}^2}{2\lambda_{opt}^3 G^3}. \tag{8}$$

3 Control Strategy of the DFIG

3.1 Active and reactive power decoupling

In order to easily control the production of electricity by the wind turbine, we will carry out an independent control of active and reactive powers by orientation of Φ_s. By choosing a reference frame linked to Φ_s, rotor currents will be related directly to the

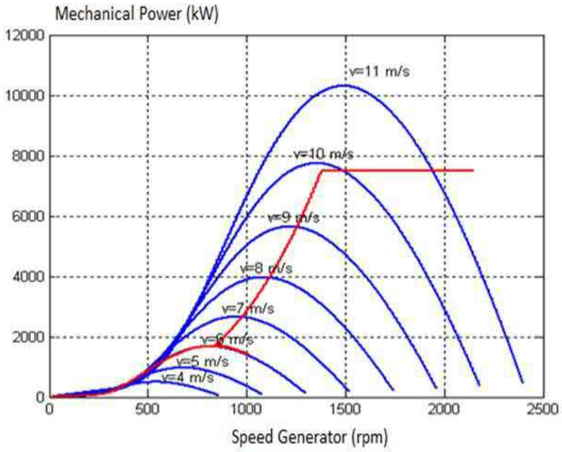

Figure 3: Mechanical power variation.

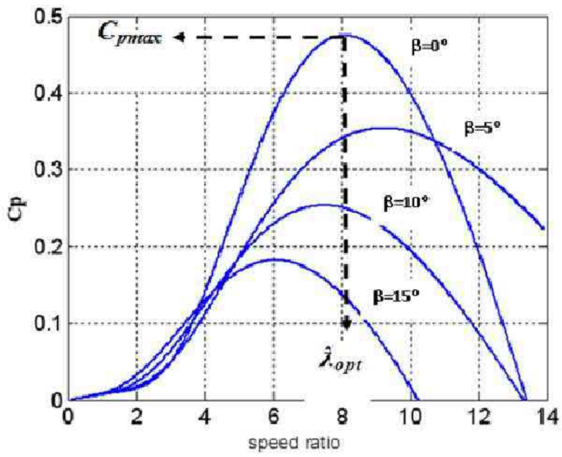

Figure 4: Power coefficient versus λ curve.

stator active and reactive power. An adapted control of these currents will thus permit to control the power exchanged between the stator and the grid. If the Φ_s is linked to the d-axis of the frame, we have

$$\begin{cases} \Phi_{sd} = \Phi_s, \\ \Phi_{sq} = 0. \end{cases} \tag{9}$$

The electromagnetic torque can then be expressed as follows:

$$C_{em} = p\frac{M}{L_s}\Phi_s i_{sq}. \tag{10}$$

By substituting (8) in (5), the following rotor flux equations are obtained:

$$\begin{cases} \Phi_s = L_s i_{sd} + M i_{rd}, \\ 0 = L_s i_{sq} + M i_{rq}. \end{cases} \tag{11}$$

In addition, the stator voltage equations are reduced to

$$\begin{cases} V_{sd} = R_s i_{sd} + \frac{d}{dt}\Phi sd, \\ V_{sq} = R_s i_{sq} + \omega_s \Phi s. \end{cases} \tag{12}$$

If the per-phase stator resistance is neglected, which is a realistic approximation for medium power machines used in the wind energy conversion, and by supposing that the electrical supply network is stable, for a simple voltage constant V_s we will have a constant stator flux ϕ_s constant. This consideration associated with (11) shows that the new stator voltage expressions can be written as follows:

$$\begin{cases} V_{sd} = 0, \\ V_{sq} = \omega_s \Phi s. \end{cases} \tag{13}$$

Using (10), a relation between the stator and rotor currents can be established:

$$\begin{cases} i_{sd} = -\frac{M}{L_s} i_{rd} + \frac{\phi_s}{L_s}, \\ i_{sq} = -\frac{M}{L_s} i_{rq}. \end{cases} \tag{14}$$

By using (4), (5), (13) and (14), the stator active and reactive powers, the rotor fluxes and the rotor voltages can be written versus rotor currents as

$$\begin{cases} P_s = -\frac{M\omega_s\Phi_s}{L_s} i_{rq}, \\ Q_s = -\frac{M\omega_s\Phi_s}{L_s} i_{rd} + \frac{\omega_s\phi_s^2}{L_s}, \end{cases} \tag{15}$$

$$\begin{cases} \phi_{rd} = \sigma L_r i_{rd} + \frac{L_m\phi_s}{L_s}, \\ \phi_{rq} = \sigma L_r i_{rq}, \end{cases} \tag{16}$$

$$\begin{cases} V_{rd} = R_r i_{rd} + \sigma L_r \frac{d}{dt} ird - \sigma\omega_s L_r i_{rq}, \\ V_{rq} = R_r i_{rq} + \sigma L_r \frac{d}{dt} irq + \sigma g \omega_s L_r i_{rd} + \omega_s \frac{L_m\phi_s}{L_s}. \end{cases} \tag{17}$$

3.2 Second-order sliding mode power control of the DFIG

The sliding mode control (SMC) is one of the most interesting nonlinear control approaches. Nevertheless, a few drawbacks arise in its practical implementation, such as the chattering phenomenon and undesirable mechanical effort. In order to reduce the effects of these problems, a high-order sliding mode seems to be a very attractive solution. This method generalizes the essential sliding mode idea by acting on the higher-order time derivatives of the sliding manifold instead of influencing the first time derivative as in the case of the SMC [10, 18]. The main feature of this control is that it only needs to drive the error to a switching surface. In this study, the errors between the measured and reference d and q rotor currents have been chosen as sliding mode surfaces, so the following expression can be written:

$$\begin{cases} S_d = i_{rd-ref} - i_{rd}, \\ S_q = i_{rq-ref} - i_{rq}. \end{cases} \tag{18}$$

Replacing the d and q rotor currents derivatives in (18) by their expressions taken from (17), one obtains

$$\begin{cases} \dot{S}_d = \dot{I}_{rd-ref} - \dot{I}_{rd} & = \frac{1}{L_r\sigma} V_{rd} + \frac{1}{L_r\sigma} \left(-R_r i_{rd} + g\omega_s L_r \sigma i_{rq}\right) + \dot{I}_{rd-ref}, \\ \dot{S}_q = \dot{I}_{rq-ref} - \dot{I}_{rq} & = \frac{1}{L_r\sigma} V_{rq} + \frac{1}{L_r\sigma} \left(-R_r i_{rd} + g\omega_s L_r \sigma i_{rd} - g\omega_s \phi_s \frac{L_m}{L_s}\right) + \dot{I}_{rq-ref}. \end{cases} \tag{19}$$

For the sliding mode surfaces given by (20), the following expression can be written:

$$\begin{cases} \ddot{S}_d = \wedge_1 (t, x) V_{rd} + Y_1 (t, x), \\ \ddot{S}_q = \wedge_2 (t, x) V_{rq} + Y_2 (t, x), \end{cases} \tag{20}$$

where $\wedge_1(t, x)$, $\wedge_2(t, x)$, Y1(t,x) and Y2(t,x) are uncertain functions which satisfy

$$\begin{cases} Y_1 > 0, |Y_1| > \lambda_1, 0 < K_{m1} < \wedge_1 < K_{M1}, \\ Y_2 > 0, |Y_2| > \lambda_2, 0 < K_{m1} < \wedge_2 < K_{M2}. \end{cases} \tag{21}$$

We define the same higher-order slip surfaces considered for power control design:

$$\begin{cases} \dot{S}_1 = F.V_{rd} + G_1, \\ \dot{S}_2 = F.V_{rq} + G_2. \end{cases} \tag{22}$$

Based on the algorithm of super twisting introduced by Levant in [12], one proposes the following command [15]:

$$\begin{cases} V_{rd} = \alpha_1 \int sign\,(S_1)\, dt + \beta_1 \left|S_1\right|^{0.5} sign\,(S_1), \\ V_{rq} = \alpha_2 \int sign\,(S_2)\, dt + \beta_2 \left|S_2\right|^{0.5} sign\,(S_2). \end{cases} \tag{23}$$

4 Simulation Results

In the objective to evaluate the performances of the $second - order$ sliding mode controller, simulation tests are realized with a 7.5 kW generator coupled to a 400V/50 Hz grid. Simulation of the whole system has been realized using Matlab/Simulink. Figure 6 illustrates the waveforms of the wind profile used in the simulation. In this figure, the wind speed is around 13 (m/s) which corresponds to the maximum power generation. Figure 7 shows also that the stator current obtained by the DFIG has a sinusoidal form, which implies a clean energy without harmonics provided by the DFIG. Figure 8 shows the simulation results of the whole system given by the bloc diagram in Figure 1. This diagram presents a DFIG model associated with a wind turbine which is controlled by

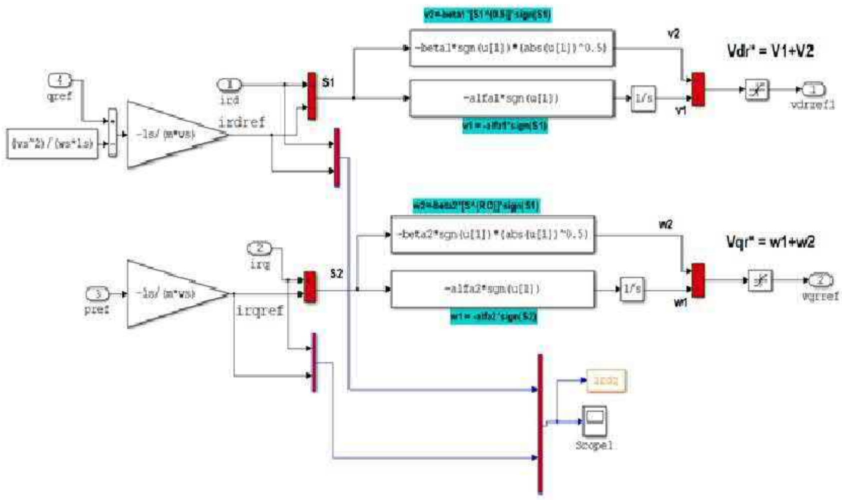

Figure 5: Algorithm of super twisting.

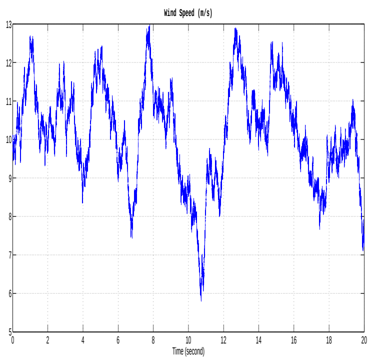

Figure 6: Wind speed profile.

the MPPT (Maximum Power Point Tracking) strategy. As is shown in this figure, for a variable wind speed, the stator active power produced by the DFIG is controlled according to the MPPT strategy and is around 7.5 kW, which represents the nominal power of the DFIG while the stator reactive power is maintained to zero. In addition, it can be noticed that the direct and quadrature rotor current take the same forms as the stator reactive and active power, respectively, as shown in Figure 9.

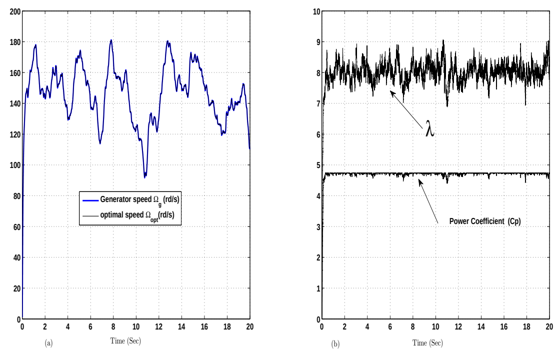

Figure 7: MPPT results: (a) generator speed, (b) coefficient power C_p and the speed ratio (λ).

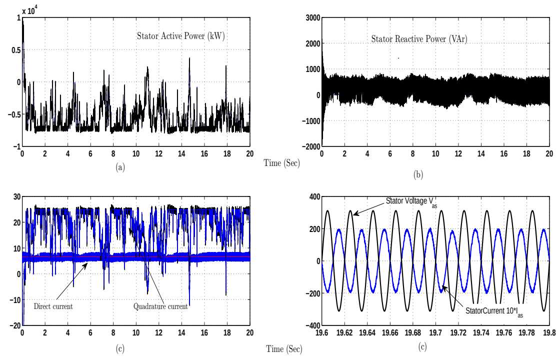

Figure 8: (a), (b) show the stator active and reactive power, (c) rotor direct and quadrature currents, (d) zoom in the stator current and grid voltage.

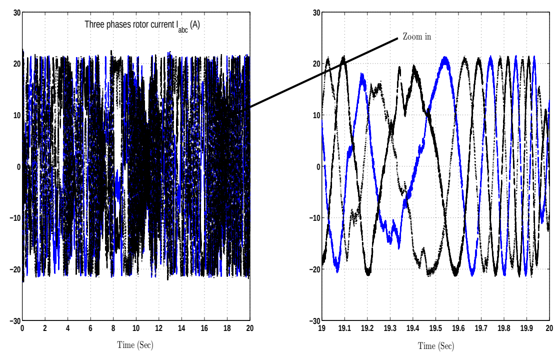

Figure 9: (a) shows rotor currents, (b) zoom in rotor currents.

5 Conclusion

In this paper, we set the higher-order sliding mode control of an energy conversion system based on the double-fed asynchronous machine. In the first step, a model of the wind turbine was proposed. Next, a control strategy by sliding mode of the wind turbine assuming an independent control of power has been recommended. Regulators of active and reactive power by sliding mode have been proposed and tested. The simulation results allowed us to determine the properties of the sliding mode control. Through the simulation results and, specifically, the response of the active and reactive power, there are good performances even in the presence of variation orders. Note that there is a sudden change during the transient. The continuation in power is perfect. The stability and convergence to the equilibrium is assured. In addition, for these types of adjustment (sliding mode) a practical control algorithm is robust and simple to implement.

Acknowledgment

The research is part of a project CNEPRU (refs :A01L07U260 1200150005, Jan 2016), realized in the laboratory of electrical engineering and automatic LREA research, University of Medea, Algeria.

References

[1] A. Moualdia, M.O. Mahmoudi and L. Nezli. Direct torque control of the DFIG and direct power control for grid side converter in wind power generation system. *The Mediterranean Journal of Measurement and Control, MEDJMC* **9**(3) (2013) 101–108.

[2] ER. Sanseverino, Di. Sanseverino, ML. Silvestre, MG. Ippolito and De. Paola. An execution, monitoring and replanting approach for optimal energy management in micro-grids. *Energy* **36**(5) (2011) 3429–3436.

[3] A. Rabiee, H. Khorramdel and A. Aghaei. A review of energy storage systems in micro-grids with wind turbines. *Renewable and Sustainable Energy Reviews* **18** (2) (2013) 316–326.

[4] A. Chalanga, S. Kamal and B. Moreno. Implementation of super-twisting control: super-twisting and higher order sliding-mode observer-based approaches. *IEEE Trans. Industrial Electronics* **63**(6) (2016) 3677–3685.

[5] G. Bartolini, A. Ferrara and E. Usai. Chattering avoidance by second-order sliding mode control. *IEEE Trans. on Automatic Control* **43** (2)(1998) 241–246.

[6] H. Pan and X. Chen. Global robust optimal sliding mode control for uncertain affine nonlinear systems. *Journal of Systems Engineering and Electronics* **20**(4)(2009) 838–843.

[7] V. Utkin. Discussion aspects of high-order sliding mode control. *IEEE Trans. Automatic Control* **61** (3)(2016) 829–833.

[8] C. Wang and H. Yau. Nonlinear dynamic analysis and sliding mode control for a gyroscope system. *Nonlinear Dynamics.* **66**(1–2)(2013) 53–65.

[9] Y. Shtessel and L. Shkolnikov. An Asymptotic Second-Order Smooth Sliding Mode Control. *Asian Journal of Control.* **5**(4) (2003) 498–504.

[10] ZH. Ismail and VW. Putranti. Second order sliding mode control scheme for an autonomous underwater vehicle with dynamic region concept. *Mathematical Problems in Engineering* **42**(12) (2015) 1–13.

[11] A. Tlemcani, K. Sebaa and N. Henin. Indirect adaptive fuzzy control of multivariable non-linear systems class with unknown parametres. *Nonlinear Dynamics and Systems Theory* **14**(2) (2014) 162–174.

[12] T. Chiew, Z. Jamaludin, AB. Hashim, K. LLeo, A. Abdullah and N. Rafan. Analysis of tracking performance in machine tools for disturbance forces compensation using sliding mode control and PID controller. *International Journal of Mechanical and Mechatronics Engineering.* **12** (2012) 34–40.

[13] M. Liserre, R. Cardenas, M. Molinas and J. Rodriguez. Overview of multi-MW wind turbines and wind parks. *IEEE Trans. Ind. Electron.* **58**(4) (2011) 1081–1095.

[14] F. Valenciaga and P.F. Puleston. Variable structure control of a wind energy conversion system based on a brushless doubly fed reluctance generator. *IEEE Trans. Energy Convers* **22**(2) (2008) 499–506.

[15] M. Tazil, V. Kumar, R.C. Bansal, S. Kong, Z.Y. Dong, W. Freitas, and H.D. Mathur. Three-phase doubly fed induction generators: An overview. *IET Elect. Power Appl.* **04**(2) (2010) 75–89.

[16] F. Hamidia, A. Abadi, A. Tlemcani and M.S. Boucherit. Dual star induction motor supplied with double photovoltaic panels based on fuzzy logic type–2. *Nonlinear Dynamics and Systems Theory* **18**(4) (2018) 359–371.

[17] A. Abadi, H. Hamidia, A. Morsli and A. Tlemcani. Optimal voltage controller using T–S fuzzy model for multimachine powersystems. *Nonlinear Dynamics and Systems Theory* **19**(2) (2019) 217–226.

[18] H. Hamidia, A. Larabi, A. Tlemcani and M.S. Boucherit. AIDTC Techniques for Induction Motors. *Nonlinear Dynamics and Systems Theory* **13**(2) (2013) 147–156.

[19] S. Bentouati, A. Tlemcani, M.S. Boucherit and L. Barasane. A DTC Neurofuzzy Speed Regulation Concept for a Permanent Magnet Synchronous Machine. *Nonlinear Dynamics and Systems Theory* **13**(4) (2013) 344–358.

Nonlinear Dynamics and Systems Theory, **19** (4) (2019) 497–511

Resonance in the Motion of a Geo-Centric Satellite Due to the Poynting-Robertson Drag and Oblateness of the Earth

Charanpreet Kaur [1*], Binay Kumar Sharma [2] and Sushil Yadav [3]

[1] *Department of Mathematics, S.G.T.B. Khalsa College, University of Delhi, Delhi-110052, India*
[2] *Department of Mathematics, S.B.S. College, University of Delhi, Delhi-110017 India*
[3] *Department of Mathematics, Maharaja Agrasen College, University of Delhi, Delhi-110096, India*

Received: December 26, 2017; Revised: September 21, 2019

Abstract: In this paper, we have investigated resonances in a geo-centric satellite under the gravitational effect of the Sun, the Earth, oblateness of the Earth and the Poynting-Robertson (P-R) drag. It is found that resonances occur due to the commensurability between satellite's mean motion and average angular velocity of the Earth around the Sun, and also between the satellite's mean motion and average angular velocity of the regression angle. Amplitudes and time periods of the oscillation at the resonance points have been determined. Effects of oblateness and P-R drag on the amplitudes and time periods of oscillation at different resonance points have been analyzed graphically. We have also compared the values of the amplitude and time period of oscillations due to the oblateness parameter and P-R drag. We have observed that amplitude as well as the time period decreases as ϕ (an orbital angle of the Earth around the Sun) increases between -90^0 to 90^0, and the effect of the P-R drag parameter is minor on the amplitudes and time periods. Also, the amplitude and time-period decrease as ψ increases between -90^0 to 90^0.

Keywords: *three-body problem; ecliptic plane; orbital plane; resonance; Poynting-Robertson drag; oblateness.*

Mathematics Subject Classification (2010): 37N05.

* Corresponding author: mailto:syadav@mac.du.ac.in

1 Introduction

One of the most important phenomena in the solar system is the occurrence of resonance which plays a significant role in the study of dynamical system. Resonance occurs when any two or more frequencies are commensurable in their ratio. The resonance in the orbital motion of the celestial bodies occurs not only due to the gravitational forces but also the non gravitational forces, for e.g., radiation pressures, oblateness, P-R drag, equatorial ellipticity of the Earth etc.

[3] discussed the motion of a geosynchronous satellite by taking the combined gravitational forces of the Sun (with radiation pressure), the Moon and the Earth. They showed for the geosynchronous satellite that angular velocity of the orbital plane lies between 0.042^0 to 0.58^0 degree per year.

[4] discussed numerically the effects of P-R drag on the equilibrium points of the photo-gravitational CR3BP including the P-R effect by taking the radiation of two massive bodies. They have used the modified bisection method to compute the position of the equilibrium points.

[7] studied the minimum fuel maneuvers to change the position of a spacecraft in orbit around the Earth. Bi-impulsive maneuver control is applied in the initial position of the satellite to send it to a transfer orbit that will cross the desired final position of the spacecraft where both the initial and the final position of satellite belong to the same Keplerian orbit.

[8] investigated the numerical search of bounded relative motion between two or more satellites. They studied the possibility of using global optimization technique to locate the initial conditions resulting into minimum drift per orbit as the perturbations such as the Earth oblateness and air drag effects are taken into account, an analytic solution appears to be more complicated.

Other pioneers in this field are [12], [6], [9], [11], [13], [5], [10], [14], [15].

The P-R effect in the three-body problem on numerical experiments in dynamical consequences has been discussed by many authors by taking only two of the three: (1) the P-R drag; (2) the three-body problem; (3) resonance. Taking all the three factors in this paper collectively, we have attempted to bridge the said gap. The motive of this paper is to investigate the resonance in the motion of geo-centric satellite due to the Poynting-Robertson drag and oblateness of the Earth in the framework of the three-body problem. Meticulous study of equations of motion in Section 2 of this paper reveals that if the regression angle is constant, there are five critical points $R_i's$, $i = 1 - 5$, at which resonance occurs in the motion of the orbiting satellite, between the mean motion of the satellite and the average angular velocity of the Earth around the Sun and if the regression angel is not constant, resonance occurs at six points $R_j''s$, $j = 1 - 6$, with two frequencies due to the oblateness of the Earth and at many points with three frequencies. Evaluation of the corresponding amplitude and time period at resonance points have been evaluated in Section 3. Discussion and conclusion are given in Section 4. In this section we have compared the amplitudes and time periods at same resonant point and for different values of q's, and also discussed the variation in the amplitudes and time periods for variation in q and ϕ at the resonant point $1 : 1$ and $1 : 2$ with the P-R drag and without the P-R drag. Further we have drawn graphs showing amplitudes and time periods due to oblateness of the Earth (J_2) at different resonant points.

2 Statement of the Problem and Equations of Motion

Let S represent the Sun, E be the Earth and $\bar{S}$ be the satellite with the masses M_S, M_E and M_P, respectively. The satellite moves around the Earth in orbital plane. Let the satellite be revolving about the Earth with the angular velocity $\vec{\omega}$ and the system be also revolving with the same angular velocity $\vec{\omega}$. Let $\vec{r}_E$, $\vec{r}_s$ and $\vec{r}$ represent the vectors from the Sun and the Earth, the Sun and the satellite and the Earth and the satellite, respectively; γ be the vernal equinox, α be the angle between the ecliptic plane and orbital plane, θ be the angle between the direction of ascending node and the direction of the satellite, ϕ be the angle between the direction of ascending node and the direction of the Sun, ψ be the regression angle, ϵ be the angle between the equatorial plane and ecliptic plane (obliquity) and c be the velocity of light. For convenience, let x, y, z be the co-ordinate system of the satellite with the origin at the center of the Earth with the unit vectors $\hat{I}$, $\hat{J}$ and $\hat{K}$ along the co-ordinates axes, respectively. Let x_0, y_0 and z_0 be another set of the co-ordinate system in the same plane, with the origin at the center of the Earth, with the unit vectors $\hat{I}_0$, $\hat{J}_0$ and $\hat{K}_0$ along the co-ordinate axes. Let X_G, Y_G and Z_G be the geo-centric reference system with the unit vectors $\hat{I_G}$, $\hat{J_G}$ and $\hat{K_G}$, respectively, along the co-ordinate axes, while the $X_G Y_G$ plane be the Earth's equatorial plane, which makes an angle $23^0 27'$ with the ecliptic plane (Figure 1).

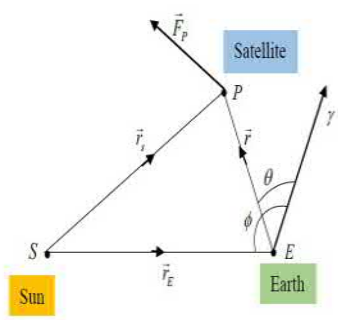

(a)

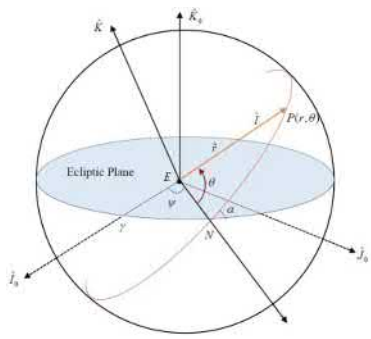

(b)

Figure 1: Configuration of the three-body problem; (a) in vector form; (b) with co-ordinate axis.

2.1 Equations of motion in polar form

Let $\vec{F}_P$ be the Poynting-Robertson drag per unit mass acting on the satellite due to the radiating body (the Sun) as shown in Figure 1, given by [4]

$$M_P \vec{F}_P = \vec{f}_1 + \vec{f}_2 + \vec{f}_3,$$

where

$\vec{f}_1 = F \dfrac{\vec{r}_s}{r_s}$ (the radiation pressure),

$\vec{f}_2 = -F \dfrac{(\vec{v} \cdot \vec{r}_s)}{c} \dfrac{\vec{r}_s}{r_s}$ (the Doppler shift owing to the motion),

$\vec{f}_3 = -F\dfrac{\vec{v}}{c}$ (the force due to the absorption and re-emission of part of the incident radiation),

$\vec{v} =$ the velocity of $\bar{S}$,

$c =$ the velocity of light,

$F =$ the measure of the radiation pressure.

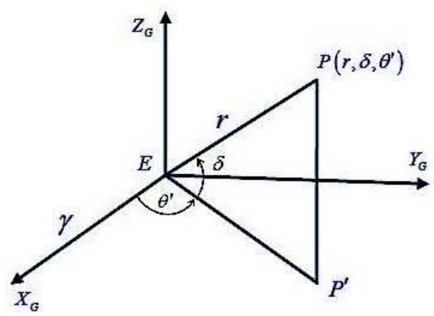

Figure 2: The coordinate system of the satellite in (X_G, Y_G, Z_G) system.

The relative motion of the satellite with respect to the Earth is obtained by

$$\ddot{\vec{r}} = \ddot{\vec{r}}_s - \ddot{\vec{r}}_E = \frac{\vec{F}_{SP} + \vec{F}_{EP} + \vec{F}_P \vec{M}_P}{M_P} - \frac{\vec{F}_{SE}}{M_E},$$

where

$$\vec{F}_{SP} = -G\frac{M_s M_p}{{r_s}^3}\vec{r}_s, \qquad \vec{F}_{SE} = -G\frac{M_s M_E}{{r_E}^3}\vec{r}_E.$$

Force of the Earth on the satellite: We take the potential of the Earth [2] at the point outside it in the form

$$U = \frac{GM_E M_P}{r}\left\{1 - \frac{J_2(R_\oplus)^2}{2r^2}\left(3\frac{(Z_G)^2}{r^2} - 1\right)\right\} + \ldots,$$

$$\vec{F}_{EP} = \frac{\partial U}{\partial r}\vec{r} + \frac{\partial U}{\partial X_G}I_G + \frac{\partial U}{\partial Y_G}J_G + \frac{\partial U}{\partial Z_G}K_G$$

$$= -\frac{GM_E}{r^3}\left(\frac{3J_2(R_\oplus)^2}{2r^2}(5\frac{(Z_G)^2}{r^2} - 1) - 1\right)\vec{r} - \frac{3J_2(R_\oplus)^2}{r^2}Z_G\hat{K}_G,$$

$G =$ the gravitational constant,

$\theta' = \angle\gamma EP' =$ the angle between the projection of the line,

EP in the plane of the equator (EP') and the vernal (Figure 2) equinox,

$J_2 =$ the coefficient due to the oblateness of the Earth,

$R_\oplus =$ the mean radius of the Earth.

Thus,

$$\ddot{\vec{r}} = -qF_g\frac{\vec{r}_s}{r_s} - \frac{GM_E}{r^3}\left(\frac{3J_2(R_\oplus)^2}{2r^2}(5\frac{(Z_G)^2}{r^2} - 1) - 1\right)\vec{r}$$

$$-\frac{3J_2(R_\oplus)^2}{r^2}Z_G\hat{K}_G+\frac{GM_s}{(r_{_E})^3}\vec{r}_{_E}-pF_g\left(\frac{(\vec{v}\cdot\vec{r}_s)\vec{r}_s}{cr_s}+\frac{\vec{v}}{c}\right),$$

where $q=1-F_p/F_g$ exhibits the relation between the gravitational force and the radiation pressure resulting from the Sun. Evidently, $0<q<1$ and $p=1-q$.

The motion of the Earth relative to the Sun is given by

$$\dot{\phi}^2=\frac{GM_s}{r_E^3},$$

also,

$$\vec{r}=r\hat{I},\ \vec{r}_{_E}=r_{_E}\hat{r}_{_E},\ \hat{r}_{_E}=\cos\phi\hat{I}_\circ+\sin\phi\hat{J}_\circ,\ \vec{r}_{_E}=r_{_E}\cos\phi\hat{I}_\circ+r_{_E}\sin\phi\hat{J}_\circ.$$

Using these values in the equation of motion of the satellite with respect to the Earth in vector form yields

$$\begin{aligned}\ddot{\vec{r}}=&-qGM_s\frac{\vec{r}_s}{r_s^3}-\frac{GM_E}{r^3}\left\{\left(-1+\frac{3J_2(R_\oplus)^2}{2r^2}(5\frac{(Z_G)^2}{r^2}-1)\right)\vec{r}\right\}\\&-\frac{3J_2(R_\oplus)^2}{r^2}Z_G\hat{K}_G+\dot{\phi}^2r_{_E}(\cos\phi\hat{I}_\circ+\sin\phi\hat{J}_\circ)-pF_g\left\{\frac{(\vec{v}\cdot\vec{r}_s)\,\vec{r}_s}{cr_s}+\frac{\vec{v}}{c}\right\}.\end{aligned}\tag{1}$$

In the rotating frame of reference with angular velocity $\vec{\omega}$ of the satellite about the center of the Earth, we have

$$\ddot{\vec{r}}=\frac{\partial^2r}{\partial t^2}\hat{I}+2\frac{\partial r}{\partial t}\left(\vec{\omega}\times\hat{I}\right)+r\left(\frac{\partial\vec{\omega}}{\partial t}\times\hat{I}\right)+r\left\{\left(\vec{\omega}\cdot\hat{I}\right)\vec{\omega}-(\vec{\omega}\cdot\vec{\omega})\,\hat{I}\right\},\tag{2}$$

where $\vec{\omega}=\dot{\theta}\hat{K}+\dot{\psi}\hat{K}_0$. Taking dot products of equations (1) and (2) with $\hat{I}$ and $\hat{J}$ and equating the respective coefficients, we get the equations of motion of the satellite in the synodic coordinate system ([3])

$$\begin{aligned}\frac{d^2r}{dt^2}-r\dot{\theta}^2+\frac{GM_E}{r^2}=&-qGM_s\frac{(\vec{r}_s\cdot\hat{I})}{r_s^3}+\dot{\phi}^2r_{_E}\{\cos\theta\cos(\phi-\psi)+\cos\alpha\sin\theta\sin(\phi-\psi)\}\\&-\frac{3GM_EJ_2R_\oplus^2[1-3(\hat{I}.K_G)^2]}{2r^4}-p\frac{GM_s}{(r_s)^2}\left\{\frac{(\vec{v}\cdot\vec{r}_s)(\vec{r}_s\cdot\hat{I})}{cr_s}+\frac{(\vec{v}\cdot\hat{I})}{c}\right\},\end{aligned}\tag{3}$$

$$\begin{aligned}\frac{d(r^2\dot{\theta})}{dt}=&-qGM_sr\frac{(\vec{r}_s\cdot\hat{J})}{r_s^3}-\dot{\phi}^2rr_{_E}\{\sin\theta\cos(\phi-\psi)-\cos\alpha\cos\theta\sin(\phi-\psi)\}\\&-\frac{3GM_EJ_2R_\oplus^2(\hat{I}.\hat{K}_G)(\hat{J}.K_G)}{2r^3}-p\frac{GM_s}{r_s^2}\left\{\frac{(\vec{v}\cdot\vec{r}_s)(\vec{r}_s\cdot\hat{J})}{cr_s}+\frac{(\vec{v}\cdot\hat{J})}{c}\right\}.\end{aligned}\tag{4}$$

	I_0	J_0	K_0
I	a_x	b_x	c_x
J	a_y	b_y	c_y
K	a_z	b_z	c_z

	I_0	J_0	K_0
I_G	1	0	0
J_G	0	$\cos\varepsilon$	$\sin\varepsilon$
K_G	0	$-\sin\varepsilon$	$\cos\varepsilon$

Table 1: Relation between coordinate system.

$$\begin{aligned}
a_x &= \cos\theta\cos\psi - \cos\alpha\sin\theta\sin\psi,\\
a_y &= -\sin\theta\cos\psi - \cos\alpha\cos\theta\sin\psi,\\
a_z &= \sin\alpha\sin\psi,\\
b_x &= \cos\theta\sin\psi - \cos\alpha\sin\theta\cos\psi,\\
b_y &= -\sin\theta\sin\psi + \cos\alpha\cos\theta\cos\psi,\\
b_z &= \cos\psi\sin\alpha,\\
c_x &= \sin\alpha\sin\theta, c_y = \sin\alpha\cos\theta,\\
c_z &= \cos\alpha.
\end{aligned}$$

Equations (3) and (4) are the required equations of motion of the satellite in polar form. These equations are not integrable, therefore we follow the perturbation technique and replace r, $\dot\theta$ and $\dot\psi$ by their steady state values r_0, $\dot\theta_0$, $\dot\psi_0$ and we may take $\theta = \dot\theta_0 t$, $\psi = \dot\psi_0 t$ and $\phi = \dot\phi t$, respectively. Putting the steady state values in the R.H.S of equations (3) and (4), we get

$$\begin{aligned}
\frac{d^2r}{dt^2} - r\dot\theta^2 + \frac{GM_E}{r^2} &= -qGM_s\frac{(\vec r_s\cdot\hat I)}{r_s^3} - \frac{3GM_EJ_2R_\oplus^2\{1-3(\hat I.\hat K_G)^2\}}{2r_0^4}\\
&\quad + \dot\phi^2 r_{_E}\{\cos\dot\theta_0 t\cos(\dot\phi-\dot\psi_0)t + \cos\alpha\sin\dot\theta_0 t\sin(\dot\phi-\dot\psi_0)t)\}\\
&\quad - p\frac{GM_s}{r_s^2}\left\{\frac{(\vec v\cdot\vec r_s)(\vec r_s\cdot\hat I)}{cr_s} + \frac{(\vec v\cdot\hat I)}{c}\right\}, \qquad (5)\\
\frac{d(r^2\dot\theta)}{dt} &= -qGM_sr_0\frac{(\vec r_s\cdot\hat J)}{r_s^3} - \frac{3GM_EJ_2R_\oplus^2(\hat I.\hat K_G)(\hat J.\hat K_G)}{2r_0^3}\\
&\quad - \dot\phi^2 r_0 r_{_E}\{\sin\dot\theta_0 t\cos(\dot\phi-\dot\psi_0)t + \cos\alpha_0\cos\dot\theta_0 t\sin(\dot\phi-\dot\psi_0)t\}\\
&\quad - pr_0\frac{GM_s}{r_s^2}\left\{\frac{(\vec v\cdot\vec r_s)(\vec r_s\cdot\hat J)}{cr_s} + \frac{(\vec v\cdot\hat J)}{c}\right\}. \qquad (6)
\end{aligned}$$

Now

$$\begin{aligned}
\vec v &= \{-r_E(\dot\phi-\dot\psi_0)\cos\dot\theta_0 t\sin(\dot\phi-\dot\psi_0)t + r_E(\dot\phi-\dot\psi_0)\cos\alpha\sin\dot\theta_0 t\cos(\dot\phi-\dot\psi_0)t\}\hat I\\
&\quad \{r_0\dot\theta_0 + r_E(\dot\phi-\dot\psi_0)\sin\dot\theta_0 t\sin(\dot\phi-\dot\psi_0)t + r_E(\dot\phi-\dot\psi_0)\cos\dot\theta_0 t\cos(\dot\phi-\dot\psi_0)t\cos\alpha_0\}\hat J\\
&\quad - r_E(\dot\phi-\dot\psi_0)\sin\alpha_0\cos(\dot\phi-\dot\psi_0)t\hat K,\\
\hat K_G &= -\sin\epsilon\hat J_0 + \cos\epsilon\hat K_0\\
&= -\sin\epsilon(\hat I b_x + \hat J b_y + \hat K b_z) + \cos\epsilon(C_x\hat I + C_y\hat J + C_z\hat K)\\
&= (-b_x\sin\epsilon + c_x\cos\epsilon)\hat I + (-b_y\sin\epsilon + c_y\cos\epsilon)\hat J + (-b_z\sin\epsilon + c_z\cos\epsilon)\hat K.
\end{aligned}$$

With the help of the above values, the transformations in Table 1 and taking $r^2\dot\theta =$ constant $= h$, $r = \frac{1}{u}$, we get

$$\frac{d^2u}{dt^2} + n^2u = K_1 + K_2\cos nt + K_3\sin nt + K_4\cos 2nt + k_5\sin 2nt$$

$$
\begin{aligned}
&+ K_6 \cos 3nt + K_7 \sin 3nt + K_8 \cos(\dot\phi + \dot\psi_0)t + K_9 \sin(\dot\phi - \dot\psi_0)t \\
&+ K_{10} \cos(n + \dot\phi - \dot\psi_0)t + K_{11} \sin(n + \dot\phi - \dot\psi_0)t + K_{12} \cos(n + \dot\phi + \dot\psi_0)t \\
&+ K_{13} \sin(n - \dot\phi + \dot\psi_0)t + K_{14} \cos(2n + \dot\phi - \dot\psi_0)t + K_{15} \sin(2n + \dot\phi - \dot\psi_0)t \\
&+ K_{16} \cos(2n - \dot\phi + \dot\psi_0)t + K_{17} \sin(2n - \dot\phi + \dot\psi_0)t + K_{18} \sin 2(\dot\phi - \dot\phi_0))t \\
&+ K_{19} \sin(2n+2\dot\phi - 2\dot\psi_0)t+K_{20} \sin(2n - 2\dot\phi+2\dot\psi_0)t+K_{21} \sin(n + 2\dot\phi - 2\dot\psi_0)t \\
&+ K_{22} \sin(n - 2\dot\phi+2\dot\psi_0)t+K_{23} \sin(3n+2\dot\phi - 2\dot\psi_0)t+K_{24} \sin(3n - 2\dot\phi + 2\dot\psi_0)t \\
&+ K_{25} \cos \dot\phi_0 t + K_{26} \cos 2\dot\phi_0 t + K_{27} \cos(2n + \dot\phi_0)t + K_{28} \cos(2n - \dot\psi_0)t \\
&+ K_{29} \cos(2n + 2\dot\psi_0)t + K_{30} \cos(2n - 2\dot\phi_0))t + K_{31} \cos(n + \dot\phi)t \\
&+ K_{32} \cos(n - \dot\phi_0)t + K_{33} \cos(n + 2\dot\psi_0)t + K_{34} \cos(n - 2\dot\psi_0)t \\
&+ K_{35} \cos(3n + 2\dot\phi_0)t + K_{36} \cos(3n - 2\dot\psi_0)t + K_{37} \cos(3n + \dot\psi_0)t \\
&+ K_{38} \cos(3n - \dot\phi_0)t. \qquad (7)
\end{aligned}
$$

The solution is given by

$$
\begin{aligned}
u &= A\cos(nt - \epsilon_1) + \frac{K_1}{n^2} - \frac{K_2 t \sin nt}{2n} + \frac{K_3 t \cos nt}{2n} + \frac{K_4 \cos 2nt}{n^2 - (2n)^2} + \frac{K_5 \sin 2nt}{n^2 - (2n)^2} \\
&+ \frac{K_6 \cos 3nt}{n^2 - (3n)^2} + \frac{K_7 \sin 3nt}{n^2 - (3n)^2} + \frac{K_8 (\dot\phi - \dot\psi_0)t}{n^2(\dot\phi - \dot\psi_0)^2 t} + \frac{K_9 \sin(\dot\phi - \dot\psi_0)t}{n^2(\dot\phi - \dot\psi_0)^2} + \frac{K_{10} \cos(n + \dot\phi - \dot\psi_0)t}{n^2 - (n + \dot\phi - \dot\psi_0)^2} \\
&+ \frac{K_{11} \sin(n + \dot\phi - \dot\psi_0)t}{n^2 - (n + \dot\phi - \dot\psi_0)t} + \frac{K_{12} \cos(n - \dot\phi + \dot\psi_0)t}{n^2 - (n - \dot\phi + \dot\psi_0)^2} + \frac{K_{13} \sin(n - \dot\phi + \dot\psi_0)t}{n^2 - (n - \dot\phi + \dot\psi_0)^2} \\
&+ \frac{K_{14} \cos(2n + \dot\phi - \dot\psi_0)t}{n^2 - (2n + \dot\phi - \dot\psi_0)^2} + \frac{K_{15} \sin(2n + \dot\phi - \dot\psi_0)t}{n^2 - (2n + \dot\phi - \dot\psi_0)^2} + \frac{K_{16} \cos(2n - \dot\phi + \dot\psi_0)t}{n^2 - (2n - \dot\phi + \dot\psi_0)^2} \\
&+ \frac{K_{17} \sin(2n - \dot\phi + \dot\psi_0)t}{n^2 - (2n - \dot\phi + \dot\psi_0)^2} + \frac{K_{18} \sin 2(\dot\phi - \dot\psi_0)t}{n^2 - 4(\dot\phi - \dot\psi_0)^2} + \frac{K_{19} \sin(2n + 2\dot\phi - 2\dot\psi_0)t}{n^2 - (2n + 2\dot\phi - 2\dot\psi_0)^2} \\
&+ \frac{K_{20} \sin(2n - 2\dot\phi + 2\dot\psi_0)t}{n^2 - (2n - 2\dot\phi + \dot\psi_0)^2} + K_{21} \frac{\sin(n + 2\dot\phi - 2\dot\psi_0)t}{n^2 - (n + 2\dot\phi - 2\dot\psi_0)^2} + K_{22} \frac{\sin(n + 2\dot\phi - 2\dot\psi_0)t}{n^2 - (n - 2\dot\phi + 2\dot\psi_0)^2} \\
&+ K_{23} \frac{\sin(3n + 2\dot\phi - 2\dot\psi_0)t}{n^2 - (3n + 2\dot\phi - 2\dot\psi_0)^2} + K_{24} \frac{\sin(3n - 2\dot\phi - 2\dot\psi_0)t}{n^2 - (3n - 2\dot\phi + 2\dot\psi_0)^2} + K_{25} \frac{\cos \dot\psi_0 t}{n^2 - \dot\psi_0^2} \\
&+ K_{26} \frac{\cos 2\dot\psi_0 t}{n^2 - (2\dot\psi_0)^2} + K_{27} \frac{\cos(2n + \dot\psi_0)t}{n^2 - (2n+\dot\psi_0)^2} + K_{28} \frac{\cos(2n + \dot\psi_0)t}{n^2 - (2n - \dot\psi_0)^2} + K_{29} \frac{\cos(2n + \dot\psi_0)t}{n^2 - (2n + \dot\psi_0)^2} \\
&+ K_{30} \frac{\cos(2n - \dot\psi_0)t}{n^2 - (2n - 2\dot\psi_0)^2} + K_{31} \frac{\cos(n+2\dot\psi_0)t}{n^2 - (n + 2\dot\psi_0)^2} + \frac{K_{32} \cos(n - \dot\psi_0)t}{n^2 - (n - \dot\psi_0)^2} + \frac{K_{33} \cos(n + \dot\psi_0)t}{n^2 - (n + \dot\psi_0)^2} \\
&+ \frac{K_{34} \cos(n - 2\dot\psi_0)t}{n^2 - (n - 2\dot\psi_0)^2} + \frac{K_{35} \cos(3n+2\dot\psi_0)t}{n^2 - (3n+2\dot\psi_0)^2} + \frac{K_{36} \cos(3n - 2\dot\psi_0)t}{n^2 - (3n - 2\dot\psi_0)^2} + \frac{K_{37} \cos(3n + \dot\psi_0)t}{n^2 - (3n + \dot\psi_0)^2} \\
&+ \frac{K_{38} \cos(3n - \dot\psi_0)t}{n^2 - (3n - \dot\psi_0)^2}. \qquad (8)
\end{aligned}
$$

The values of constant $K_i's$ are given in Appendix 'A' (which can be obtained from the authors).

2.2 Resonance

It is clear that the motion becomes indeterminate if any one of the denominator vanishes in equation (8), and hence the resonance occurs at these points, called the critical points. It is found that resonance occurs at many points with three frequencies and at six points $R_1'(n = \dot{\psi})$, $R_2'(3n = \dot{\psi})$, $R_3'(2n = \dot{\psi})$, $R_4'(3n = 2\dot{\psi})$, $R_5'(n = 2\dot{\psi})$ and $R_6'(4n = \dot{\psi})$ with two frequencies due to oblateness. Also, it is found that resonance occurs at five points $(n = \dot{\phi})$, $(n = 2\dot{\phi})$, $(3n = \dot{\phi})$, $(2n = \dot{\phi})$, $(3n = 2\dot{\phi})$ in the frequencies n and $\dot{\phi}$. The $1 : 1$ resonance repeated four times, $2 : 1$ resonance occurs thrice while other four resonances occur once only. If we take the solar radiation pressure as a perturbing force, then there are only three points at which resonance occurs. If we consider the velocity dependent terms of the P-R drag, then five points of resonance occur, where three points of resonance are same, and $1 : 2$ and $3 : 2$ resonances occurs only due to the velocity dependent terms of the P-R drag.

3 Time Period and Amplitude at the Resonance Point

3.1 Time period and amplitude at $n = 2\dot{\phi}$

We follow the method in [1] to determine the time period and amplitude at $n = 2\dot{\phi}$. It is suggested to obtain the solution of (7) when that of

$$\frac{d^2u}{dt^2} + n^2u = 0 \tag{9}$$

is periodic and is known. The solution of (9) is

$$u = k\cos s,$$

where

$$s = nt + \epsilon, \quad n = \frac{k_1}{k} = \text{the function of } k; \tag{10}$$

k, k_1 and ϵ are arbitrary constants. As we are probing the resonance in the motion of the satellite at the point $n = 2\dot{\phi}$, in our case, the resulting equation. (7) can be written as

$$\frac{d^2u}{dt^2} + n^2u = HA'\cos n't = H\psi',$$

where

$$H = \frac{pF_g(r_E)^2\dot{\phi}}{4ca(r_s)(1-e^2)} = \text{constant}, n' = 2\dot{\phi}, \quad A' = -\sin^2\alpha,$$

$$\psi' = \frac{\partial\psi}{\partial u} = A'\cos 2n't, \psi = uA'\cos n't, \quad \psi = \frac{A'k}{2}\{\cos(2n't + s) + \cos(2n't - s)\}. \tag{11}$$

Then

$$\frac{dk}{dt} = \frac{H}{W}\frac{\partial u}{\partial s}\psi' = \frac{H}{W}\frac{\partial\psi}{\partial s}, \tag{12}$$

$$\frac{ds}{dt} = n - \frac{H}{W}\frac{\partial u}{\partial k}\psi' = n - \frac{H}{W}\frac{\partial \psi}{\partial k}, \tag{13}$$

where

$$W = \frac{\partial}{\partial k}(n\frac{\partial u}{\partial s})\frac{\partial u}{\partial s} - n\frac{\partial^2 u}{\partial s^2}\frac{\partial u}{\partial k} = \textbf{a function of } k \textbf{ only.}$$

Since n and W are the function of k only, we can put (12) and (13) into canonical form with new variables defined by

$$dk_1 = Wdk, \tag{14}$$

$$dB = -ndk_1 = -nWdk, \tag{15}$$

(14) and (15) can be put in the form

$$\frac{dk_1}{dt} = \frac{\partial}{\partial s}(B + H\psi), \quad \frac{ds}{dt} = -\frac{\partial}{\partial s}(B + H\psi).$$

Differentiating (13) with respect to t and substituting the expression for $\frac{ds}{dt}$ and $\frac{dk}{dt}$, we have

$$\frac{d^2 s}{dt^2} = \frac{H}{W}\left(\frac{\partial n}{\partial k}\frac{\partial \psi}{\partial s} - n\frac{\partial^2 \psi}{\partial s \partial k} - \frac{\partial^2 \psi}{\partial k \partial t}\right) + \frac{H^2}{K^2}\left(\frac{\partial^2 \psi}{\partial s \partial k}\frac{\partial \psi}{\partial k} - W\frac{\partial}{\partial k}\left(\frac{1}{W}\frac{\partial \psi}{\partial k}\right)\frac{\partial \psi}{\partial s}\right). \tag{16}$$

Since the last expression of (16) has the factor H^2, it may, in general, be neglected in a first approximation. In (11) we find s and t are present in ψ' as a sum of the periodic terms with argument

$$s' = s - n't,$$

the affected term in our case is

$$\psi = \frac{kA' \cos s'}{2}. \tag{17}$$

Equation (16) for s' is then

$$\frac{d^2 s'}{dt^2} + (n - 2n')^2 \frac{H}{W}\frac{\partial}{\partial k}\left(\frac{1}{n - n'}\frac{\partial \psi}{\partial s'}\right) = 0 \tag{18}$$

or

$$\frac{d^2 s'}{dt^2} - (n - 2n')^2 \frac{H}{2W}\frac{\partial}{\partial k}\left(\frac{kA'}{n - n'}\right)\sin s' = 0. \tag{19}$$

At first approximation, we put constants $k = k_0, \quad n = n_0, \quad W = W_0$. Then (19) can be written as

$$\frac{d^2 s'}{dt^2} - (n - 2n')^2 \frac{H}{2W}\frac{\partial}{\partial k}\left(\frac{kA'}{n - n\prime}\right)\sin s' = 0. \tag{20}$$

If the oscillations are small intervals, then (20) may be put in the form

$$\frac{d^2 s'}{dt^2} - (n - 2n')^2 \frac{H}{2W}\frac{\partial}{\partial k}\left(\frac{kA'}{n - n\prime}\right)s' = 0$$

or

$$\frac{d^2s'}{dt^2} + p_1^2 s' = 0, \tag{21}$$

where

$$p_1 = \sqrt{\frac{pF_g(r_{_E})^2\dot{\phi}\sin^2\alpha}{8ca(r_s)(1-e^2)}}\sqrt{\frac{\sqrt{k_1}}{W_0 k_0}}, \tag{22}$$

$$\begin{aligned} W_0 = (W)_0 &= \frac{\partial}{\partial k}(n\frac{\partial y}{\partial s})\frac{\partial y}{\partial s} - n\frac{\partial^2 y}{\partial s^2}\frac{\partial y}{\partial k}_0 = (\sqrt{k}_1\cos^2(2n't+\epsilon)_0), \\ &= \sqrt{k}_1\cos^2(2\dot{\phi}t+\epsilon_0). \end{aligned} \tag{23}$$

The solution of (21) is given by

$$s' = A\sin(p_1 t + \lambda_0),$$

where

$$A = \frac{\sqrt{k}_2}{p_1}, \qquad k_2, \lambda_0 = \text{the constants of integration}, \qquad s' = s - 2n't.$$

The equation for s gives

$$s = 2n't + A\sin(p_1 t + \lambda_0). \tag{24}$$

Using (12), (19) and (22) the equation for k gives

$$k = k_0 + HA'\left(\frac{q}{W}\right)_0 \frac{A}{p_1}\cos(p_1 t + \lambda_0), \tag{25}$$

where k_0 is determined from $n_0 = n'$. Since n_0 is a known function of k_0, the amplitude 'A' and the time period T are given by

$$A = \frac{\sqrt{k}_2}{p_1}, \quad T = \frac{2\pi}{p_1},$$

where k_2 is an arbitrary constant,

$$p_1 = \frac{\sqrt{pF_g(r_{_E})^2\dot{\phi}\sin^2\alpha}}{\sqrt{8car_s(1-e^2)k_0}\cos(2\dot{\phi}+\epsilon_0)}.$$

Using equation (13), k_0 may be written as

$$k_0 = \frac{\sqrt{k}_1}{n_0}.$$

We may choose the constants of integration $k_1 = 1$, $k_2 = 1$, $\epsilon_0 = 0$ [12].

The amplitude and time period are given by

$$A = \frac{2\sqrt{2car_s(1-e^2)}}{\sqrt{pF_g n_0\dot{\phi}r_{_E}}\sin\alpha}\cos 2\phi, \quad T = \frac{4\pi\sqrt{2ca(r_s)(1-e^2)}}{\sqrt{pF_g n_0\dot{\phi}r_{_E}}\sin\alpha}\cos 2\phi.$$

In the same manner we have calculated the amplitudes and time periods at other points also. Thereafter two cases arise.

Case 1: Regression angle is constant.

- If we take the solar radiation pressure as a perturbing force, then there are only three points at which resonance occurs. The corresponding amplitudes and time periods are given in Table 2 below.

- In addition to the above, if we consider the velocity dependent terms of the P-R drag, then at five points $R_1(n = \dot{\phi})$, $R_2(3n = \dot{\phi})$, $R_3(2n = \dot{\phi})$, $R_4(3n = 2\dot{\phi})$, $R_5(n = 2\dot{\phi})$ resonance occurs, where three points of resonance are same as in subcase 1, and 1 : 2 and 3 : 2 resonances occur only due to the velocity dependent terms of the P-R drag. But the amplitudes and time periods at all resonance points are not same as in the case of the solar radiation pressure. The corresponding amplitude and time period are given in Table 3.

Case 2: Regression angle is not constant.

It is found that resonance occurs at many points with three frequencies and at six points $R'_1(n = \dot{\psi})$, $R'_2(3n = \dot{\psi})$, $R'_3(2n = \dot{\psi})$, $R'_4(3n = 2\dot{\psi})$, $R'_5(n = 2\dot{\psi})$ and $R'_6(4n = \dot{\psi})$ with two frequencies. The corresponding amplitudes and time-periods are given in Table 4.

	Resonance	Amplitude	Time Period
1	$n = \dot{\phi}$	A_1, A_2	T_1, T_2
2	$2n = \dot{\phi}$	A_5	T_5
3	$3n = \dot{\phi}$	A_9	T_9

Table 2: Amplitudes A_i's and time periods T_i's at resonance points with only radiation pressure as a perturbing force when the regression angle is constant.

	Resonance	Amplitude	Time Period
1	$n = \dot{\phi}$	A_3, A_4	T_3, T_4
2	$2n = \dot{\phi}$	A_6	T_6
3	$n = 2\dot{\phi}$	A_7, A_8	T_7, T_8
4	$3n = 2\dot{\phi}$	A_{10}	T_{10}

Table 3: Amplitudes A_i's and time periods T_i's at resonance points for the velocity dependent terms of the P-R drag when the regression angle is constant.

Resonance	Amplitude	Time Period
$n = \dot{\psi}$	$A_{11}, A_{12}, A_{13}, A_{14}$	$T_{11}, T_{12}, T_{13}, T_{14}$
$2n = \dot{\psi}$	A_{15}, A_{16}	T_{15}, T_{16}
$n = 2\dot{\psi}$	A_{17}, A_{18}	T_{17}, T_{18}
$3n = \dot{\psi}$	A_{19}	T_{19}
$3n = 2\dot{\psi}$	A_{20}	T_{20}
$4n = \dot{\psi}$	A_{21}	T_{21}

Table 4: Amplitudes A_i's and time periods T_i's at resonance points for two frequencies when the regression angle is not constant.

where A_i's and T_i's are are given in the Appendix A and Appendix B, respectively (which can be obtained from the authors).

4 Discussion and Conclusion

We have investigated the resonance in the motion of a satellite in the Earth-Sun system due to oblateness of the Earth and the P-R drag. Firstly, the equations of motion of the geo-centric satellite in vector as well as in polar form has been evaluated by taking the velocity of the satellite as v. Secondly, the velocity of the satellite in the P-R drag have been deduced by using an operator and then substituted in the equations of motion. We get resonances at many points with three frequencies, and at eleven points with two frequencies between n and $\dot{\phi}$ and n and $\dot{\psi}$.

Two resonance points 3 : 2 and 1 : 2 occur only due to the velocity dependent terms of the P-R drag. We have shown the effect of the P-R drag and oblateness on the amplitude and time period by using the following data of the satellite:

$$a = 6921000m; \quad e = .0065; n = 0.0628766\frac{deg}{sec}; \quad \dot{\phi} = 0.0000114077\frac{deg}{sec};$$
$$r_s = 149599 \times 10^6 m; \quad r_{_E} = 149.6 \times 10^9 m; \quad c = 3 \times 10^8 \frac{m}{sec}.$$

We make the above quantities dimensionless by taking

$$M_E + M_s = 1\text{unit}, \quad G = 1\text{unit},$$
$$r_s = \text{the distance between the Earth and the Sun} = 1\text{unit}.$$

From Figure 3, we observe that the amplitude and time period increase when q increases and it is maximum at $\phi = 0$. p is the factor of the velocity dependent terms of the P-R drag, when q increases, p decreases, and hence, when the P-R decreases, then the amplitude as well as the time period increase.

Figure 4 explains the variation in A_1 and time-period T_1, respectively, for $-90^0 < \phi < 90^0$ and $0 < q < 1$, at resonance 1 : 1 with the P-R drag. The below graphs show that the amplitude and time period decrease as ϕ increases.

(a) (b)

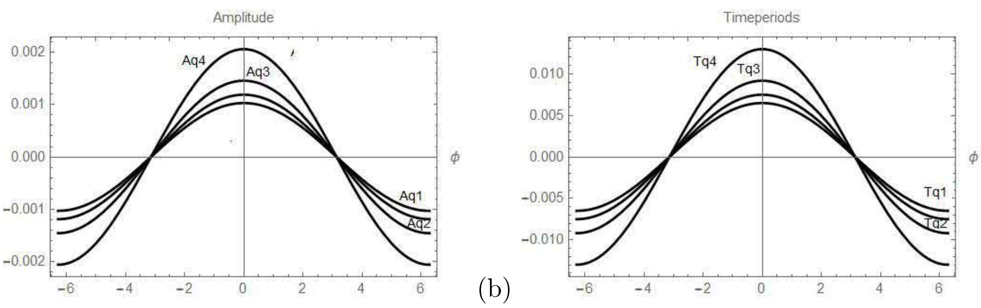

Figure 3: (a) Comparison of amplitudes at same resonant points and for different $q's$: $Aq1 = 0.20$ (Red); $Aq2 = 0.40$ (Green); $Aq3 = 0.60$ (Gray) and $Aq4 = 0.80$ (Blue). (b) Comparison of time periods at same resonant points and for different $q's$: $Tq1 = 0.20$ (Red); $Tq2 = 0.40$ (Green); $Tq3 = 0.60$ (Gray) and $Tq4 = 0.80$ (Blue), at resonance 1:1.

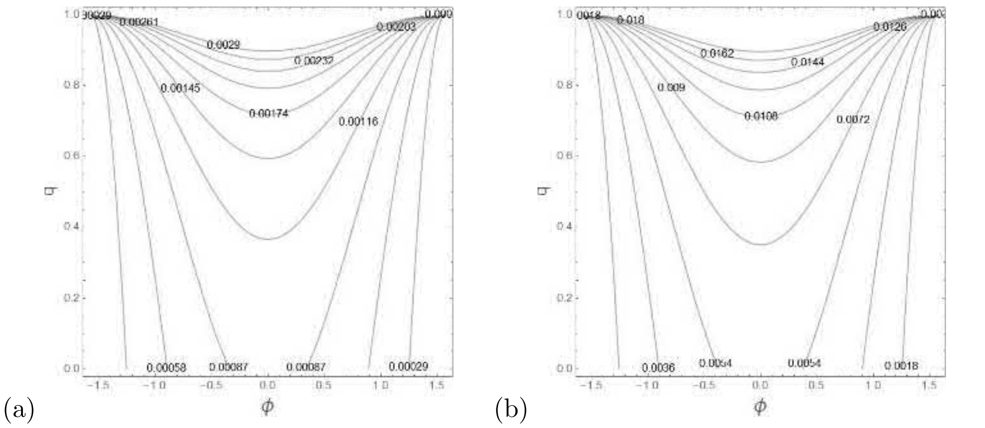

Figure 4: (a) Variation in amplitude, (b) variation in time period 'T' for $0^0 < \phi < 90^0$ and q $(0 < q < 1)$ at resonance 1:1 with the P-R drag.

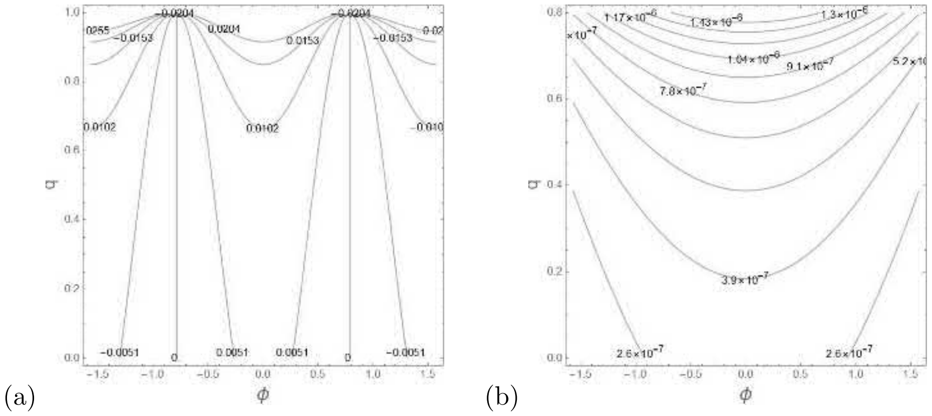

Figure 5: (a) Variation in amplitude 'A' w.r.t. ϕ , at resonance 1:2. (b) Time period 'T' at resonance 1:1, for $-1^0 < \phi < 1^0$ and q $(0 < q < 1)$ without the P-R drag

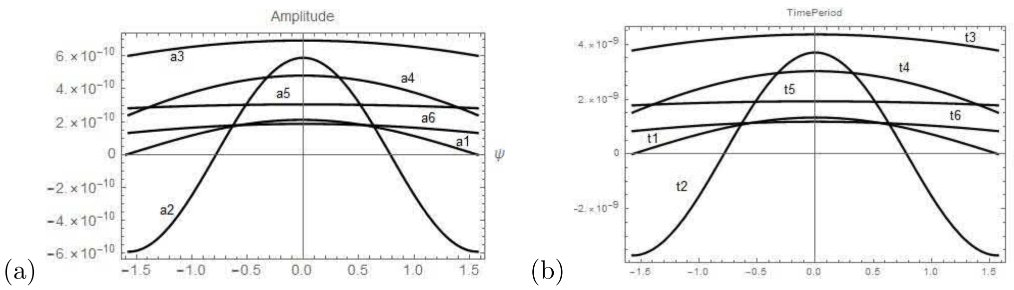

Figure 6: (a) Comparison of amplitude. (b) Comparison of time periods due to the coefficient of oblateness of the Earth (J_2) at different resonant points.

Figure 4 explains the variation in A_1 and time period T_1, respectively, for $-90^0 <$

$\phi < 90^0$ and $0 < q < 1$ at resonance $1:1$ with the P-R drag. The above graphs show that the amplitude and time-period decrease as ϕ increases.

Figure 5 also explains the amplitude and time period with respect to ϕ. In this case it can be observed that the amplitude becomes very high of greater range of ϕ but it is not in the case of the velocity dependent terms of the P-R drag. Similarly, Figure 5 explains the variation in amplitude for $-90^0 < \phi < 90^0$ and $0 < q < 1$ at resonance $1:2$. The graphs show that the amplitude is periodic with respect to ϕ and it increases (decreases) as q increases (decreases).

Figure 6 also explains the amplitudes and time periods due to oblateness of the Earth (J_2). In these graphs we have shown the comparison of the amplitude and time period at different critical points, where resonance occurs, and it is clear from the figures that the value of the amplitudes and time periods is different at different critical points. The present study is becoming of more interest in the commensurable orbits, for example, the interacting and navigation satellite system.

References

[1] E.W. Brown, and C.A. Shook *Planetary Theory.* Cambridge University Press, Cambridge, 1933.

[2] C.H. Zee. Effects of Earth oblateness and equator ellipticity on a asynchrounous satellite. *Asstr. Acta.* **16** (1971) 143–152.

[3] K.B. Bhatnagar and M. Mehra. Motion of Geosyncronous satellite-1. *Indian J. Pure Appl. Math.* **17** (12) (1986) 1438–1452.

[4] O. Ragos, F.A. Zafiropoulos and M.N. Vrahatis. A numerical study of influence of the Poynting Robertson effect on the equilibrium points of the photo gravitational restricted three body problem (out of plane case). *Astron. Astrophys.* **300** (1995) 579–590.

[5] A. Celletti and L. Chierchia. Hamiltonian stability of spin-orbit resonances in celestial mechanics. *Celest. Mech. Dyn. Astr.* **76** (2000) 229–240.

[6] N. Callegari and T. Yokoyama. Some aspects of the dynamics of fictitious Earth's satellites. *Planetary and Space Science* **49** (2001) 35–46.

[7] A. Prado. Satellite maneuvers using the Henon's orbit transfer problem: Application to geostationary satellites. *Nonlinear Dynamics and Systems Theory* **5(4)** (2005) 407–417.

[8] M. Sabatini, R. Bevilacqua, M. Pantaleoni and D. Izzo. Numerical search of bounded relative satellite. *Nonlinear Dynamics and Systems Theory* **6(4)** (2006) 411–419.

[9] C. Pardini and L. Anselmo. Long-term evolution of geosynchronous orbital debris with high area-to-mass ratios. *Transactions of Journal of the Japan Society for Aeronautical and Space Science* **51** (2008) 22–27.

[10] A. Celletti, L. Stefanelli, E. Lega and C. Froeschle. Some results on the global dynamics of the regularized restricted three-body problem with dissipation. *Celest. Mech. Dyn. Astr.* **109** (2011) 265–284.

[11] B. Quarles, Z.E. Musielak and M. Cuntz. Study of resonances for the restricted 3-body problem. *Asron. Nachr.* **00** (2012) 1–10.

[12] S. Yadav and R. Aggarwal. Resonance in the Earth-moon system around the sun including Earth's equatorial ellipticity. *Astrophysics Space Sci.* **348** (2013) 367–375.

[13] E.D. Kuznetsov, P.E. Zakharova, D.V. Glamazda and S.O. Kudryavtsev Effect of the high-order resonances on the orbital evolution of objects near geostationary orbit. *Solar System Research* **48** (2014) 446–459.

[14] A. Celletti and C. Gale Dynamical investigation of minor resonances for space debris. *Celestial Mechanics and Dynamical Astronomy* **123** (2015) 203–222.

[15] J. Daquin, F. Deleflie and J. Perez. Comparison of mean and osculating stability in the vicinity of the (2:1) tesseral resonant surface. *Acta Astronautica* **111** (2015) 170–177.

Nonlinear Dynamics and Systems Theory, **19** (4) (2019) 512–522

(G'/G)-Expansion Method and Weierstrass Elliptic Function Method Applied to Coupled Wave Equation

E.V. Krishnan [1,*], M. Al Ghabshi [1] and M. Alquran [2]

[1] *Department of Mathematics, Sultan Qaboos University, P.O. Box 36, Al Khod 123, Muscat, Sultanate of Oman*
[2] *Department of Mathematics and Statistics, Jordan University of Science and Technology, P.O. Box (3030), Irbid (22110), Jordan*

Received: December 5, 2018; Revised: October 9, 2019

Abstract: This paper deals with the exact solutions of a nonlinear coupled wave equation. The (G'/G)-expansion method has been applied to derive kink solutions and singular wave solutions. The restrictions on the coefficients of the governing equations have also been investigated. Solitary wave solutions have also been derived for this system of equations using the Weierstrass elliptic function method.

Keywords: *(G'/G)-expansion method; coupled wave equation; kink wave solutions; singular wave solutions; solitary wave solutions; Jacobi and Weierstrass elliptic functions.*

Mathematics Subject Classification (2010): 74J35, 34G20, 93C10.

1 Introduction

Nonlinear evolution equations (NLEEs) govern several physical phenomena which appear in various branches of science and engineering [1–5]. Exact solutions of NLEEs shed more light on the various aspects of the problem, which, in turn, leads to the applications. Several methods such as the tanh method [6–11], exponential function method [12], Jacobi elliptic function (JEF) method [13–16], mapping methods [17–22], Hirota bilinear method [23, 24] and trigonometric-hyperbolic function methods [25–27] have been applied in the last few decades and the results have been reported. Also, many physical phenomena have been governed by systems of partial differential equations (PDEs) and there have been significant contributions in this area [28, 29].

In this paper, we use the (G'/G)-expansion method [30–34] to find some exact solutions for a nonlinear coupled wave equation [35]. The paper is organized as follows. In Section 2, we give a mathematical analysis of the (G'/G)-expansion method, in Section 3, we find kink solutions and singular wave solutions of the nonlinear coupled wave equation, in Section 4, we use the Weierstrass elliptic function (WEF) method [36] to derive SWSs of the system of equations, in Section 5 we write down the conclusion.

* Corresponding author: mailto:krish@squ.edu.om

2 The (G'/G)-Expansion Method

Consider the nonlinear partial differential equation (PDE)

$$P(u, u_t, u_x, u_{tt}, u_{xt}, u_{xx}, ...) = 0, \tag{1}$$

where $u(x, t)$ is an unknown function, P is a polynomial in $u = u(x, t)$ and its various partial derivatives. The traveling wave variable $\xi = x - ct$ reduces the PDE (1) to the ordinary differential equation (ODE)

$$P(u, -cu', u', -c^2u'', -cu'', u'', ...) = o, \tag{2}$$

where $u = u(\xi)$ and $'$ denotes differentiation with respect to ξ.

We suppose that the solution of equation (2) can be expressed by a polynomial in $\left(\dfrac{G'}{G}\right)$ as follows:

$$u(\xi) = \sum_{i=0}^{m} a_i \left(\frac{G'}{G}\right)^i, \quad a_m \neq 0, \tag{3}$$

where $a_i (i = 0, 1, 2, ..)$ are constants. Here, G satisfies the second order linear ODE

$$G''(\xi) + \lambda G'(\xi) + \mu G(\xi) = 0, \tag{4}$$

with λ and μ being constants. The positive integer m can be determined by a balance between the highest order derivative term and the nonlinear term appearing in equation (2). By substituting equation (3) into equation (2) and using equation (4), we get a polynomial in G'/G. The coefficients of various powers of G'/G give rise to a set of algebraic equations for a_i $(i = 0, 1, 2, ..., m)$, λ and μ.

The general solution of equation (4) is a linear combination of sinh and cosh or of sine and cosine functions if $\Delta = \lambda^2 - 4\mu > 0$ or $\Delta = \lambda^2 - 4\mu < 0$, respectively. In this paper we consider only the first case and so,

$$G(\xi) = e^{-\lambda\xi/2}\left(C_1 \sinh(\frac{\sqrt{\lambda^2 - 4\mu}}{2}\xi) + C_2 \cosh(\frac{\sqrt{\lambda^2 - 4\mu}}{2}\xi)\right), \tag{5}$$

where C_1 and C_2 are arbitrary constants.

3 A Coupled Wave Equation

Consider the system of PDEs

$$u_t + \alpha v^2 v_x + \beta u^2 u_x + \eta u u_x + \gamma u_{xxx} = 0, \tag{6}$$

$$v_t + \sigma(uv)_x + \epsilon v v_x = 0, \tag{7}$$

where, $\alpha, \beta, \eta, \gamma, \sigma$ and ϵ are constants.

We seek TWSs of equations (6) and (7) in the form $u = u(\xi)$, $\quad v = v(\xi)$, $\quad \xi = x - ct$. Then equations (6) and (7) give

$$-cu' + \alpha v^2 v' + \beta u^2 u' + \eta u u' + \gamma u''' = 0, \tag{8}$$

$$-cv' + \sigma(uv)' + \epsilon vv' = 0. \tag{9}$$

Integrate equation (9) with respect to ξ

$$-cv + \sigma(uv) + \frac{\epsilon}{2}v^2 = k, \tag{10}$$

where k is the integration constant. Dividing equation (10) by v, we obtain

$$-c + \sigma u + \frac{\epsilon}{2}v = \frac{k}{v}. \tag{11}$$

So, for the solutions to be uniformly valid, the integration constant k should be set equal to 0. Therefore, equation (11) can be written as

$$v = \frac{2(c - \sigma u)}{\epsilon}. \tag{12}$$

Substituting equation (12) into equation (8), we obtain

$$-cu' - \frac{8\alpha\sigma}{\epsilon^3}(c^2 - 2c\sigma u + \sigma^2 u^2)u' + \beta u^2 u' + \eta uu' + \gamma u''' = 0. \tag{13}$$

Integrating equation (13) with respect to ξ and assuming the boundary conditions $u, u', u'' \longrightarrow 0$ as $|\xi| \longrightarrow \infty$, we have

$$\gamma u'' - \left\{c + \frac{8\alpha\sigma c^2}{\epsilon^3}\right\}u + \left\{\frac{\eta}{2} + \frac{8\alpha\sigma^2 c}{\epsilon^3}\right\}u^2 + \left\{\frac{\beta}{3} - \frac{8\alpha\sigma^3}{3\epsilon^3}\right\}u^3 = 0. \tag{14}$$

We rewrite equation (14) as

$$\gamma u'' + Au + Bu^2 + Cu^3 = 0, \tag{15}$$

where

$$A = -\left\{c + \frac{8\alpha\sigma c^2}{\epsilon^3}\right\}, \quad B = \left\{\frac{\eta}{2} + \frac{8\alpha\sigma^2 c}{\epsilon^3}\right\}, \quad C = \left\{\frac{\beta}{3} - \frac{8\alpha\sigma^3}{3\epsilon^3}\right\}. \tag{16}$$

With the change of variable $w = u + \delta$, equation (15) can be reduced to

$$\gamma w'' + c_1 w + c_2 w^3 + c_3 = 0, \tag{17}$$

where

$$\delta = -\frac{B}{3C}, \quad c_1 = \frac{3AC - B^2}{3C}, \quad c_2 = C, \quad c_3 = \frac{2B^3 - 9ABC}{27C^2}. \tag{18}$$

Assuming the expansion $w(\xi) = \sum_{i=0}^{m} a_i \left(\frac{G'}{G}\right)^i$, $a_m \neq 0$ in equation (17) and balancing the nonlinear term and the derivative term, we get $m + 2 = 3m$ so that $m = 1$.

So, we assume the solution of equation (17) in the form

$$w(\xi) = a_0 + a_1\left(\frac{G'}{G}\right), \; a_1 \neq 0. \tag{19}$$

So, we can obtain

$$w'(\xi) = -a_1\left(\frac{G'}{G}\right)^2 - \lambda a_1\left(\frac{G'}{G}\right) - \mu a_1, \tag{20}$$

$$w''(\xi) = 2a_1\left(\frac{G'}{G}\right)^3 + 3a_1\lambda\left(\frac{G'}{G}\right)^2 + (a_1\lambda^2 + 2a_1\mu)\left(\frac{G'}{G}\right) + a_1\lambda\mu, \tag{21}$$

$$w^3(\xi) = a_1^3\left(\frac{G'}{G}\right)^3 + 3a_0a_1^2\left(\frac{G'}{G}\right)^2 + 3a_0^2a_1\left(\frac{G'}{G}\right) + a_0^3. \tag{22}$$

Now, substituting equations (19), (21) and (22) into equation (17) and collecting the coefficients of $\left(\frac{G'}{G}\right)^i$, $i = 0, 1, 2, 3$, we get

$$\gamma a_1\lambda\mu + c_1a_0 + c_2a_0^3 + c_3 = 0, \tag{23}$$

$$\gamma a_1\lambda^2 + 2\gamma a_1\mu + c_1a_1 + 3c_2a_0^2a_1 = 0, \tag{24}$$

$$3a_1\lambda\gamma + 3a_0a_1^2c_2 = 0, \tag{25}$$

$$2\gamma a_1 + c_2a_1^3 = 0. \tag{26}$$

From equation (26), we get

$$a_1 = \pm\sqrt{-\frac{2\gamma}{c_2}}. \tag{27}$$

Equation (25) leads to

$$a_0 = \pm\frac{1}{2}\lambda\sqrt{-\frac{2\gamma}{c_2}}. \tag{28}$$

When $\mu = 0$ in equation (24), we get $\lambda = \pm\sqrt{\frac{2c_1}{\gamma}}$, and when $\lambda = 0$, we get $\mu = -\frac{c_1}{2\gamma}$. In both cases, $\Delta = \lambda^2 - 4\mu = \frac{2c_1}{\gamma}$. Equation (23) gives a constraint condition on the coefficients in the governing equation.

Case 1: $\mu = 0,\ \lambda = \sqrt{\frac{2c_1}{\gamma}}$.

$$u_1(x,t) = \pm\sqrt{-\frac{c_1}{c_2}}\left[1 + \frac{(C_1 - C_2)\left(1 - \tanh\frac{1}{2}\sqrt{\frac{2c_1}{\gamma}}(x - ct)\right)}{C_1\tanh\frac{1}{2}\sqrt{\frac{2c_1}{\gamma}}(x - ct) + C_2}\right] + \frac{B}{3C}. \tag{29}$$

Case 2: $\mu = 0,\ \lambda = -\sqrt{\dfrac{2c_1}{\gamma}}$.

$$u_2(x,t) = \pm\sqrt{-\frac{c_1}{c_2}}\left[1 + \frac{(C_1 + C_2)\left(1 - \tanh\frac{1}{2}\sqrt{\frac{2c_1}{\gamma}}(x - ct)\right)}{C_2 - C_1\tanh\frac{1}{2}\sqrt{\frac{2c_1}{\gamma}}(x - ct)}\right] + \frac{B}{3C}. \tag{30}$$

Case 3: $\lambda = 0,\ \mu = -\dfrac{c_1}{2\gamma}$.

$$u_3(x,t) = \pm\sqrt{-\frac{c_1}{c_2}}\left[\frac{C_1 + C_2\tanh\frac{1}{2}\sqrt{\frac{2c_1}{\gamma}}(x - ct)}{C_1\tanh\frac{1}{2}\sqrt{\frac{2c_1}{\gamma}}(x - ct) + C_2}\right] + \frac{B}{3C}. \tag{31}$$

In all three cases, γ and c_1 should have the same signs and c_2 should be of the opposite sign and $C_1 \neq \pm C_2$.

Figure 1 and Figure 2 represent the solutions given by equation (29).

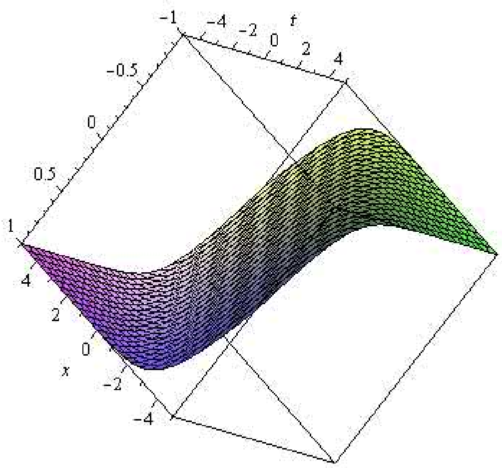

Figure 1: The solution for $u(x,t)$, $C_1 = 0, C_2 = 1$.

Using equation (12), we can write down the corresponding solutions $v_1(x,t)$, $v_2(x,t)$ and $v_3(x,t)$.

4 Weierstrass Elliptic Function Solutions of the Coupled Wave Equation

The Weierstrass elliptic function (WEF) $\wp(\xi; g_2, g_3)$ with invariants g_2 and g_3 satisfy

$$\wp'^2 = 4\wp^3 - g_2\wp - g_3, \tag{32}$$

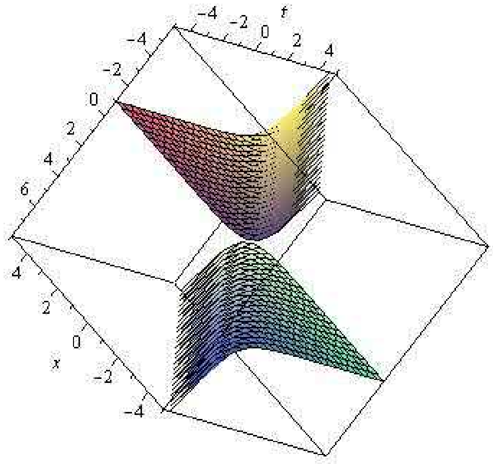

Figure 2: The solution for $u(x,t)$, $C_1 = 1, C_2 = 0$.

where g_2 and g_3 are related by the inequality

$$g_2^3 - 27g_3^2 > 0. \tag{33}$$

The WEF $\wp(\xi)$ is related to the JEFs by the following relations:

$$\mathrm{sn}(\xi) = [\wp(\xi) - e_3]^{-1/2}, \tag{34}$$

$$\mathrm{cn}(\xi) = \left[\frac{\wp(\xi) - e_1}{\wp(\xi) - e_3}\right]^{1/2}, \tag{35}$$

$$\mathrm{dn}(\xi) = \left[\frac{\wp(\xi) - e_2}{\wp(\xi) - e_3}\right]^{1/2}, \tag{36}$$

where e_1, e_2, e_3 satisfy

$$4z^3 - g_2 z - g_3 = 0 \tag{37}$$

with

$$e_1 = \frac{1}{3}(2 - m^2), \;\; e_2 = \frac{1}{3}(2m^2 - 1), \;\; e_3 = -\frac{1}{3}(1 + m^2). \tag{38}$$

From equation (38), one can see that the modulus m of the JEF and the $e's$ of the WEF are related by

$$m^2 = \frac{e_2 - e_3}{e_1 - e_3}. \tag{39}$$

We consider the ODE of order $2k$ given by

$$\frac{d^{2k}\phi}{d\xi^{2k}} = f(\phi; r+1), \tag{40}$$

where $f(\phi; r+1)$ is an $(r+1)$ degree polynomial in ϕ. We assume that

$$\phi = \gamma Q^{2s}(\xi) + \mu \tag{41}$$

is a solution of equation (40), where γ and μ are arbitrary constants and $Q^{(2s)}(\xi)$ is the $(2s)^{\text{th}}$ derivative of the reciprocal Weierstrass elliptic function (RWEF) $Q(\xi) = \dfrac{1}{\wp(\xi)}$, $\wp(\xi)$ being the WEF.

It can be shown that the $(2s)^{\text{th}}$ derivative of the RWEF $Q(\xi)$ is a $(2s+1)$ degree polynomial in $Q(\xi)$ itself. Therefore, for ϕ to be a solution of equation (40), we should have the relation

$$2k - r = 2rs. \tag{42}$$

So, it is necessary that $2k \geq r$ for us to assume a solution in the form of equation (41). But this is in no way a sufficient condition for the existence of the PWS in the form of equation (41).

Now, we shall search for the WEF solutions of equation (17). We introduce a restriction on the coefficients in the form $2B^2 = 9AC$, so that equation (17) reduces to

$$\gamma w'' + c_1 w + c_2 w^3 = 0, \tag{43}$$

where $c_1 = -\dfrac{1}{2}A,\ c_2 = C$.

For a solution of equation (43) in the form of equation (41), we should have $r = 2$ and $k = 1$ so that $s = 0$. So, our solution will be

$$u(\xi) = \frac{\tau}{\wp(\xi)} + \zeta. \tag{44}$$

Substituting equation (44) into equation (43) and equating the coefficients of like powers of $\wp(\xi)$ to zero, we obtain

$$\wp^3(\xi): \quad 2\gamma\tau - \frac{1}{2}A\zeta + C\zeta^3 = 0, \tag{45}$$

$$\wp^2(\xi): \quad -\frac{1}{2}A\tau + 3C\tau\zeta^2 = 0, \tag{46}$$

$$\wp(\xi): \quad -\frac{3}{2}\gamma\tau g_2 + 3C\tau^2\zeta = 0, \tag{47}$$

$$\wp^0(\xi): \quad -2\gamma\tau g_3 + C\tau^3 = 0. \tag{48}$$

From equations (46) through (48), it can be found that

$$\tau = \pm\sqrt{\frac{2\gamma g_3}{C}}, \tag{49}$$

$$\zeta = \pm\sqrt{\frac{A}{6C}}, \tag{50}$$

$$g_2 = 2\sqrt{\frac{A g_3}{3\gamma}}. \tag{51}$$

From equations (49) through (51), one can conclude that if $g_3 > 0$, A, C and γ should all be of the same signs, whereas for $g_3 < 0$, A and C should be of the same signs and γ should be of the opposite sign.

Equation (45) leads us to the value of g_3 given by

$$g_3 = \frac{A^3}{432\gamma^3}. \tag{52}$$

The condition $g_2^3 - 27g_3^2 > 0$ gives the relation

$$\frac{8}{9} > \frac{3}{4}, \tag{53}$$

which is remarkably true for any value of the coefficients in the governing equation.

The equations (34) through (36) will give rise to the same PWS of equation (43) which can be obtained using equation (44) with the help of equation (38). Thus the PWS of equation (43) in terms of JEFs can be written as

$$u(\xi) = \frac{\tau\,\mathrm{sn}^2(\xi)}{1 - \frac{1}{3}(1+m^2)\mathrm{sn}^2(\xi)} + \zeta. \tag{54}$$

As $m \to 1$, the SWSs of the coupled wave equation given by equations (6) and (7) with the restriction $2B^2 = 9AC$ are

$$u(x,t) = \frac{B}{3C} + \frac{\tau\tanh^2(x-ct)}{1 - \frac{2}{3}\tanh^2(x-ct)} + \zeta, \tag{55}$$

$$v(x,t) = \frac{2c}{\epsilon} - \frac{2\sigma}{\epsilon}\left[\frac{B}{3C} + \frac{\tau\tanh^2(x-ct)}{1 - \frac{2}{3}\tanh^2(x-ct)} + \zeta\right], \tag{56}$$

where τ and ζ are given by equations (49) and (50).

5 Conclusions

The (G'/G)-expansion method has been applied to a nonlinear coupled wave equation. The kink wave solution and the singular wave solution have been graphically illustrated. It was found that there are some restrictions on the coefficients in the governing equation for the solutions in terms of hyperbolic functions to exist. The WEF method has also been applied to the system of equations to derive SWSs. The condition $g_2^3 - 27g_3^2 > 0$ was found to be identically satisfied, which is a remarkable result and has never been reported in the literature. We intend to apply these methods for higher order and higher dimensional PDEs of physical interest.

References

[1] A. Biswas. Solitary wave solution for KdV equation with power law nonlinearity and time-dependent coefficients. *Nonlinear Dynamics* **58** (2009) 345–348.

[2] A. Biswas. Solitary waves for power-law regularized long wave equation and R(m,n) equation. *Nonlinear Dynamics* **59** (2010) 423–426.

[3] R. Sassaman and A. Biswas. Topological and non-topological solitons of the Klein-Gordon equations in $(1+2)$-dimensions. *Nonlinear Dynamics* **61** (2010) 23-28.

[4] A. Biswas, A.H. Kara, A.H. Bokhari and F.D. Zaman. Solitons and conservation laws of Klein-Gordon equation with power law and log law nonlinearities. *Nonlinear Dynamics* **73** (2013) 2191–2196.

[5] M. Mirzazadeh, M. Eslami, E. Zerrad, M.F. Mahmood, A. Biswas and M. Belic. Optical solitons in nonlinear directional couplers by sine-cosine function method and Bernoulli's equation approach. *Nonlinear Dynamics* **81** (2015) 1933–1949.

[6] W. Malfliet. The tanh method: Exact solutions of nonlinear evolution and wave equations. *Physica Scripta* **54** (1996) 563–568.

[7] M. Alquran and K. Al-Khaled K. Sinc and Solitary Wave Solutions to the Generalized Benjamin-Bona-Mahony-Burgers Equations. *Physica Scripta* **83** (2011) 065010 (6 pp).

[8] M. Alquran and K. Al-Khaled. The tanh and sine-cosine methods for higher order equations of Korteweg-de Vries type. *Physica Scripta* **84** (2011) 025010 (4 pp).

[9] S. Shukri and K. Al-Khaled. The Extended Tanh Method For Solving Systems of Nonlinear Wave Equations. *Applied Mathematics and Computation* **217** (2010) 1997–2006.

[10] M. Alquran, H.M. Jaradat and M. Syam. A modified approach for a reliable study of new nonlinear equation: two-mode Korteweg-de Vries-Burgers equation. *Nonlinear Dynamics* **91**(3) (2018) 1619–1626.

[11] A. Jaradat, M.S.M. Noorani, M. Alquran and H.M. Jaradat. A Variety of New Solitary-Solutions for the Two-mode Modified Korteweg-de Vries Equation. *Nonlinear Dynamics and Systems Theory* **19**(1) (2019) 88–96.

[12] J.H. He and X.H. Wu. Exp-function method for nonlinear wave equations. *Chaos Solitons and Fractals* **30** (2006) 700–708.

[13] J. Liu, L. Yang and K. Yang. Jacobi elliptic function solutions of some nonlinear PDEs. *Physics Letters A* **325** (2004) 268–275.

[14] M. Alquran and A. Jarrah. Jacobi elliptic function solutions for a two-mode KdV equation. *Journal of King Saud University-Science* (2017). https://doi.org/10.1016/j.jksus.2017.06.010.

[15] M. Alquran, A. Jarrah and E.V. Krishnan. Solitary wave solutions of the phi-four equation and the breaking soliton system by means of Jacobi elliptic sine-cosine expansion method. *Nonlinear Dynamics and Systems Theory* **18**(3) (2018) 233–240.

[16] M. Al Ghabshi, E.V. Krishnan and M. Alquran. Exact solutions of a Klein-Gordon system by (G'/G)-expansion method and Weierstrass elliptic function method. *Nonlinear Dynamics and Systems Theory* **19**(3) (2019) 386–395.

[17] Y. Peng. Exact periodic wave solutions to a new Hamiltonian amplitude equation. *J. of the Phys. Soc. of Japan* **72** (2003) 1356–1359.

[18] Y. Peng. New Exact solutions to a new Hamiltonian amplitude equation. *J. of the Phys. Soc. of Japan* **72** (2003) 1889–1890.

[19] Y. Peng. New Exact solutions to a new Hamiltonian amplitude equation II. *J. of the Phys. Soc. of Japan* **73** (2004) 1156–1158.

[20] E.V. Krishnan and Y. Peng. A new solitary wave solution for the new Hamiltonian amplitude equation. *J. of the Phys. Soc. of Japan* **74** (2005) 896–897.

[21] J.F. Alzaidy. Extended mapping method and its applications to nonlinear evolution equations. *Journal of Applied Mathematics* **2012(2012)** Article ID 597983, 14 pages.

[22] M. Al Ghabshi, E.V. Krishnan, K. Al-Khaled and M. Alquran. Exact and Approximate Solutions of a System of Partial Differential Equations, *International Journal of Nonlinear Science.* **23** (2017) 11–21.

[23] M. Syam, H.M. Jaradat and M. Alquran. A study on the two-mode coupled modified Korteweg-de Vries using the simplified bilinear and the trigonometric-function methods. *Nonlinear Dynamics* **90**(2)(2017) 1363–1371.

[24] H.M. Jaradat, M. Syam and M. Alquran. A two-mode coupled Korteweg-de Vries: multiple-soliton solutions and other exact solutions. *Nonlinear Dynamics* **90**(1)(2017) 371–377.

[25] M. Alquran. Bright and dark soliton solutions to the Ostrovsky-Benjamin-Bona-Mahony (OS-BBM) equation. *Journal of Mathematical and Computational Science* **2**(1) (2012) 15–22.

[26] M. Alquran, R. Al-Omary and Q. Katatbeh. New explicit solutions for homogeneous KdV equations of third order by trigonometric and hyperbolic function methods. *Applications and Applied Mathematics* **7**(1) (2012) 211–225.

[27] M. Alquran. Solitons and periodic solutions to nonlinear partial differential equations by the sine-cosine method. *Applied Mathematics and Information Sciences* **6**(1) (2012) 85–88.

[28] R. Hirota and J. Satsuma. Soliton solutions of a coupled Korteweg-de Vries equation. *Physics Letters A* **85** (1981) 407–408.

[29] R. Dodd and A.P. Fordy. On the integrability of a system of coupled KdV equations. *Physics Letters A* **89** (1982) 168–170.

[30] H. Gao and R.X. Zhao. New application of the (G'/G)-expansion method to high-order nonlinear equations. *Appl. Math Computation* **215** (2009) 2781–2786.

[31] F. Chand F. and A.K. Malik. Exact traveling wave solutions of some nonlinear equations using (G'/G)-expansion method. *International Journal of Nonlinear Science* **14** (2012) 416–424.

[32] M. Alquran and A. Qawasmeh. Soliton solutions of shallow water wave equations by means of (G'/G)-expansion method. *Journal of Applied Analysis and Computation* **4** (2014) 221–229.

[33] O. Yassin and M. Alquran. Constructing New Solutions for Some Types of Two-Mode Nonlinear Equations. *Applied Mathematics and Information Sciences* **12**(2) (2018) 361–367.

[34] M. Alquran and O. Yassin. Dynamism of two-mode's parameters on the field function for third-order dispersive Fisher: Application for fibre optics. *Optical and Quantum Electronics* **50**(9) (2018) 354.

[35] E.V. Krishnan. Remarks on a system of coupled nonlinear wave equations. *Journal of Mathematical Physics* **31** (1990) 1155–1156.

[36] D.W. Lawden. *Elliptic Functions and Applications*. Springer Verlag, Berlin, 1989.

Nonlinear Dynamics and Systems Theory, **19** (4) (2019) 523–536

Control, Stabilization and Synchronization of Fractional-Order Jerk System

A. Senouci * and T. Menacer

Department of Mathematics, Faculty of Exact Sciences, University of Biskra, Algeria

Received: May 31, 2019; Revised: October 14, 2019

Abstract: In this work we study the fractional-order jerk system stability by using the fractional Routh-Hurwitz conditions. These conditions have also been used to control the chaos of the proposed systems towards their equilibrium. It has been shown that the fractional-order systems are controlled at their equilibrium point unlike those of fractional order. The synchronization between two different coupled fractional systems is also achieved via the auxiliary system approach. The numerical simulation coincides with the theoretical analysis.

Keywords: *chaos; chaotic fractional-order system; Routh-Hurwitz criteria; chaos control; chaos synchronization.*

Mathematics Subject Classification (2010): 34C23, 34H10, 34H15, 34A34, 34D06, 37N35, 37C75, 37N30.

1 Introduction

Fractional calculus is a topic more than 300 years old. The idea of fractional calculus has been known since the regular calculus, with the first reference probably being associated with Leibniz and L'Hospital in 1695. Its applications to physics and engineering are just a recent focus of interest. It was found that many systems in interdisciplinary fields can be elegantly described with the help of fractional derivatives. In 1996, Hans Gottlieb thought,'What is the simplest jerk equation that gives chaos ?', by which he meant an equation of the form

$$\dddot{x} = f(\ddot{x}, \dot{x}, x).$$

* Corresponding author: mailto:assia.senouci@univ-biskra.dz

The term 'jerk' comes from the fact that in a mechanical system in which x is the displacement, $\dot{x}$ is the velocity, and $\ddot{x}$ is the acceleration, the quantity $\dddot{x}$ is called the 'jerk' (Schot, 1978). It is the lowest derivative for which an ODE with smooth continuous functions can give chaos.

In this paper, we investigate the chaotic behaviors of the fractional-order simple autonomous jerk system with cubic non-linearity. The system is a linear transformation of the MO4 and MO11 models introduced for the first time in [14]. We find that chaos exists in the fractional-order model MO4 and MO11 systems with an order less than 3. Many other studies on the dynamics in fractional-order systems are presented, in particular, in [13–15]. In addition, the auxiliary system method, generalized to the fractional-order, is also presented to synchronize the fractional chaotic order between MO4 and MO11. Both approaches, based on the theory of the stability of fractional order systems, are simple and theoretically rigorous. The results of the simulation are used to visualize and illustrate the effectiveness of the proposed synchronization methods.

2 Preliminaries

2.1 Fractional calculus

Fractional calculus is a generalization of integration and differentiation to the noninteger-order fundamental operator ${}_aD_\alpha^t$, where a and t are the bounds of the operation and $\alpha \in \mathbf{R}$. The continuous integro-differential operator is defined as

$$ {}_aD_\alpha^t = \begin{cases} \frac{d^\alpha}{dt^\alpha}, & \alpha > 0, \\ 1, & \alpha = 0, \\ \int_a^t (d\tau)^\alpha, & \alpha < 0. \end{cases} $$

In this paper, we will use the Caputo fractional derivatives defined by

$$ {}_aD_\alpha^t f(t) = \frac{1}{\Gamma(n-\alpha)} \int_a^t \frac{f^n(\tau)}{(t-\tau)^{\alpha-n+1}} d\tau \qquad \text{for } n-1 < \alpha < n. $$

2.2 Numerical method for solving fractional differential equations

For numerical simulation of the fractional-order system a predictor-corrector method has also been proposed [16]. It is suitable for Caputo's derivative because it just requires the initial conditions and for the unknown function it has a clear physical meaning. The method is based on the fact that the fractional differential equation

$$ \begin{cases} D_\alpha^t x(t) = f(t, x(t)), & 0 \le t < T, \\ x^{(k)}(0) = x_0^{(k)}, & k = 0, 1, ..., n-1, \end{cases} $$

is equivalent to the Volterra integral equation

$$ x(t) = \sum_{k=0}^{[\alpha]-1} x_0^{(k)} \frac{t^k}{k!} + \frac{1}{\Gamma(\alpha)} \int_0^t (t-\tau)^{\alpha-1} f(\tau, x(\tau)) d\tau. \tag{1} $$

Set $h = \frac{T}{N}$, $t_n = nh$, $n = 0, 1, ..., N$, then (1) can be discredited as follows:

$$\begin{aligned} x_h(t_{n+1}) &= \sum_{k=0}^{[\alpha]-1} x_0^{(k)} \frac{t_{n+1}^k}{k!} + \frac{h^\alpha}{\Gamma(\alpha+2)} f\left(t_{n+1}, x_h^p(t_{n+1})\right) \\ &\quad + \frac{h^\alpha}{\Gamma(\alpha+2)} \sum_{j=0}^{n} a_{j,n+1} f\left(t_j, x_h(t_j)\right), \end{aligned}$$

where

$$a_{j,n+1} = \begin{cases} n^{\alpha+1} - (n-\alpha)(n+1)^\alpha, & j = 0, \\ (n-j+2)^{\alpha+1} + (n-j)^{\alpha+1} - 2(n-j+1)^{\alpha+1}, & 1 \le j \le n, \\ 1, & j = 1, \end{cases}$$

$$x_h^p(t_{n+1}) = \sum_{k=0}^{[\alpha]-1} x_0^{(k)} \frac{t_{n+1}^k}{k!} + \frac{1}{\Gamma(\alpha)} \sum_{j=0}^{n} b_{j,n+1} f\left(t_j, x_h(t_j)\right),$$

$$b_{j,n+1} = \frac{h^\alpha}{\alpha}\left((n+1-j)^\alpha + (n-j)^\alpha\right), \qquad 0 \le j \le n \quad .$$

This method, the error is estimated as

$$\varepsilon = \max_{j=0,1,\ldots,N} \left| x(t_j) - x_h(t_j) \right| = o\left(h^p\right),$$

where $p = \min(2, 1+\alpha)$.

2.3 Fractional-order Routh-Hurwitz stability conditions

Let us consider the following three-dimensional fractional-order commensurate system:

$$D^\alpha x = f(x),$$

where $\alpha \in \left]0, 1\right]$, $x \in \mathbf{R}^3$. We suppose that x_{eq} is an equilibrium point of this system, then its characteristic equation is given as

$$P(\lambda) = \lambda^3 + a_1\lambda^2 + a_2\lambda + a_3 = 0,$$

its discriminant is given by

$$D(P) = 18a_1a_2a_3 + (a_1a_2)^2 - 4a_3(a_1)^3 - 4(a_2)^3 - 27(a_3)^2.$$

We have the following fractional-order Routh–Hurwitz conditions:

1. If $D(P) > 0$, then the necessary and sufficient condition for the equilibrium point E to be locally asymptotically stable is $a_1 > 0, a_3 > 0$ and $a_1a_2 - a_3 > 0$.
2. If $D(P) < 0, a_1 \ge 0, a_2 \ge 0, a_3 > 0$, then E is locally asymptotically stable for $\alpha < 2/3$. However, if $D(P) < 0, a_1 < 0, a_2 < 0, \alpha > 2/3$, then E is unstable.
3. If $D(P) < 0, a_1 > 0, a_2 > 0, a_1a_2 - a_3 = 0$, then E is locally asymptotically stable for all $\alpha \in]0, 1[$.
4. The necessary condition for the equilibrium point E to be locally asymptotically stable is $a_3 > 0$.

3 Description and Analysis of the Models

3.1 First model

The mathematical model of the jerk system considered in this work is expressed by the following set of three coupled first-order nonlinear differential equations:

$$\begin{cases} \frac{d^\alpha x}{dt^\alpha} = y, \\ \frac{d^\alpha y}{dt^\alpha} = z, \\ \frac{d^\alpha z}{dt^\alpha} = -\mu z - y - \beta e^x + \delta, \end{cases} \tag{2}$$

where the parameters μ, β and δ are positive reals and μ is the fractional-order of system (2) which has the only equilibrium point, which is found by equating the right-hand sides of system (2) to zero and is given as follows: $E\left(\ln \frac{\delta}{\beta} 0, 0\right)$.

3.1.1 Stability of the equilibrium point

Proposition 3.1 *1. If $\mu < \sqrt{3}$, then E is asymptotically stable for $\alpha < 2/3$. In addition to this condition, if $\beta = \mu$, then E is locally asymptotically stable for all $\alpha \in]0, 1[$.*

2. If $\mu > \sqrt{3}$ and $\beta < \frac{1}{3}\mu - \frac{2}{27}\mu^3 + \frac{2}{27}\sqrt{\left(\mu^2-3\right)^3}$, then the first stability condition holds.

Proof. The characteristic polynomial of the equilibrium point $E\left(\ln \frac{\delta}{\beta} 0, 0\right)$ is given by

$$\lambda^3 + \mu\lambda^2 + \lambda + \beta = 0,$$

so

$$a_1 = \mu > 0, a_2 = 1 > 0, a_3 = \beta > 0$$

and

$$D_E(p) = -4\mu^3\beta + \mu^2 + 18\mu\beta - 27\beta^2 - 4.$$

1. If $\mu < \sqrt{3}$, then $D_E(p) < 0$. Thus achieving the second of the stability conditions, therefore E is asymptotically stable for $\alpha < 2/3$. Moreover, if $\beta = \mu$ is verified, which means fulfilling the condition

$$a_1 \times a_2 - a_3 = 0.$$

From all of the foregoing, we arrive at the realization of the third stabilization conditions and from it, we conclude that the equilibrium point E is locally asymptotically stable for all $\alpha \in]0, 1[$.

2. If $\mu > \sqrt{3}$ and $\beta < \frac{1}{3}\mu - \frac{2}{27}\mu^3 + \frac{2}{27}\sqrt{\left(\mu^2-3\right)^3}$, both conditions result in satisfaction of $D(P) > 0$ and $a_1 > 0, a_3 > 0$ and $a_1 a_2 - a_3 > 0$, then the first stability condition holds.

3.1.2 Chaos

For the parameter values $\mu = 0.5$, $\beta = 1$ and $\delta = 5$, the integer-order form of the system (2) presents chaotic behavior, with the largest exponent of Lyapunov calculated numerically $LE = 0.035$, and its equilibrium $E(\ln 5, 0, 0)$ is locally asymptotically stable when $\alpha < 2/3$ and their eigenvalues are given as: $\lambda_1 = -1.6787$, $\lambda_{2,3} = 0.58933 \pm 1.6221i$. The equilibrium point is a saddle point of index 2, thus the necessary condition for the fractional-order system (2) to remain chaotic is $\alpha > \frac{2}{\pi} \arctan\left(\frac{|\lambda_{2,3}|}{\mathrm{Re}\,\lambda_{2,3}}\right)$. Consequently, the lowest fractional order α, for which the fractional-order system (2) demonstrates chaos at the above-mentioned parameters, is given by the inequality
$\alpha > 0.79051$, see Figs.1 and 2.

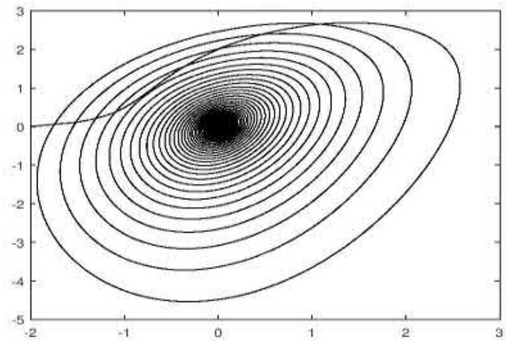

Figure 1: Phase plots of attractor generated by (2) y-z plane with $\mu = 0.5$, $\beta = 1$ and $\delta = 5$, at $\alpha = 0.77$.

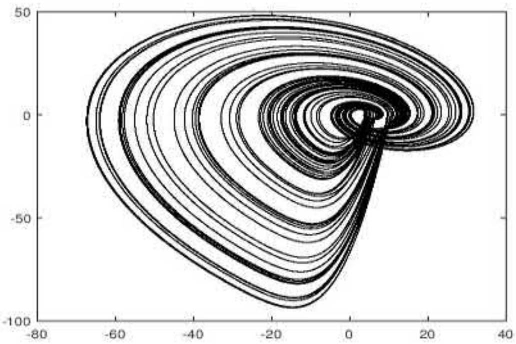

Figure 2: Phase plots of attractor generated by (2) y-z plane with $\mu = 0.5$, $\beta = 1$ and $\delta = 5$, at $\alpha = 0.97$.

3.1.3 Chaos control of the fractional-order systems

A three-dimensional fractional-order chaotic system and the control of chaos are described as follows:

$$\begin{cases} \frac{d^{\alpha}X}{dt^{\alpha}} = F\left(X\right), \\ \frac{d^{\alpha}X}{dt^{\alpha}} = F\left(X\right) - K\left(X - X^{*}\right), \end{cases}$$

where $\alpha = (\alpha_1, \alpha_2, \alpha_3) \in \mathbf{R}^3$, $\alpha_i > 0$, is the fractional order and the systems are chaotic. K is a coupling matrix. For simplicity, let K have the form $K = diag(k_1, k_2, k_3)$, where $k_i \geq 0$. The error is $e = X - X^*$ and the aim of the control is to design the coupling matrix so that $||e(t)|| \to 0$ as $t \to +\infty$. Let us consider the system (2). The controlled fractional-order system associated with the system (2) is given by

$$\begin{cases} \frac{d^{\alpha}x}{dt^{\alpha}} = y - k_1(x - x^*), \\ \frac{d^{\alpha}y}{dt^{\alpha}} = z - k_2(y - y^*), \\ \frac{d^{\alpha}z}{dt^{\alpha}} = -\alpha z - y - \beta e^x + \delta - k_3(z - z^*), \end{cases} \tag{3}$$

where (x^*, y^*, z^*) represents an arbitrary equilibrium point of system (2). The goal is to drive the system trajectories to any of the three unstable equilibrium point E. For simplicity, we are going to choose the feedback gains $K = diag(0, k_2, 0)$.

3.1.4 Stabilizing the equilibrium point

Sufficient conditions for the stabilization of the controlled systems (3) are given in the following proposition.

Proposition 3.2 *If* $k_2 = -\frac{1}{2\mu}\left(-\sqrt{-2\mu^2 + \mu^4 + 4\mu\beta + 1} + \mu^2 + 1\right)$ *and the parameter* β *satisfies* $\beta > 0$*, then the trajectories of the controlled system* (3) *are driven to the unstable equilibrium point* E*.*

Proof. The characteristic equation of the controlled system (3) at E is given as

$$\lambda^3 + \left(k_2 + \mu\right)\lambda^2 + \left(\mu k_2 + 1\right)\lambda + \beta.$$

Choose the parameter $\beta > \mu$ and the feedback control gain

$$k_2 = -\frac{1}{2\mu}\left(-\sqrt{-2\mu^2 + \mu^4 + 4\mu\beta + 1} + \mu^2 + 1\right).$$

If $D(p) < 0$ for the found value of the parameter k_2, then the stability condition (3) holds and the trajectories of the controlled system (3) are driven to the stable equilibrium point E for all $\alpha \in]0, 1[$.

3.1.5 Numerical results

In this section, we apply the result in the previous system (2) for the purpose of control chaos, we take $\mu = 0.5$, $\beta = 1, \delta = 5$ and the fractional order $q = 0.97$, by Proposition 3.2 we have $k_2 = 0.35078$, $k_1 = k_3 = 0$. It follows that $D(p){=}{-22.25} < 0$, $a_1 > 0$, $a_2 > 0$, $a_1 a_2 = a_3$. Therefore, the stability conditions (3) and (4) are checked. This implies that the trajectories of the controlled fractional-order system (3) converge to the equilibrium point as shown in Fig. 3. But in the integer-order case, there are two pure imaginary eigenvalues of the characteristic equation. This means that the integer-order form of the controlled system (3) is not stabilized to the same equilibrium point when choosing the above-mentioned parameter values and feedback control gains see Fig. 4.

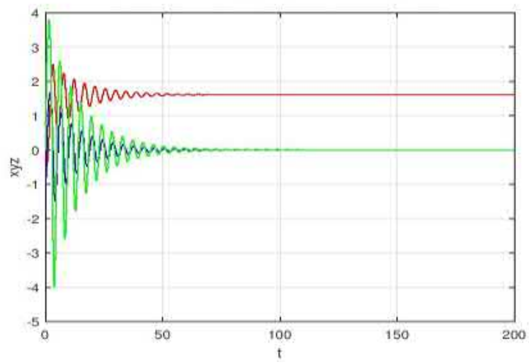

Figure 3: The trajectories of the controlled system (3), $\mu = 0.5$,$\beta = 1, \delta = 5$ and the controllers $k_2 = 0.35078$, $k_1 = k_3 = 0$. Stabilized to the equilibrium point E for $\alpha = 0.97$.

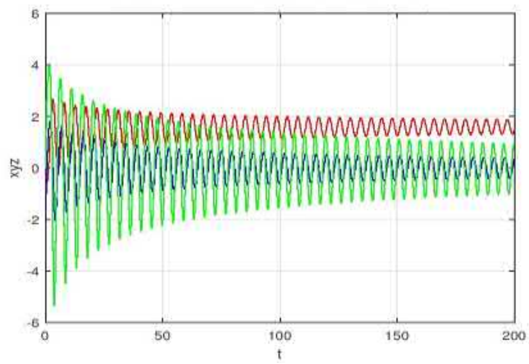

Figure 4: The trajectories of the controlled system (3), $\mu = 0.5$, $\beta = 1, \delta = 5$ and the controllers $k_2 = 0.35078$, $k_1 = k_3 = 0$. Not stabilized to the equilibrium point E for $\alpha = 1$.

3.2 Second model

The mathematical model of the jerk system considered in this work is expressed by the following set of three coupled first-order nonlinear differential equations:

$$\begin{cases} \frac{d^\alpha x}{dt^\alpha} = y, \\ \frac{d^\alpha y}{dt^\alpha} = z, \\ \frac{d^\alpha z}{dt^\alpha} = -\mu z - y - \sigma x\left(x-1\right), \end{cases} \tag{4}$$

where the parameters μ and σ are positive reals and α is the fractional-order. The system (4) has two equilibrium points which are found by equating the right-hand sides of (4) to zero and are given as follows: $E_1\,(0,0,0)\,, E_2\,(1,0,0)\,.$

3.2.1 Stability of the equilibrium points

The characteristic polynomial of the equilibrium point E_1 is given by

$$\lambda^3 + \mu\lambda^2 + \lambda - \sigma = 0.$$

So $a_3 = -\sigma < 0$, then E_2 is unstable. The characteristic polynomial of the equilibrium point E_2 is given by

$$\lambda^3 + \mu\lambda^2 + \lambda + \sigma = 0.$$

So $a_1 = \mu > 0$, $a_2 = 1 > 0$, $a_3 = \sigma > 0$ and $\mu^2 + 18\mu\sigma - 27\sigma^2 - 4$.

If $\mu < \sqrt{3}$, then $D_E\,(p) < 0$ and E_2 is asymptotically stable for $\alpha < 2/3$. However, if $\sigma = \mu$, then E_2 is locally asymptotically stable for all $\alpha \in]0,1[$ according to the third condition of the Routh-Hurwitz criterion.

If $\mu > \sqrt{3}$ and $\sigma < \frac{1}{3}\mu - \frac{2}{27}\mu^3 + \frac{2}{27}\sqrt{(\mu^2-3)^3}$, then the first condition of the Routh-Hurwitz criterion holds. From which stability is achieved.

3.2.2 Chaos

For the parameter values $\mu = 0.5$ and $\sigma = 1$, the integer-order form of the system (4) presents chaotic behavior, with the largest exponent of Lyapunov calculated numerically $LE = 0.094$, and its equilibrium E_1 is unstable and $E_2(1,0,0)$ is locally asymptotically stable when $\alpha < 2/3$ and their eigenvalues are given as E_2:$\lambda_1 = -0.803\,76$, $\lambda_{2,3} = 0.151\,88 \pm 1.105i$ $E_2 : \lambda_1 = 0.601\,49$, $\lambda_{2,3} = -0.550\,75 \pm 1.165\,9i$. The equilibrium point E_2 is a saddle point of index 2, thus the necessary condition for the fractional-order system (4) to remain chaotic is $\alpha > \frac{2}{\pi}\arctan\left(\frac{|\lambda_{2,3}|}{\operatorname{Re}\lambda_{2,3}}\right)$. Consequently, the lowest fractional order α, for which the fractional-order system (4) demonstrates chaos at the above-mentioned parameters, is given by the inequality $\alpha > 0.913\,84$, see fig. 5 and 6.

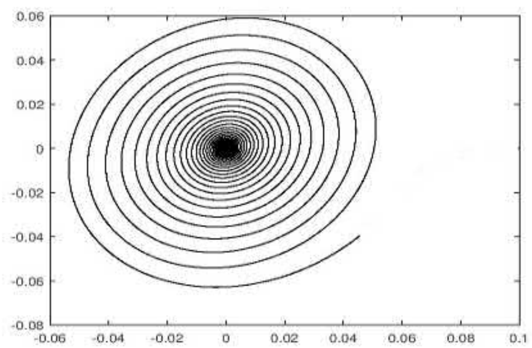

Figure 5: Phase plots of attractor generated by (3) y-z plane with $\mu = 0.5$ and $\sigma = 1$, at $\alpha = 0.99$.

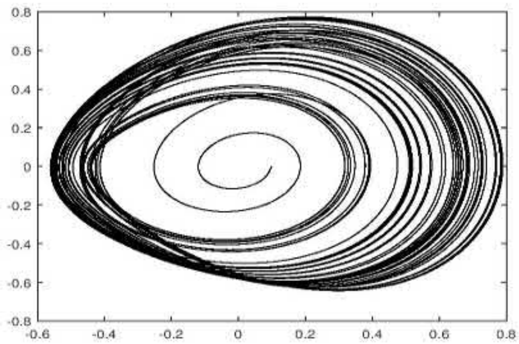

Figure 6: Phase plots of attractor generated by (3) y-z plane with $\mu = 0.5$ and $\sigma = 1$, at $\alpha = 0.99$.

3.2.3 Chaos control of the fractional-order systems

The controlled fractional-order system assisted with system (4) is given by

$$\begin{cases} \frac{d^\alpha x}{dt^\alpha} = y - k_1(x - x^*), \\ \frac{d^\alpha y}{dt^\alpha} = z - k_2(y - y^*), \\ \frac{d^\alpha z}{dt^\alpha} = -\mu z - y - \sigma x\,(x-1) - k_3(z - z^*), \end{cases} \tag{5}$$

where (x^*, y^*, z^*) represents an arbitrary equilibrium point of system (4). The goal is to drive the system trajectories to any of the two unstable equilibrium points E_1 and E_2. As in the previous model we chose the feedback gains $K = diag(0, k_2, 0)$.

3.2.4 Stabilizing the equilibrium points

Sufficient conditions for the stabilization of the controlled systems (5) are given in the following proposition.

Proposition 3.3 • *The trajectories of the system* (5) *are not driven to the unstable equilibrium point* E_1.

- *If* $k_1 = -\frac{1}{2\mu}\left(-\sqrt{-2\mu^2 + \mu^4 + 4\mu\sigma + 1} + \mu^2 + 1\right)$ *and the parameter* σ *satisfies* $\sigma > 0$, *then the trajectories of the controlled system* (5) *are driven to the stable equilibrium point* E_1 *for all* $q \in]0, 1[$.

Proof. • The characteristic equation of the controlled system at E_1 is given as

$$\lambda^3 + (k_2 + \mu)\,\lambda^2 + (k_2\mu + 1)\,\lambda - \sigma = 0.$$

We have $a_3 = -\sigma$, according to the fourth condition of the Routh -Hurwitz criterion, the system (5) can not be stable.

• By choosing the parameter $\sigma > \alpha$ and the feedback control gain

$$k_2 = -\frac{1}{2\mu}\left(-\sqrt{-2\mu^2 + \mu^4 + 4\mu\sigma + 1} + \mu^2 + 1\right)$$

and assuming that $D(p) < 0$, the stability condition (3) is satisfied and the trajectories of the controlled system (5) are driven to the stable equilibrium point E_2 for all $\alpha \in]0, 1[$.

3.2.5 Numerical results

In this section, we take $\alpha = 0.5$, $\sigma = 1$ and the fractional-order $\alpha = 0.98$, by Proposition 3.3 we have $k_2 = 0.35078$, $k_1 = k_3 = 0$. It follows that $D(p) < 0, a_1 > 0, a_2 > 0, a_1 a_2 = a_3$. Therefore, the stability conditions (3) and (4) are checked. This implies that the trajectories of the controlled fractional-order system (5) converge to the equilibrium point E_2 as shown in Fig. 7. But in the integer-order case, there are two pure imaginary eigenvalues of the characteristic equation. This means that the integer-order form of the controlled system (5) is not stabilized to the same equilibrium point when choosing the above-mentioned parameter values and feedback control gains, Fig. 8.

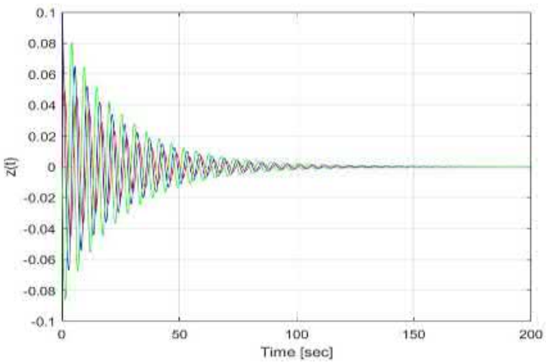

Figure 7: The trajectories of the controlled system (5) for $\mu = 0.5$, $\sigma = 1$, $k_2 = 0.35078$ and $k_1 = k_3 = 0$. Stabilized to the equilibrium point E_2 for $\alpha = 0.98$.

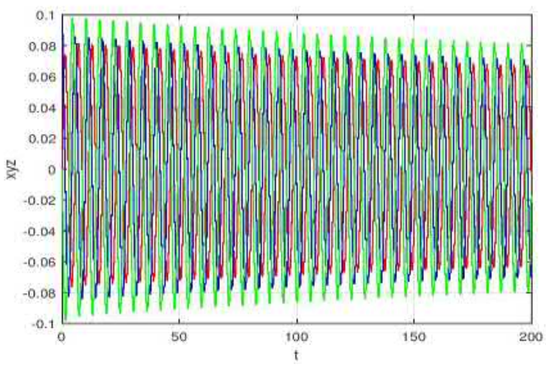

Figure 8: The trajectories of the controlled system (5) for $\mu = 0.5$, $\sigma = 1$, $k_2 = 0.35078$ and $k_1 = k_3 = 0$. Not stabilized to the equilibrium point E_2 for $\alpha = 1$.

4 Chaos Synchronization

In this section, we realize the synchronization between two different fractional-order systems via the auxiliary system approach. We choose as a master system the following system:

$$\begin{cases} \frac{d^\alpha x_1}{dt^\alpha} = y_1, \\ \frac{d^\alpha y_1}{dt^\alpha} = z_1, \\ \frac{d^\alpha z_1}{dt^\alpha} = -\mu z_1 - y_1 - \beta e^{x_1} + \delta, \end{cases} \tag{6}$$

and the slave system is

$$\begin{cases} \frac{d^\alpha x_2}{dt^\alpha} = y_2 - k_1(x_2 - x_1), \\ \frac{d^\alpha y_2}{dt^\alpha} = z_2 - k_2(y_2 - y_1), \\ \frac{d^\alpha z_2}{dt^\alpha} = -\mu z_2 - y_2 - \sigma x_2\,(x_2 - 1) - k_3(z_2 - z_1). \end{cases} \tag{7}$$

The master system is coupled with the slave system only by the scalar $x(t)$. We choose the auxiliary system that is identical to the slave system (7) (with different initial conditions)

$$\begin{cases} \frac{d^\alpha x_3}{dt^\alpha} = y_3 - k_1(x_3 - x_1), \\ \frac{d^\alpha y_3}{dt^\alpha} = z_3 - k_2(y_3 - y_1), \\ \frac{d^\alpha z_3}{dt^\alpha} = -\mu z_3 - y_3 - \sigma x_3\,(x_3 - 1) - k_3(z_3 - z_1). \end{cases} \tag{8}$$

The substraction of two systems (7) and (8) yields the fractional-order synchronization error system which can be written as follows:

$$\begin{cases} \frac{d^q e_1}{dt^q} = e_2 - k_1 e_1, \\ \frac{d^q e_2}{dt^q} = e_3 - k_2 e_2, \\ \frac{d^q e_3}{dt^q} = -\alpha e_3 - e_2 - \sigma e_1 x_3 - \sigma e_1 x_2 - e_{1-} k_3 e_3, \end{cases} \tag{9}$$

where $e_1 = x_3 - x_2$, $e_2 = y_3 - y_2$ and $e_3 = z_3 - z_2$. Further (9) can be written as

$$\frac{d^\alpha e}{dt^\alpha} = Ae + \varphi(x_{2,3}, y_{2,3}, z_{2,3}), \tag{10}$$

where $e = [e_1, e_2, e_3]^T$

$$A = \begin{bmatrix} -k_1 & 1 & 0 \\ 0 & -k_2 & 1 \\ -1 & -1 & -\mu - k_3 \end{bmatrix}, \quad \varphi(x_{2,3}, y_{2,3}, z_{2,3}) = \begin{pmatrix} 0 \\ 0 \\ -\sigma e_1\,(x_2 + x_3) \end{pmatrix},$$

$\varphi(x_{2,3}, y_{2,3}, z_{2,3})$ is a nonlinear function satisfying the Lipschitz condition, so, near to zero, it converges to zero. To study the stability of the system (10), we use the conditions of the Routh-Hurwitz criterion generalized in fractional order. The characteristic polynomial of matrix A is given by

$\lambda^3 + (\mu + k_1 + k_2 + k_3)\lambda^2 + ((\mu + k_3)\,(k_1 + k_2) + k_1 k_2 + 1)\lambda + (k_1 + k_1 k_2(\mu + k_3) + 1)$.

For simplicity, we choose the feedback gains $k_1 = k_2 = 0$ and $k_3 = k$. The characteristic polynomial becomes

$$P(\lambda) = \lambda^3 + (k + \mu)\lambda^2 + \lambda + 1. \tag{11}$$

Its discriminant is as follows:

$$D(p) = -3k^2 + (18 - 6\mu)k - 3\mu^2 + 18\mu - 31,$$

which is always negative for all values of k and μ, now for the condition $a_1 \times a_2 - a_3 = 0$ to be satisfied, it is enough that $k = 1 - \mu$. Therefore the zero solution of the system (9) is locally asymptotically stable for all $\alpha \in]0; 1[$. In this case, the fractional-order drive and response systems (6) and (7) are synchronized.

4.1 Numerical results

In numerical simulations, we set the parameters of the drive system as $\mu = 0.5$, $\beta = 1$ and $\delta = 5$, the parameters of the response and auxiliary systems as $\mu = 0.5$ and $\sigma = 1$ with the fractional-order $\alpha = 0.98$ and the coefficient of control function $k = 0.5$. We also have the initial conditions $x_1(0) = 1, y_1(0) = 2, z_1(0) = 5$ for the drive system, the initial conditions $x_2(0) = 10, y_2(0) = 32, z_2(0) = 7$ for the slave system, and $x_3(0) = 9, y_3(0) = 28, z_3(0) = 8$ for the auxiliary system. Numerical results show that the synchronization of two different fractional-order systems is achieved, see Fig. 9.

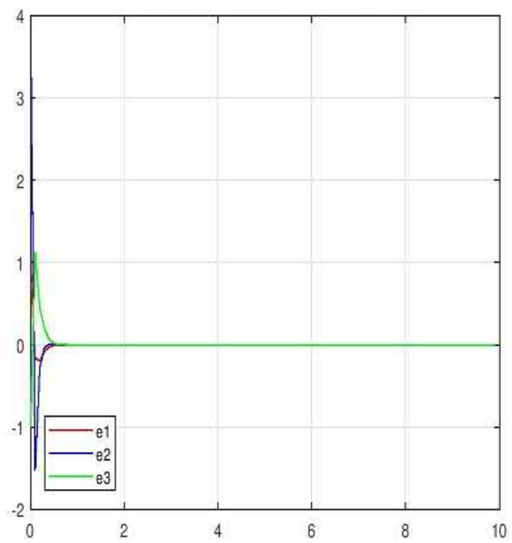

Figure 9: Synchronization error of the coupled systems.

5 Conclusion

In this study, we examined the local stability of the equilibrium in fractional system by using the fractional Routh-Hurwitz conditions which are also used to control chaos in the proposed systems towards their equilibrium by choosing some specific linear controllers. We showed that the fractional-order systems are controlled to their equilibrium points, however, their integer-order counterparts are not. This fact gives an advantage to the fractional-order systems compared with their integer-order counterparts, the effect of the fractional system on the synchronization of the chaos of these systems was also presented. And the numerical simulation matches with the theoretical analysis.

References

[1] A. A. Taher Azar, S. Vaidyanathan and A. Ouannas. *Fractional Order Control and Synchronization of Chaotic Systems*. Springer, 2017.

[2] A. E. Matrouk. Chaos, feedback control and synchronization of a fractional order modified Autonomous Van der Pol-Duffing circuit. *J. Communications in Nonlinear Science and Numerical Simulation* **16** (2010) 975–986.

[3] A. Hajipour and S. S. Aminabadi. Synchronization of Chaotic Arneodo System of Incommensurate Fractional Order with Unknown Parameters using Adaptive Method. *Optik* **127** (19)(2016) 7704–7709.

[4] A. Khan and M. A. Bhat. Hybrid Projective Synchronization of Fractional Order Chaotic Systems with Fractional Order in the Interval (1,2). *Nonlinear Dynamics and Systems Theory* **16** (1)(2016) 350–365.

[5] C. Li, X. Liao and J. Yu. Synchronization of fractional order chaotic systems. *Phys. Rev. E* **68** (2003) 067203.

[6] C. Li and G. Chen. Chaos and hyperchaos in fractional order Rossler equations. *Physica A.* **341** (2004) 55–61.

[7] D. Cafagna and G. Grassi. Fractional-order Chua's circuit: Time-doma analysis, bifurcation chaotic behavior and test for chaos. *Int. J. Bifurcation and Chaos* **358** (2008) 615–639.

[8] D. Chen, R. Zhang and J. C. Sprott, Synchronization between integer-order chaotic systems and a class of fractional-order chaotic system based on fuzzy sliding mode control. *Nonlinear Dynamics* **70** (2012) 1549-1561.

[9] E. Ahmed, A. M. A. El-Sayed and H. A. El Saka. On some Routh-Hurwitz conditions for fractional order differential equations and their applications in Lorenz, Rosler, Chua and Chen Systems. *Phys. Lett. A* **358** (1) (2006) 1–4.

[10] G. L. Jun. Chaotic dynamics and synchronization of fractional-order Arneodo's systems. *Chaos, Solitons and Fractals* **26** (2005) 1125–1133.

[11] H. Taghvafard and G. H. Erjaee. Phase and anti-phase synchronization of fractional order chaotic systems via active control. *J. Commun Nonlinear Sci. Numer Simulat.* **16** (2011) 4079–4088.

[12] I. Petras. Fractional-Order Nonlinear Systems: Modeling, Analysis and Simulation. *Nonlinear Physical Science* 2011.

[13] J. C. Sprott. Some simple chaotic jerk functions. *Am. J. Phys.* **65** (1997) 537–543.

[14] J. C. Sprott. Simple chaotic systems and circuits. *Am. J. Phys.* **68** (2000) 758–763.

[15] J. C. Sprott. *Elegant Chaos: Algebraically Simple Flow.* World Scientific Publishing, Singapore, 2010.

[16] K. Diethelm N. D. Ford and A. D. Freed. A Predictor-Corrector Approach for the Numerical Solution of Fractional Differential Equations. *Nonlinear Dyn.* **29** (2002) 3–22.

[17] L. M. Pecora and T. L. Carroll, Synchronization in chaotic systems. *J. Physical Review Letters* **64** (1990) 821–824.

[18] L. Pan, W. Zhou L. G. Zhou, K. and Sun K. Chaos synchronization between two different fractional-order hyperchaotic systems. *J. Common Nonlinear Sci. Numer. Simulat.* **16** (2011) 2628–2640.

[19] P. Louodop, M. Kountchou, H. Fotsin, and S. Bowong. Practical finite-time synchronization of jerk systems: theory and experiment. *Nonlinear Dyn.* **78** (2014) 597–607.

[20] S., Kaouache and M.S. Abdelouahab. Generalized Synchronization Between Two Chaotic Fractional Non-Commensurate Order Systems with Different Dimensions. *Nonlinear Dynamics and Systems Theory* **18** (3) (2018) 273–284.

[21] T. Menacer and N. Hamri. Synchronization of different chaotic fractional-order systems via approached auxiliary system the modified Chua oscillator and the modified Van der Pol-Duffing oscillator. *Electronic Journal of Theoretical Physics, EJTP* **25** (8) (2011) 253–266.

[22] W. Ahmada, R. El-Khazalib and A. Al-Assaf. Stabilization of generalized fractional order chaotic systems using state feedback control. *Chaos, Solitons and Fractals* **22** (2004) 141–150.

[23] W. M. Ahmad and J. C. Sprott. Chaos in fractional-order autonomous nonlinear systems. *Chaos, Solitons and Fractals* **16** (2003) 339–351.

[24] W. Laouira and N. Hamri. Feedback Control of Chaotic Systems by Using Jacobian Matrix Conditions. *Nonlinear Dynamics and Systems Theory* **18** (3) (2018) 285–296.

[25] Y. Xu, W. Zhou, J. Fang, W. Sun and L. Pan. Adaptive synchronization of stochastic time-varying delay dynamical networks with complex-variable systems. *Nonlinear Dynamics* **81** (2015) 1717–1726.

[26] Z. Jindao, L. Chunbiao, S. Bing and H. Wen. Synchronisation control of composite chaotic systems. *International Journal of Systems Science* **47** (16) (2016) 3952–3959.

Nonlinear Dynamics and Systems Theory, **19** (4) (2019) 537–550

Existence and Stability of Equilibrium Points in the Problem of a Geo-Centric Satellite Including the Earth's Equatorial Ellipticity

Sushil Yadav [1], Vinay Kumar [2*] and Rajiv Aggarwal [3].

[1] *Maharaja Agrasen College, University of Delhi, Delhi, India*
[2] *Zakir Husain Delhi College, University of Delhi, Delhi, India*
[3] *Sri Aurobindo College, University of Delhi, Delhi, India*

Received: November 12, 2017; Revised: September 26, 2019

Abstract: This paper deals with the existence and stability of the equilibrium points in the problem of a geo-centric satellite including the earth's equatorial ellipticity. We have determined the equations of motion of the geo-centric satellite which include the earth's equatorial ellipticity parameter Γ (the satellite's angular position relative to the minor axis of the earth's equatorial section) and then we have investigated the existence and stability of equilibrium points. It is observed that there exists an infinite number of equilibrium points which lie on a circle for different values of Γ. It is shown that the effect of the earth's equatorial ellipticity parameter Γ on the location of equilibrium points is very small (i.e., the coordinates of the equilibrium points are different after the fifth decimal places). Further, we have observed that the collinear points are unstable for different values of Γ. The non-collinear points lying on the y-axis are unstable for different values of Γ. We have also found that some of the non-collinear points lying on the circle are stable and others are unstable for different values of Γ.

Keywords: *geo-centric satellite; earth's equatorial ellipticity; equilibrium points and stability.*

Mathematics Subject Classification (2010): 70F07, 70F10, 70F15.

* Corresponding author: mailto:vkumar@zh.du.ac.in

1 Introduction

The motion of an artificial satellite is affected by various forces, some of which are the earth's gravitational field, atmospheric drag, solar radiation pressure, lunar and solar gravitational fields, relativistic effect and Poynting-Robertson drag. In recent years, the idea of establishing an artificial satellite in a synchronous equatorial orbit about the earth has become increasingly attractive. Since such a satellite would remain above the same position on the earth's equator, it could be used as a communication relay station between any two points on the earth which are within its field of view.

Sehnal [8] discussed the influence of the equatorial ellipticity of the earth's gravitational field on the motion of a close satellite. The method of variation of constants is applied to discuss the perturbation of angular elements. Blitzer [4] discussed the motion of a satellite under the influence of the longitude-dependent terms of the geopotential in a frame of reference rotating with the mean motion of the spacecraft. Allan [1] investigated the motion in longitude of a nominally geostationary satellite due to the tesseral harmonics. He further developed the corrective impulses required for the principal $J_{2,2}$ term. Wagner [9] investigated the motion of 24-hour near equatorial earth satellites in an earth gravity field through the 4^{th} order. Bhatnagar and Mehra [3] discussed the motion of a satellite under the gravitational forces of the sun, moon, earth (including the ellipticity of the earth's equator) and solar radiation pressure. They studied the orientation of the orbital plane of a geosynchronous satellite. It is shown that the significant effect of the earth's equatorial ellipticity is to produce a change in the relative angular position Γ of the satellite as seen from the earth. Bhatnagar and Kaur [2] studied the in-plane perturbation of the satellite caused by the attraction of the sun, moon and oblate earth including the earth's equatorial ellipticity. Gilthorpe and Moore [6] developed a theory for the motion of a satellite in a nearly circular orbit perturbed by zonal harmonic terms in the earth's gravity field. Mark [7] developed a first-order analytical theory of the tesseral harmonic J_2^2 effects on satellite orbits. Correa et al. [13] investigated two models of the restricted three-body and four-body problems. They determined the transfer orbits from a parking orbit around the Earth to the halo orbit in both the dynamical models. They also compared the total velocity increment to both the models. Prado [14] studied space trajectories in the circular restricted three-body problem. He assumed that the spacecraft moves under the gravitational forces of two massive bodies which are in circular orbits. He also determined orbits which can be used to transfer a spacecraft from one body back to the same body or to transfer a spacecraft from one body to the respective Lagrangian points L4 and L5. Yadav and Aggarwal [10] investigated resonances resulting from the commensurability between the mean motion of a geo-centric satellite and the earth's equatorial ellipticity parameter. Kumari and Kushvah [11] studied the stability regions of equilibrium points in the restricted four-body problem with oblateness effects. Camargo et al. [12] studied the attitude synchronization of two dumbbell shaped satellites by using a generalized Hamiltonian systems approach. They presented the numerical results of the synchronization behavior of the satellites.

In this paper, we aim to investigate the impact of the earth equatorial ellipticity parameter Γ on the location and stability of the equilibrium points, which exist in the problem of a geo-centric satellite. The effect of the earth's equatorial ellipticity parameter Γ is also analyzed on the zero-velocity curves by taking different values of the Jacobi constants.

This paper is organized as follows. We write the equations of motion of geo-centric satellite and find the Jacobi integral of the system in Section 2. In Section 3, we determine equilibrium points and describe the zero-velocity curves whereas, in Section 4, we examine the stability of the equilibrium points. Finally, Section 5 includes the discussion and conclusions of the paper.

2 Configuration and the Equation of Motion

The equations of motion of the geo-centric satellite $P(r, \theta, \phi)$ moving around the earth E in the equatorial plane are given in [5]:

$$M_s\left(\ddot{r} - r\dot{\theta}^2\cos^2\phi - r\dot{\phi}^2\right) = \frac{\partial U}{\partial r}, \tag{1}$$

$$M_s\left(\frac{1}{r\cos\phi}\frac{d}{dt}\left(r^2\dot{\theta}\cos\phi\right)\right) = \frac{1}{r\cos\phi}\frac{\partial U}{\partial \theta}, \tag{2}$$

$$M_s\left(\frac{1}{r}\frac{d}{dt}\left(r^2\dot{\phi}\right) + r\dot{\theta}^2\cos\phi\sin\phi\right) = \frac{1}{r}\frac{\partial U}{\partial \theta}. \tag{3}$$

Here U is known as the earth's gravitational potential which can be written as

$$\mathrm{U} = \frac{g_0{R_0}^2}{r}\left\{1 - \frac{J_2{R_0}^2}{r^2}\left(\frac{3\sin^2\phi - 1}{2}\right)\right\} + \frac{3g_0{R_0}^2}{r}\left(\frac{{J_2}^{(2)}{R_0}^2}{r^2}\cos^2\phi\cos 2\Gamma\right), \tag{4}$$

where:

$g_0 = 9.8\mathrm{m/sec}^2$ = gravitational acceleration on the earth's surface,

r = radial distance of the satellite from the centre of the earth,

M_s = mass of the satellite,

$J_2 = 1.08219 \times 10^{-3}$ = coefficient due to the oblateness of the earth,

$R_0 = 6367.4 \times 10^5\mathrm{cm}$ = mean radius of the earth,

$J_2^{(2)} = 2.32 \times 10^{-6}$ = coefficient due to the earth's equatorial ellipticity,

$\phi = \angle PEM$ = latitude of the satellite (Fig.1(a)),

$\theta = \angle XEF$ = longitude of the satellite (Fig.1(a)),

$\Gamma = \angle MEF = \theta - \theta_E$ = satellite angular position relative to minor axis of the earth's equatorial section (Fig. 1(a)),

$\theta_E = \angle XEF$ = angular position of the minor axis of the earth's equatorial section ,

$\dot{\theta}_E$ = angular rate of rotation of the earth (Fig. 1(b)),

X, Y, Z=inertial coordinate system with the origin at the centre of the earth and XY plane in the earth's equatorial plane.

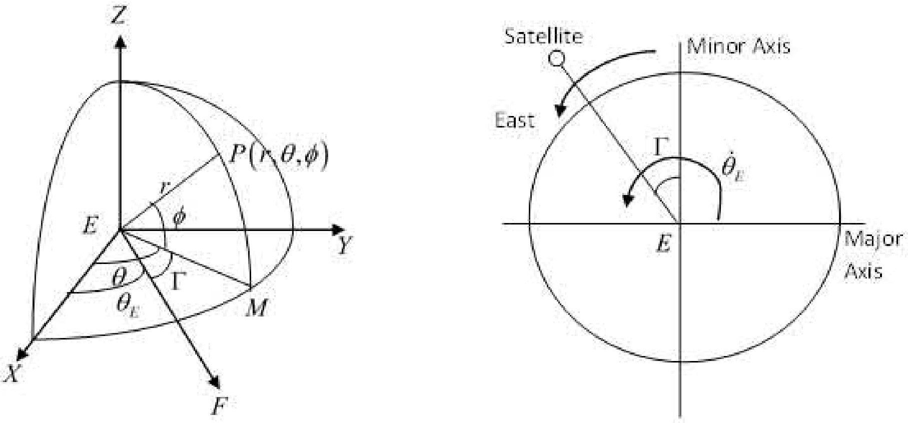

(a) Configuration of the satellite P (b) The earth's equitorial ellipticity parameter Γ

Figure 1: Configuration of the geo-centric satellite.

Substituting the value of U from (4) in equations (1), (2) and (3), we obtain

$$\ddot{r} - r\dot{\theta}^2\cos^2\phi - r\dot{\phi}^2 = -\frac{g_0{R_0}^2}{r^2} + 3\frac{J_2 g_0{R_0}^4}{2r^4}\left(3\sin^2\phi - 1\right) - 9\frac{J_2^{(2)} g_0{R_0}^4}{r^4}\cos^2\phi\cos 2\Gamma, \tag{5}$$

$$\frac{1}{r\cos\phi}\frac{d}{dt}\left(r^2\dot{\theta}\cos\phi\right) = -6\frac{J_2^{(2)} g_0{R_0}^4}{r^4}\cos\phi\sin 2\Gamma, \tag{6}$$

$$\frac{1}{r}\frac{d}{dt}\left(r^2\dot{\phi}\right) + r\dot{\theta}^2\cos\phi\sin\phi = -3\frac{J_2 g_0{R_0}^4}{2r^4}\sin\phi\cos\phi - 6\frac{J_2^{(2)} g_0{R_0}^4}{r^4}\sin\phi\cos\phi\cos 2\Gamma. \tag{7}$$

We assume that the satellite P lies in the equatorial plane i.e., $\phi = 0$.
Equations (5) and (6) become

$$\ddot{r} - r\dot{\theta}^2 = -\frac{g_0{R_0}^2}{r^2} - 3\frac{J_2 g_0{R_0}^4}{2r^4} - 9\frac{J_2^{(2)} g_0{R_0}^4}{r^4}\cos 2\Gamma, \tag{8}$$

$$\frac{1}{r}\frac{d}{dt}\left(r^2\dot{\theta}\right) = r\ddot{\theta} + 2\dot{r}\dot{\theta} = -6\frac{J_2^{(2)} g_0{R_0}^4}{r^4}\sin 2\Gamma. \tag{9}$$

In the synodic coordinate system, we have

$$\ddot{\bar{r}} = (\ddot{r} - r\dot{\theta}^2)\hat{e_r} + (r\ddot{\theta} + 2\dot{r}\dot{\theta})\hat{e_\theta} + \ddot{z}\hat{k},$$

where

$$\begin{aligned}
&\hat{e_r} = \cos\theta\ \hat{i} + \sin\theta\ \hat{j} \quad \hat{e_\theta} = -\sin\theta\ \hat{i} + \cos\theta\ \hat{j},\\
&\ddot{\bar{r}} = \frac{d}{dt}\left(\frac{d\bar{r}}{dt}\right) = \frac{d}{dt}\left(\frac{\partial\bar{r}}{\partial t} + \hat{w}\times\hat{r}\right) = \frac{\partial^2\bar{r}}{\partial t^2} + 2\bar{w}\times\frac{\partial\bar{r}}{\partial t} + \bar{w}\times(\bar{w}\times\bar{r}),\\
&\bar{w} = n\hat{k},\\
&\bar{r} = r\hat{e_r} = r\cos\theta\ \hat{i} + r\sin\theta\ \hat{j} = x\ \hat{i} + y\ \hat{j}.
\end{aligned}$$

We take the origin of coordinates at the centre of mass of the earth, the plane of motion of the infinitesimal satellite P is in the xy-plane orthogonal to the line of motion of the centre of mass of the earth and the motion of the earth takes place on the z-axis. The equations of the motion of $P(x, y)$ in the synodic coordinate system and dimensionless variables, i.e., the distance between the synchronous satellite and the earth is unity, the mass of the earth is unity and choose time t such that the universal gravitational constant G is unity, are

$$\ddot{x} - 2n\dot{y} - n^2 x = \frac{1}{r}\left[(\ddot{r} - r\dot{\theta}^2)x - (r\ddot{\theta} + 2\dot{r}\dot{\theta})y\right],$$
$$\ddot{y} + 2n\dot{x} - n^2 y = \frac{1}{r}[(\ddot{r} - r\dot{\theta}^2)y + (r\ddot{\theta} + 2\dot{r}\dot{\theta})x].$$

We may take

$$r^2\dot{\theta} = h \text{ (constant)}.$$

Differentiating with respect to t, we get

$$r\ddot{\theta} + 2\dot{r}\dot{\theta} = 0.$$

The equations of the motion of P in the synodic coordinate system and dimensionless variables are

$$\ddot{x} - 2n\dot{y} - n^2 x = \frac{1}{r}[(\ddot{r} - r\dot{\theta}^2)x],$$
$$\ddot{y} + 2n\dot{x} - n^2 y = \frac{1}{r}[(\ddot{r} - r\dot{\theta}^2)y].$$

Using equation (8), we get

$$\ddot{x} - 2n\dot{y} = n^2 x + \frac{1}{r}\left(-\frac{g_0 {R_0}^2}{r^2} - 3\frac{J_2 g_0 {R_0}^4}{2r^4} - 9\frac{J_2^{(2)} g_0 {R_0}^4}{r^4}\cos 2\Gamma\right)x, \tag{10}$$

$$\ddot{y} + 2n\dot{x} = n^2 y + \frac{1}{r}\left(-\frac{g_0 {R_0}^2}{r^2} - 3\frac{J_2 g_0 {R_0}^4}{2r^4} - 9\frac{J_2^{(2)} g_0 {R_0}^4}{r^4}\cos 2\Gamma\right)y. \tag{11}$$

Now, we define a function F such that

$$F = \frac{n^2}{2}(x^2 + y^2) + \frac{g_0 {R_0}^2}{r} + \frac{g_0 {R_0}^4}{3r^3}\left(\frac{3}{2}J_2 + 9J_2^{(2)}\cos 2\Gamma\right).$$

Hence, equations (10) and (11) become

$$\ddot{x} - 2n\dot{y} = F_x, \tag{12}$$
$$\ddot{y} + 2n\dot{y} = F_y, \tag{13}$$

where F_x and F_y are the partial derivatives of F with respect to x and y, respectively. The integral analogous to the Jacobi integral is

$$\dot{x}^2 + \dot{y}^2 = 2F - C. \tag{14}$$

The perturbed mean motion of the earth is governed by

$$n(\Gamma) = \sqrt{g_0 {R_0}^2\left(1 + \frac{3}{2}{R_0}^2 J_2 + 9J_2^{(2)}\cos 2\Gamma\right)}.$$

3 Location of Equilibrium Points

The points described by $F_x = 0$ and $F_y = 0$ are called the equilibrium points. In fact, all the derivatives of the co-ordinates with respect to time are zero at these points. Therefore the satellite P placed at the equilibrium points with zero velocity, will stay there. The terms "Libration points" and "Lagrangian points" are also used in place of equilibrium points.

Thus, we have

$$F_x = 0 \text{ implies } \quad x \times f(x,y) = 0,$$
$$F_y = 0 \text{ implies } \quad y \times f(x,y) = 0,$$

where

$$f(x,y) = n^2 - \frac{g_0 {R_0}^2}{(x^2+y^2)^{\frac{3}{2}}} + \frac{g_0 {R_0}^4}{3(x^2+y^2)^{\frac{5}{2}}} \left(\frac{3}{2} J_2 + 9 J_2^{(2)} \cos 2\Gamma \right).$$

3.1 Collinear points

Solving the above equations for $f(x,y) = 0$ when $y = 0$ and by taking different values of the earth's equatorial ellipticity parameter Γ, we obtained two collinear points on the x-axis. In Table 1, we have shown the coordinates of these collinear points for different values of the earth's equatorial ellipticity parameter Γ. We noticed the one equilibrium point is on the positive side of the x-axis, while the other equilibrium point lies on the negative side of the x-axis for different values of the earth's equatorial ellipticity parameter Γ. Also, the effect of the earth's equatorial ellipticity parameter Γ on the location of equilibrium points on the x-axis is very small (i.e., the coordinates of the equilibrium points are different after the fifth decimal places) and the number of equilibrium points remains same for different values of Γ.

3.2 Non-collinear points lying on the y-axis

The non-collinear points lying on the y-axis are the solution of the equations $f(x,y) = 0$ when $x = 0$. We have found that there exist two non-collinear points lying on the y-axis for different values of the earth's equatorial ellipticity parameter Γ (Table 2). Also, the effect of the earth's equatorial ellipticity parameter Γ on the location of non-equilibrium points lying on the y-axis is very small and the number of equilibrium points remains same for different values of Γ.

3.3 Non-collinear points lying on the circle

The non-collinear points lying on the y-axis are the solution of the equations $f(x,y) = 0$ when $x \neq 0$ and $y \neq 0$. We observed that there exists an infinite number of non-collinear points lying on the circle. We have shown the location of some of the non-collinear points lying on the circle in Table 3.

3.4 Zero-velocity curves

Equation (14) represents the relation between the positions and square of the velocity of the satellite P in the rotating coordinate system. Using initial conditions, the Jacobi constant C can be found numerically. Therefore the contour curves describing the

Γ	Collinear Equilibrium Points	Stability
$0°$	$(-0.9994650500230987, 0)$ $(0.9994650500230987‘, 0)$	Unstable
$5°$	$(-0.9994751560349406‘, 0)$ $(0.9994751560349406‘, 0)$	Unstable
$10°$	$(-0.9994753049325603, 0)$ $(0.9994753049325603, 0)$	Unstable
$15°$	$(-0.999475391830673, 0)$ $(0.999475391830673, 0)$	Unstable
$20°$	$(-0.9994754533738673, 0)$ $(0.9994754533738673, 0)$	Unstable
$25°$	$(-0.9994750068339644, 0)$ $(0.9994750068339644, 0)$	Unstable
$30°$	$(-0.9994752431809284, 0)$ $(0.9994752431809284, 0)$	Unstable
$35°$	$(-0.9994753527773587, 0)$ $(0.9994753527773587, 0)$	Unstable
$40°$	$(-0.9994754248202805, 0)$ $(0.9994754248202805, 0)$	Unstable
$45°$	$(-0.9994754785409711, 0)$ $(0.9994754785409711, 0)$	Unstable

Table 1: Location and stability of collinear equilibrium points.

boundaries of the permitted region within the infinitesimal satellite P move freely and can be found by using equation (14). These curves obtained in the XY-plane by taking $\dot{x} = \dot{y} = 0$ are known as zero-velocity curves and are given by $2F = C$. Fig. 3 shows zero-velocity curves at $\Gamma = 0°$, for different values of the Jacobi constant C taken in increasing order. Fig. 4 indicates zero-velocity curves at $\Gamma = 15°$, for different values of the Jacobi constant C taken in increasing order. Fig. 5 shows zero-velocity curves at $\Gamma = 30°$, for different values of the Jacobi constant C taken in increasing order. Fig. 6 indicates zero-velocity curves at $\Gamma = 45°$, for different values of the Jacobi constant C taken in increasing order. It is observed that at a fixed value of the earth's equatorial ellipticity parameter Γ, on increasing the values of the Jacobi constant C, the represented possible boundary regions decrease, where the satellite can move freely. We also noticed that the possible boundary regions depend on the Jacobi constant, while the effect of the earth's equatorial ellipticity parameter Γ on the possible boundary regions is minimal.

4 Stability of Equilibrium Points

To study the stability of equilibrium points, we denote the location of equilibrium points by (x_0, y_0) and consider a small displacement (ξ, η) from the point such that

$$x = x_0 + \xi, \; y = y_0 + \eta.$$

Γ	Non-Collinear Equilibrium Points lying on the y-axis	Stability
$0°$	$(0, -0.9994650500230987)$ $(0, 0.9994650500230987)$	Unstable
$5°$	$(0, -0.9994751560349406)$ $(0, 0.9994751560349406)$	Unstable
$10°$	$(0, -0.9994753049325603)$ $(0, 0.9994753049325603)$	Unstable
$15°$	$(0, -0.999475391830673)$ $(0, 0.999475391830673)$	Unstable
$20°$	$(0, -0.9994754533738673)$ $(0, 0.9994754533738673)$	Unstable
$25°$	$(0, -0.9994750068339644)$ $(0, 0.9994750068339644)$	Unstable
$30°$	$(0, -0.9994752431809284)$ $(0, 0.9994752431809284)$	Unstable
$35°$	$(0, -0.9994753527773587)$ $(0, 0.9994753527773587)$	Unstable
$40°$	$(0, -0.9994754248202805)$ $(0, 0.9994754248202805)$	Unstable
$45°$	$(0, -0.9994754785409711)$ $(0, -0.9994754785409711)$	Unstable

Table 2: Location and stability of non-collinear equilibrium points lying on the y-axis.

Substituting these values in equations of motion (12) and (13), we obtain the variational equations as

$$\ddot{\xi} - 2n\dot{\eta} = \left(F^0_{xx}\right)\xi + \left(F^0_{xy}\right)\eta, \tag{15}$$

$$\ddot{\eta} + 2n\dot{\xi} = \left(F^0_{yx}\right)\xi + \left(F^0_{yy}\right)\eta, \tag{16}$$

where the superscript '0' indicates that the partial derivatives are evaluated at the equilibrium point (x_0, y_0). Let the solution of the variational equations (15) and (16) be

$$\xi = Ae^{\lambda t}, \eta = Be^{\lambda t},$$

where A, B and λ are constants. Then equations (15) and (16) will have a non-trivial solution for A and B when

$$\begin{vmatrix} \lambda^2 - F^0_{xx} & -2n\lambda - F^0_{xy} \\ 2n\lambda - F^0_{yx} & \lambda^2 - F^0_{xx} \end{vmatrix} = 0.$$

On expanding the determinant, we obtain the characteristic equation corresponding to the variational equations (15) and (16) as

$$\lambda^4 - (F^0_{xx} + F^0_{yy} - 4n^2)\lambda^2 + F^0_{xx}F^0_{yy} - \left(F^0_{xy}\right)^2 = 0. \tag{17}$$

The four roots of characteristic equation (17) play an important role for determining the stability of equilibrium points. An equilibrium point will be stable if the above equation

Γ	Non-Collinear Equilibrium Points lying on the circle	Stability
0°	$(0.027075043161954526, -0.9990982575580011)$	Unstable
	$(0.950631409170543, 0.3085940863271852)$	Stable
5°	$(0.02706787135141031, -0.9991084123488571)$	Unstable
	$(0.9506385809810823, 0.3086042411180343)$	Stable
10°	$(0.027067763883445894, -0.9991085645161091)$	Stable
	$(-0.446978878143267, 0.893957756286534)$	Unstable
15°	$(0.446978974966415, -0.8939578053071354)$	Stable
	$(0.9506387512193974, 0.3086044821637891)$	Unstable
20°	$(0.027067656634011672, -0.9991087163739373)$	Unstable
	$(0.9506387956984799, 0.3086045451431129)$	Stable
25°	$(0.02706762217188341, -0.9991087651699426)$	Stable
	$(-0.4469789651947475, -0.893957932725505)$	Unstable
30°	$(0.9945151859441937, 0.09945151482739278)$	Unstable
	$(0.95063885829031, 0.3086046337688429)$	Stable
35°	$(0.027067570280104203, -0.9991088386451358)$	Stable
	$(-0.9945152184903229, 0.0994515209075532)$	Unstable
40°	$(0.9945152473685147, -0.09945151908563067)$	Unstable
	$(0.9506389026192351, 0.3086046965355544)$	Stable
45°	$(0.027067531585647564, -0.999108893433827)$	Stable
	$(0.9506389207468378, 0.30860472220299384)$	Unstable

Table 3: Location and stability of non-collinear equilibrium points lying on the circle.

evaluated at the equilibrium point has four pure imaginary roots or complex roots with negative real parts.

4.1 Stability of collinear points

At the collinear point $(-0.9994650500230987,\ 0)$, at $(\Gamma = 0^\circ)$, the characteristic roots are given by $\lambda_1 = -0.00125276$ $\lambda_2 = -0.12927\iota, \lambda_3 = 0.12927\iota, \lambda_4 = 0.00125276$. At the collinear point $(0.9994650500230987, 0)$ at $(\Gamma = 0^\circ)$, the characteristic roots are given by $\lambda_1 = -0.00125276, \lambda_2 = -0.12927\iota, \lambda_3 = 0.12927\iota, \lambda_4 = 0.00125276$. Thus both the collinear points are unstable. For $\Gamma = 45^\circ$, at the non-collinear point $(0.9994754785409711,\ 0)$ the characteristic roots are given by $\lambda_1 = -1.81113 \times 10^{-9}\iota, \lambda_2 = 1.81113 \times 10^{-9}\iota, \lambda_3 = -0.129266\iota, \lambda_4 = 0.129266\iota$. For $\Gamma = 45^\circ$, at the non-collinear point $(-0.9994754785409711,\ 0)$ the characteristic roots are given by $\lambda_1 = -1.81113 \times 10^{-9}\iota, \lambda_2 = 1.81113 \times 10^{-9}\iota, \lambda_3 = -0.129266\iota, \lambda_4 = 0.129266\iota$. Similarly, we have also examined that both the collinear points are unstable for other values of the earth's equatorial ellipticity parameter Γ (Table 1).

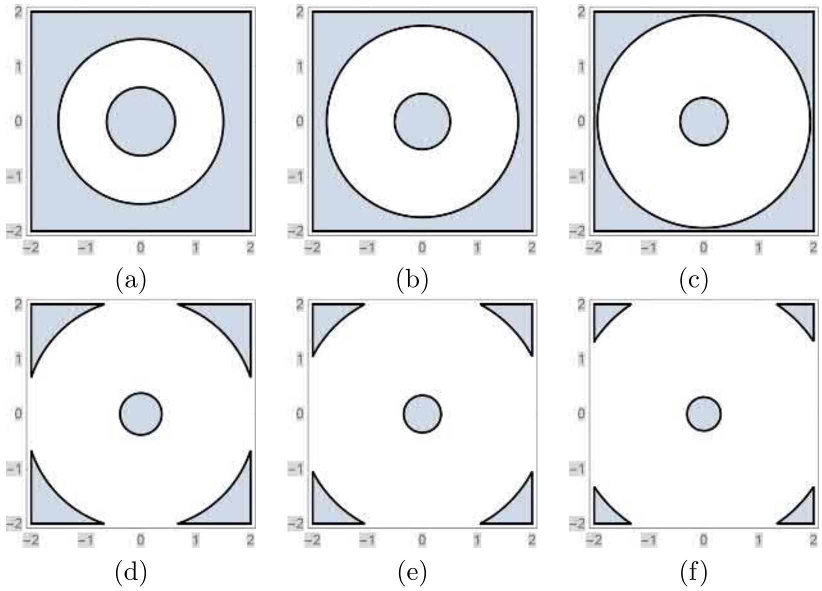

Figure 2: Effect on zero-velocity curves at the ellipticity parameter $\Gamma = 0^\circ$ and different values of the Jacobi constants: (a) $\Gamma = 0^\circ$ and C=0.06; (b) $\Gamma = 0^\circ$ and C=0.07; (c) $\Gamma = 0^\circ$ and C=0.08; (d) $\Gamma = 0^\circ$ and C=0.09; (e) $\Gamma = 0^\circ$ and C=0.10; (f) $\Gamma = 0^\circ$ and C=0.11.

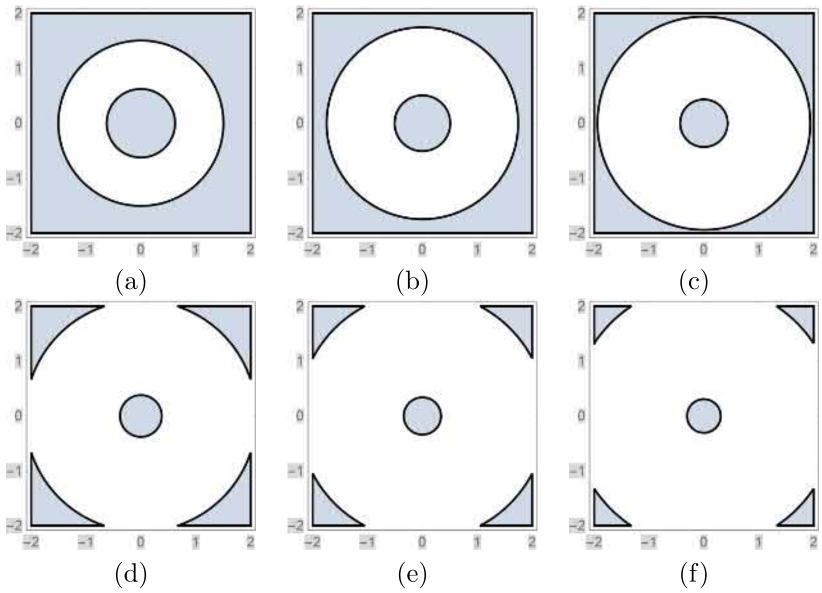

Figure 3: Effect on zero-velocity curves at the ellipticity parameter $\Gamma = 15^\circ$ and different values of the Jacobi constants: (a) $\Gamma = 15^\circ$ and C=0.06; (b) $\Gamma = 15^\circ$ and C=0.07; (c) $\Gamma = 15^\circ$ and C=0.08; (d) $\Gamma = 15^\circ$ and C=0.09; (e) $\Gamma = 15^\circ$ and C=0.10; (f) $\Gamma = 15^\circ$ and C=0.11.

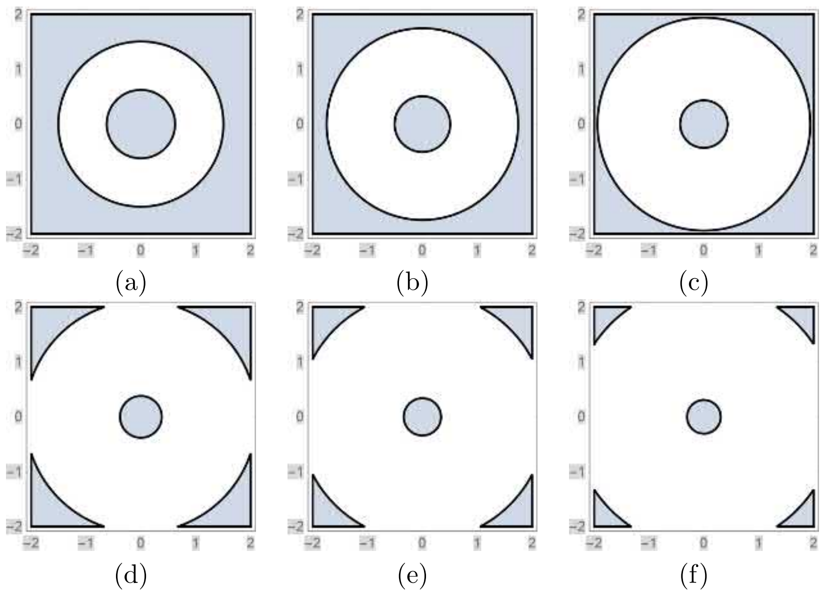

Figure 4: Effect on zero-velocity curves at the ellipticity parameter $\Gamma = 30^\circ$ and different values of the Jacobi constants: (a) $\Gamma = 30^\circ$ and C=0.06; (b) $\Gamma = 30^\circ$ and C=0.07; (c) $\Gamma = 30^\circ$ and C=0.08; (d) $\Gamma = 30^\circ$and C=0.09; (e) $\Gamma = 30^\circ$ and C=0.10; (f) $\Gamma = 30^\circ$ and C=0.11.

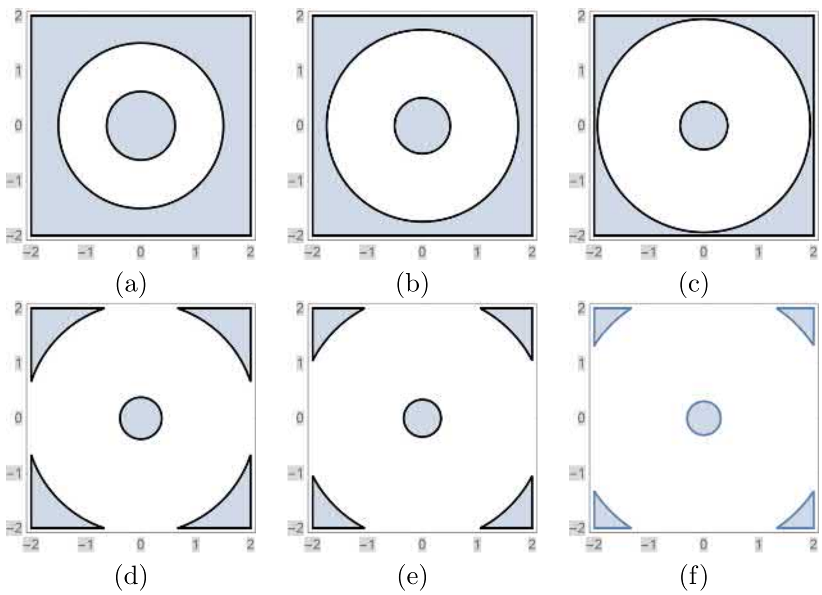

Figure 5: Effect on zero-velocity curves at the ellipticity parameter $\Gamma = 45^\circ$and different values of the Jacobi constants: (a) $\Gamma = 45^\circ$and C=0.06, (b) $\Gamma = 45^\circ$and C=0.07, (c) $\Gamma = 45^\circ$and C=0.08, (d) $\Gamma = 45^\circ$and C=0.09, (e) $\Gamma = 45^\circ$and C=0.10, (f) $\Gamma = 45^\circ$and C=0.11.

4.2 Stability of non-collinear points lying on the y-axis

At the non-collinear point $(0, 0.9994650500230987)$ for $\Gamma = 0^\circ$ (i.e., in the case of a geo synchronous satellite), the characteristic roots are given by $\lambda_1 = -0.00125276, \lambda_2 =$

$-0.12927\iota, \lambda_3 = 0.12927\iota, \lambda_4 = 0.00125276$. At the non-collinear point $(0, -0.99946505\ 00230987)$ (at $\Gamma = 0°$), the characteristic roots are given by $\lambda_1 = -0.00125276, \lambda_2 = -0.12927\iota, \lambda_3 = 0.12927\iota, \lambda_4 = 0.00125276$. Thus both the non-collinear points lying on the y-axis are unstable for $\Gamma = 0°$. For $\Gamma = 45°$, at the non-collinear point $(0\ , 0.9994754785409711)$ the characteristic roots are given by $\lambda_1 = -1.81113 \times 10^{-9}\iota, \lambda_2 = 1.81113 \times 10^{-9}\iota, \lambda_3 = -0.129266\iota, \lambda_4 = 0.129266\iota$. For $\Gamma = 45°$, at the non-collinear point $(0\ , -0.9994754785409711)$ the characteristic roots are given by $\lambda_1 = -1.81113 \times 10^{-9}\iota, \lambda_2 = 1.81113 \times 10^{-9}\iota, \lambda_3 = -0.129266\iota, \lambda_4 = 0.129266\iota$. Similarly, we have examined that both the non-collinear points lying on the y-axis are unstable for other values of Γ (Table 2).

4.3 Stability of non-collinear points lying on the circle

From the roots of the characteristic equation (17), we have noted that some of the non-collinear points lying on the circle are stable and others are unstable for different values of the earth's equatorial ellipticity parameter Γ. In Table 3, we have shown the stability of two non-collinear points for different values of Γ.

4.4 Stability regions of equilibrium points

From characteristic equation (17), an equilibrium point will be stable if the above equations evaluated at the equilibrium points has purely imaginary roots or complex roots with negative real parts. This happens if the following three conditions

$$\begin{aligned} (F^0_{xx} + F^0_{yy} - 4n^2)^2 - \left(F^0_{xx}F^0_{yy} - (F^0_{xx})^2\right) > 0, \\ F^0_{xx} + F^0_{yy} - 4n^2 > 0, \\ F^0_{xx}F^0_{yy} - (F^0_{xx})^2 > 0, \end{aligned}$$

evaluated at the equilibrium point are satisfied simultaneously.

We have plotted the stability regions of the equilibrium points for different values of the earth's equatorial ellipticity parameter Γ (Fig. 6). We observed that there is a very small change in the stability region as the value of Γ increases.

5 Discussion and Conclusion

We have studied the locations and stability of the equilibrium points in the problem of a geo-centric satellite including the earth's equatorial ellipticity parameter Γ. First, we write the equations of motion of the geo-centric satellite P moving around the earth in the equatorial plane. We assume that the satellite P lies in the equatorial plane. We choose the origin of coordinates at the centre of mass of the earth. The plane of motion of the infinitesimal satellite P is in the XY-plane orthogonal to the line of motion of the centre of mass of the earth, and the motion of the earth takes place on the z-axis. We write the Jacobi integral of the system, and then we calculate the perturbed mean motion n which is a function of Γ. The possible boundary regions for the motion of an infinitesimal satellite P are obtained with the help of zero-velocity curves at different values of the Jacobi constant by fixing the values of the earth's equatorial ellipticity parameter Γ. In Figs. 2–5, we observed that at a fixed value of the earth's equatorial ellipticity parameter Γ, on increasing the values of the Jacobi constant C, the possible boundary regions decrease. We also observed that the possible boundary regions depend

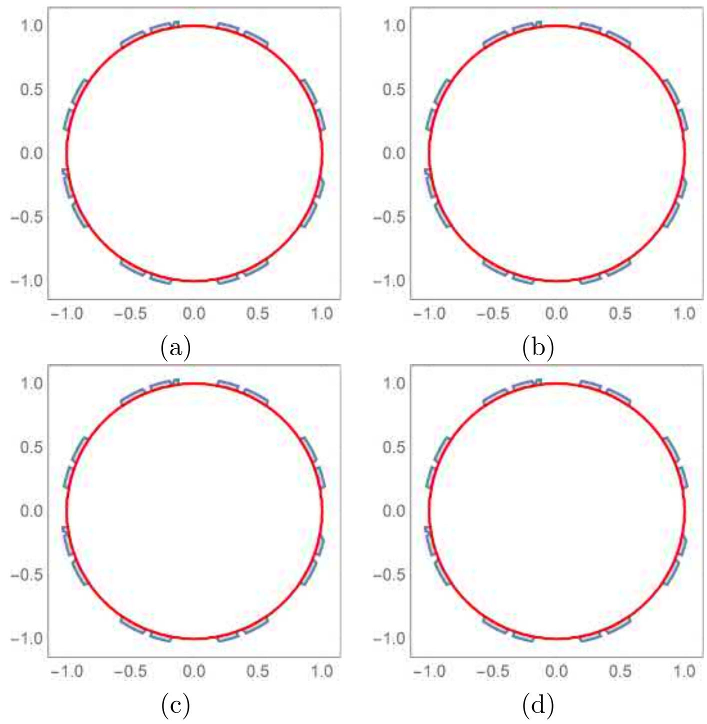

Figure 6: Stability regions of equilibrium points for different values of Γ: (a) $\Gamma = 0°$; (b) $\Gamma = 15°$; (c) $\Gamma = 30°$; (d) $\Gamma = 45°$.

on the Jacobi constant, while the effect of the earth's equatorial ellipticity parameter Γ on possible boundary regions is very small. We have also investigated the existence and stability of the equilibrium points of the system for different values of Γ. We observed that there exist two collinear points and both of them are unstable for different values of Γ (Table 1). It is shown that the effect of earth's equatorial ellipticity parameter Γ on the location of equilibrium points is very small and the number of equilibrium points remains the same for different values of Γ. We also observe that there exist non-collinear points lying on the y-axis and both of them are unstable for different values of Γ (Table 2). Further, we have found that there exist an infinite number of non-collinear points lying on the circle. Some of them are stable, and others are unstable. Two non-collinear points for different values of Γ and their stability are shown in Table 3. Finally, we have plotted the stability regions of the equilibrium points for different values of Γ (Fig. 6). We notice that there is a minimal change in the stability regions of the equilibrium points as the value of Γ increases.

Acknowledgment

We are thankful to Centre of Fundamental Research in Space Dynamics and Celestial Mechanics (CFRSC), Delhi, India for providing necessary facilities required for this research work.

References

[1] R. R. Allan. Perturbations of a geostationary satellite by the longitude-dependent terms in the Earth's gravitational field. *Planetary and Space Science* **11** (11) (1963) 1325–1334.

[2] K. B. Bhatnagar and Manjeet Kaur. The in-plane motion of a Geosynchronous Satellite under the Gravitational Attraction of the Sun, the Moon and the Oblate Earth. *Journal of Astrophysics and Astronomy* **11** (1) (1990) 1–10.

[3] K. B. Bhatnagar and M. Mehra. The Motion of a Geosynchronous Satellite-I. *Indian J. Pure Appl. Math* **17** (1986) 1438–1452.

[4] L. Blitzer. Synchronous and Resonant Satellite Orbits Associated with Equatorial Ellipicity. *ARS J* **32** (1966) 1016–1019.

[5] R. H. Frick and T. B. Garber. *Perturbations of a Synchronous Satellite*. The RAND Corporation, R-399 NASA, 1962.

[6] M. S. Gilthorpe and P. Moore. A combined theory for zonal harmonic and resonance perturbations of a near-circular orbit with applications to COSMOS 1603 (1984-106A). *Celestial Mechanics and Dynamical Astronomy* **54** (1992) 363–391.

[7] T. Lane Mark. An Analytical Treatment of Resonance Effects on Satellite Orbits. Massachusetts Institute of Technology. *Lincoln Laboratory* Lexington Ma (1988) 02173–0073.

[8] L. Sehnal. The influence of the equatorial ellipticity of the earth gravitational field on the motion of a close satellite. *Astronomical Institute of the Czechoslovak Academy of Sciences* Ondrejov (1959) 90–93.

[9] C. A. Wagner. The drift of a 24-hour Equatorial satellite due to an earth gravity field through 4th order. *Goddard Space Flight Centre Greenbelt*, Maryland National Aeronautics and Space Administration, Washington, D. C. NASA TN D-2103 (1964).

[10] S. Yadav and R. Aggarwal. Resonance in a geo-centric satellite including earth's equatorial ellipticity. *Astrophysics and Space Science* **347** (2013) 249–259.

[11] B. Kumari and B. S. Kushvah. Stability regions of equilibrium points in restricted four-body problem with Oblateness effects. *Astrophysics and Space Science* **349** (2014) 693–704.

[12] L. O. Arriaga-Camargo et al. Synchronization of Dumbbell Satellites: Generalized Hamiltonian Systems Approach. *Nonlinear Dynamics and Systems Theory* **15** (4) (2015) 334–343.

[13] A. A. Correa. et al. Comparison of Transfer Orbits in the Restricted Three and Four-Body Problems. *Nonlinear Dynamics and Systems Theory* **7** (3) (2007) 267–277.

[14] A. F. B. A. Prado. A Survey on Space Trajectories in the Model of Three Bodies. *Nonlinear Dynamics and Systems Theory* **6** (4) (2006) 389–400.

Nonlinear Dynamics and Systems Theory, **19** (4) (2019) 551–554

Contents of Volume 19, 2019

Volume 19 Number 1 2019

Volume 19 Number 1-SI 2019

Volume 19 Number 2 2019

Volume 19 Number 3 2019

Volume 19 Number 4 2019